Title
Advancing the plant fossil record across the Permo-Triassic boundary with a focus on phytoliths

Author
Kirchholtes, Renske

Publication Date
2018

Peer reviewed|Thesis/dissertation

Advancing the plant fossil record across the Permo-Triassic boundary with a focus on phytoliths

by

Renske Kirchholtes

A dissertation submitted in partial satisfaction of the

requirements for the degree of

Doctor of Philosophy

in

Integrative Biology

in the

Graduate Division

of the

University of California, Berkeley

Committee in charge:

Professor Cindy V. Looy, Chair

Professor Anthony D. Barnosky

Professor Paul R. Renne

Fall 2018

Abstract

Advancing the plant fossil record across the Permo-Triassic boundary with a focus on phytoliths

by

Renske Kirchholtes

Doctor of Philosophy in Integrative Biology

University of California, Berkeley

Professor Cindy V. Looy, Chair

The end-Permian mass extinction (~252 Ma ago) drastically altered ecosystems worldwide, not just in the oceans, but also on land. The effects were so profound that it was not until 4-5 million years into the Triassic that the ecosystem of what was then the eastern part of equatorial Pangea, showed signs of recovery. The flora responsible for this recovery appears to have invaded European habitats after their Early Triassic origination elsewhere. Hitherto, no direct evidence exists of where the refugional source areas of the immigrants could have been located. Here, we suggest that North America could be a potential source area for European Triassic conifers. This body of work aims to advance the plant fossil record across the Permo-Triassic boundary in this geographical region.

The first part of chapter one focusses on our current understanding of the potential causes of the end-Permian biotic crisis. While there may be a singular cause that set off a cascade of events, the intricate nature of the Earth's system makes it difficult to identify the specific drivers behind the ecosystem collapse. It appears that many factors have contributed to some degree to the biotic crisis. The second part of this chapter is focused on the effects the biotic crisis had on life on land, particularly on plants and the data that we have available to study these extinction patterns. Analysis of the data that is currently available through various online databases, suggests that the information is insufficient to adequately study extinction patterns.

The second chapter is a literature review of the role of silica in plants. Silica is absorbed by plant roots in the form of monosilicic acid, which originates from the dissolution of crystalline silicate and weathering of biogenic silicates in the soil. Silica absorption, once thought to be a passive process, has been shown to be driven by active transport mechanisms. Depending on where the silica is deposited in the plant, the crystalized shape—the phytolith—may adopt a shape unique to that plant cell or tissue. However, before it crystalizes, the silica plays an important role in the plant's defense mechanisms. Once crystalized, the opaline silica continues to beneficial; it not only reduces biotic and abiotic stress, it also appears to provide structural benefits.

Chapter three examines the Permian and Triassic phytolith record and its potential to support (bio)stratigraphic investigations. In Caprock Canyons State Park and Palo Duro State Park in Texas, the Permian-Triassic boundary is well-preserved and the stratigraphy has been resolved in detail. The phytolith assemblages recovered from the Permian and Triassic strata appear to have limited potential for

regional biostratigraphy. However, these phytoliths do form the first evidence of plant life at the western portion of the supercontinent Pangea, a region previously believed to be entirely barren.

Table of contents

Introduction

Everyone always likes a good “biggest”, “tallest” or “oldest”. It makes objects, features and characters seem more impressive, more important. The world’s biggest marine mammal, the tallest tree in the United States, the second deepest lake east of the Mississippi, or the oldest fossil ever found in Iceland. But really, the oldest fossils in Iceland are of Pliocene age, which compared to ones found in the rest of the Europe can hardly be considered extremely old. Whenever reading about the end-Permian biotic crisis, the first paragraph almost always talks about it being the worst extinction event of all time, or something to that effect. I will not dispute that this event has not had a great effect on life on our planet, but I will argue for a bit of nuance, because it does depend on your perspective. Not all organisms are affected equally by extinction events. During the great freeze, the Huronian glaciation that started some 2400 Mya ago and lasted about 300 Mya, many organisms went extinct. Most likely, almost all of them. Only a few had a narrow escape. But since these single-celled organisms generally leave a poor trace in the fossil record, we conveniently forget about it or chose to ignore it because we do not really care about single-celled organisms until they turn milk into yogurt or give us a belly ache. So to be precise, the end-Permian biotic crisis, colloquially also known as the Great Dying, the end-Permian Extinction. the Great Permian Extinction, or the Permian-Triassic extinction event, is the greatest extinction event of multicellular organisms in the last 530 Mya that we know of. Granted that it is unlikely that we will find (evidence for) events that exceeded the end-Permian extinction event in severity, it is best to be as accurate as possible. While it is considered to be the greatest extinction event, it is not the most studied one. That honor goes to the meteorite mediated exit of the dinosaurs, potentially because some feel that dinosaurs are more charismatic than trilobites. But again, that’s a matter of perspective.

Independent of your perspective, it is obvious that the end-Permian biotic crisis had a profound effect on life on Earth. This, combined with the knowledge that the end-Permian biotic crisis unfolded within a relative short timeframe, making it obvious that a biotic status quo can be overturned fairly quickly, makes the events that took place in the end-Permian a very interesting and relevant topic. The present is the key to the past, but the past may also be the key to the future. While few harbor the illusion that we even fully comprehend the present, our understanding of the past is worse still. If you like to envision paleontology like detective work, then comparing it to an Agatha Christie novel with all but a few pages ripped out, is not much of a stretch. Reconstructing the full (hi-)story, based on a few titbits is most certainly a challenge and yet that is what paleontology and adjacent scientific fields are about. The following pages contain my two cents.

Acknowledgements

This work would not have been possible without the help and support of numerous people to whom I am hugely indebted.

First of all, thanks to my advisor Cindy Looy for being such a supportive PI. Thank you for allowing me to take on this—in a way—risky project and for making the lab feel like such welcoming place. Thanks also to my other committee members, Tony Barnosky and Paul Renne for the feedback, support and encouragement throughout this process.

I would also like to thank Neil Tabor of Southern Methodist University, who took time out his incredibly busy schedule to help me find sites, collect samples, teach me about the local stratigraphy of Caprock Canyon State Park and the surrounding area.

Thanks also to the entire UC Museum of Paleontology community, and particularly Ivo Duijnstee for all his scientific insights and Diane Erwin for keeping me and all the other people safe while working countless hours in the windowless UCMP labs. And thank you Chris Meija, for helping me fax official documents whenever I hit an administrative rough patch.

This study was funded in part by fellowships and research grants from the Dutch Geological Survey, University of California Museum of Paleontology, Paleontological Society of America, Sigma Xi Grants-in-Aid of Research, GRAC Research Funds from the UC-Berkeley Integrative Biology Department, Graduate Division Travel Award and IB Summer Research Grant. I would like to highlight the funding I received from the Dutch Geological Survey (TNO) and the person who went out of his way to make that happen, Tom van Hoof.

I want to thank my lab mates, especially Dori, Jeff, Ben, Nick and Jeamin for distracting me. Equally or even more distracting were Mel, Lucy, Rosemary, Camilla, Dwight, Leanne, Jun, Ash and Adam. Thank you for board games, barbeques and indulging my love for theater, Shakespeare and—let's be frank—Benedict!

I would also like to thank my co-GSIs, Andrew, Alex, Jim, Clay and particularly Rebecca. Teaching with you, taught me a lot.

Last but not least, I want to thank my family and friends outside of academia. Kim, Nina, Florence and Suzan, thank you for your unwavering friendship. Thank you mom, for your unwavering support. Sorry for being a tad tetchy at times.

Most of all, I want to thank Ate! Thank you for all your patience, your help, your amazing dinners and ... did I mention your endless patience? ♪ *You and me ...* ♫

CHAPTER 1: The end Permian Biotic Crisis and its reflection in the fossil record

A very brief introduction to the end-Permian biotic crisis

The end-Permian biotic crisis (~252 million years ago) is the largest known extinction event in the Paleozoic. It profoundly altered ecosystems worldwide, both on land and in the ocean (McElwain and Punyasena 2007). In the ocean, 286 of the known invertebrate genera disappear entirely, which translates to ~96% overall loss of marine species (Shen et al. 2011; Clapham and Payne 2011). On land, the fauna is hit almost just as hard with 70% of terrestrial vertebrate species and insects 83% of insect genera going extinct (Erwin 1989; Labandeira 2005; Benson and Upchurch 2013). Plants however, seem to escape a similar fate. For plants, the Permian-Triassic boundary is marked by a community turn-over rather than a sudden mass extinction (Silvestro et al. 2015; Niklas 2015; Knoll 1984).

To understand the course of events, we must look at both the causes and effects of this crisis. This chapter is therefore split in two parts. The first part is focused on a number of causes that have most likely all contributed to some degree to the extinction event, whilst the second part is focused on the effects it had on life on land, particularly on plants and the data that we have available to study the patterns. The conclusion to both these parts will validate the ongoing need for further investigation and why other avenues deserve exploration in an effort to elucidate patterns previously undetected.

PART 1 : "Murder on the Paleozoic Express": they all did it?

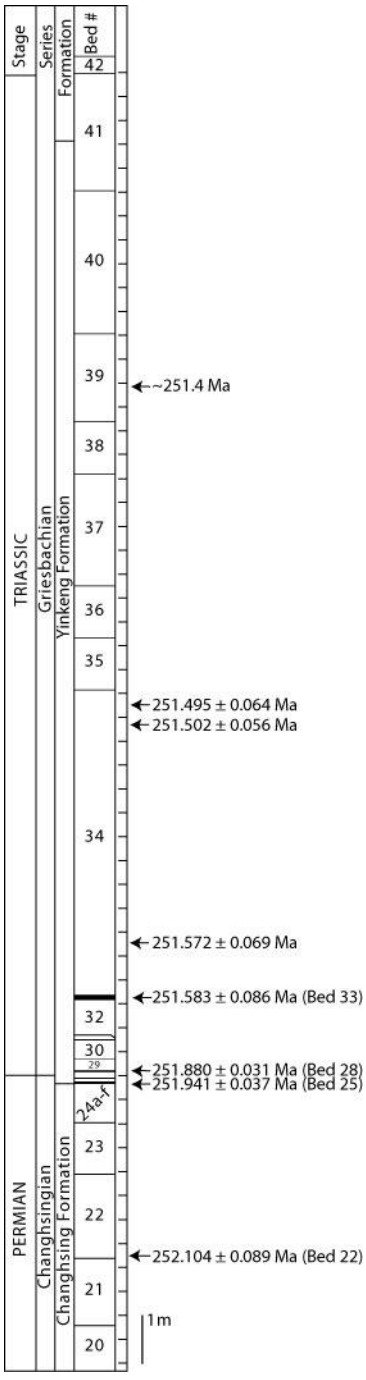

Many mechanisms and triggers have been proposed to explain the events of the end-Permian extinction by just as many groups of researchers. Understandably, investigators oftentimes seek answers that lie in their own realm of expertise. Although the causes and mechanisms are presented here as separate entities, they certainly do not act independently; feedback and interactions oftentimes impede definitive discrimination between these various causes (Shen and Bowring 2014). Douglas Erwin therefore called it Murder on the Orient Express, after the famous Agatha Christie book in which more than one character had a hand in the victim's fate and the murder involved multiple causes (Erwin 1993).

1.1 In search of the ultimate cause of the end-Permian biotic crisis

When evaluating the suggested causes of the end-Permian biotic crisis, it is important to specifically look for two aspects of time: (1) timing and (2) duration. In other words, when did it happen and how long did it take to unfold? When assessing the validity of the causes suggested, whether it is direct result or circumstantial evidence, it is critical to evaluate these two aspects of time.

The first written work that alludes to the end-Permian biotic crisis was that of John Phillips in 1860. He recognized that there was a sharp decrease in the number of fossils between two time periods that he dubbed the Paleozoic and the Mesozoic. His discovery however did not spark much interest in exploring the potential causes of this event. The pattern in the fossil record was merely observed and recorded as it presented in the strata. It would take more than a century before a renewed interest, and the work of Sepkoski on marine invertebrates, prompted the question as to why the fauna in the end of the Permian was hit so hard.

Fig 1. *Stratigraphy for the Permian-Triassic GSSP at Meishan, China. Based on Burgess et al 2104.*

From the outset it was apparent that the cause of the extinction is not cut-and-dry; there is a plethora of potential culprits. When examining these potential culprits for their contribution to the biotic crisis, one of the most important criteria is to establish if the pattern of extinction can be explained by the characteristics of the triggering mechanism. Determining the ultimate cause of the end-Permian extinction has proven to be difficult, in part because the apparent, and seemingly all-encompassing decline in biodiversity, particularly in the marine realm. However, the asynchronous timing and the different pattern of extinction observed in the various realms (terrestrial-marine, flora-fauna) provides important clues as to what may have caused or contributed to the biotic crisis. The coincidence, in the literal sense of the word, and interplay makes it challenging if not impossible to distinguish between these—potentially ultimate—causes.

However, in the past decade the time resolution of the Permian-Triassic boundary has dramatically improved. The resolution went from roughly millions of years, to a resolution high enough to observe variation in Milankovitch cycles (*e.g.* Wu et al. 2013; Burgess et al 2014). This higher resolution now allows the end-Permian crisis to be tied to the rate and/or severity of the currently ongoing extinction. This much improved dating of the end-Permian events (*e.g.* Wu et al. 2013; Burgess et al 2014. See Fig. 1) also demonstrated that the onset of events, based on the duration of the carbonate carbon isotope excursion, took place rather quickly, spanning between 2,100 and 18,800 years, with the extinction interval itself bracketed it within 0.061 ± 0.048 Mya. Whether the current, human-driven so-called *6th Mass Extinction* is already underway is the topic of much debate and subject of a lot of research. However, in 2011 Barnosky *et al.* and Ceballos *et al.* (2015) firmly established that the present day rates of extinction are higher than the regular background extinction rates. Suddenly, the analogy between the rapid environmental transition observed during the end-Permian Biotic Crisis and current events does not seem so farfetched at all.

The improved resolution and a closer study of 537 marine species showed that in the marine realm there were actually pulses to the end-Permian biotic crisis (Song et al. 2012). These two pulses were approximately 180,000-years apart and affected different taxonomic groups. Song *et al* concluded that, because the two pulses showed different extinction selectivity, they may have had different environmental causes. However, it should be noted that the first pulse already eliminated around 57% of the species. Even though this process seems to have been selective, taking out most plankton, some benthic groups, including algae, rugose corals, and fusulinids, it is hard to imagine a game with different players on the field to unfold in the same manner as what occurred 180,000-years previously.

1.2 Impact theory

Scientists as people are generally not portrayed as particularly trendy in the media, however their work is most certainly susceptible to the *mode de la jour*. Four years prior to the publication of Sepkoski's diversity curve of marine fauna in the Phanerozoic, the first publication suggesting a meteor impact as possible cause for the Cretaceous-–Paleogene (K–Pg) mass extinction rolled off the presses (Alvarez et al 1980). This inevitably led researchers to seek an extraterrestrial explanation for the end Permian crisis as well (*e.g.* Becker et al. 2004)

The fact that Permian biotic crisis and the Cretaceous–Paleogene (K–Pg) extinction event are different on many levels such as severity, duration, recovery etc., is widely agreed upon. However, studying the K–Pg boundary does demonstrate what an impact boundary would or could look like; a fast-acting medium with synchronous global aftereffect. This medium would leave recoverably traces in the form of stratum containing iridium-rich clay, shocked quarts and/or fullerenes (spherical fullerenes are colloquially known as "buckyballs"). While not all meteorites contain equally large quantities of iridium, at least 86% of the ones the hit Earth (chondrites) contain on average around 330 ppb iridium whereas the Earth's crust only contains 2 ppb (Ehmann and Baedecker 2015).

The Earth is constantly pelted with meteorites from outer space. Most burn up in the atmosphere - some make it to the Earth's surface. Meteorites are reduced in size as they are plasmatized in the atmosphere, and because they are more likely to hit water than not, these meteorites often leave little to no trace. And it is only if the erosional processes left the visible scar intact, that we can find these impact craters. Therein lies the crucial point; no crater of the correct age and size has been found. There are claims of an impact feature in northwestern Australia, the Bedout structure, but uncertainty regarding the age, the lack of a spherule layer, and the lack of tsunamite has few scientists convinced (Wignall et al. 2004; Kerr 2004; Renne et al. 2004).

Another indicator of an impact by a chondrite or Ca-poor achondrite type meteorite would be an iridium-rich layer, as found at the K-Pg boundary. Again, as with the impact structure, some claim to have found just such layer in China, but a different group of researchers found no quantities of iridium that could not be explained by regular accumulation over time (Dao-Yi et al. 1985). Ever since the impact theory was coined, people have been looking for iridium-rich layers. From Hungary to China, and from Australia to Japan, no evidence of K-Pg-like iridium spike has been found (Zajzon et al. 2012). Fullerenes collected from lower Triassic layer in Gifu, central Japan were analyzed for their iridium content. However, these fullerenes also contained little to no iridium, in the order of parts per billion, versus parts per million as found in the K-Pg boundary layer (Yabushita and Kawakami 2007). Another theory that has been put forward is that perhaps the bolide was too small to leave an observable impact crater and

may not have been the ultimate cause of the extinction, but perhaps an impact at the right location may have triggered another event: massive volcanism. This will be discussed in the next paragraph.

1.3 Volcanism (UV and CO_2)

The Siberian Traps, the most voluminous flood basalt provinces on Earth, are found in the middle of modern-day northern Russia. The traps cover a vast area, about the combined size of the US states of Texas, New Mexico, Utah, Nevada and California (~2000,000 km2) and enough volume to cover the entire state of Texas in a layer of roughly 4 kilometer (Saunders and Reichow 2009). The traps were probably even more extensive at one point, but due to erosion and burial it is impossible to determine its exact dimensions. The lava is very thick in places, with the maximum thickness estimated at 6,500m. High precision $^{40}Ar/^{39}Ar$ and U/Pb dating put the traps right around 251.7 ± 0.4 to 251.1 ± 0.3 Ma, which makes this large igneous province (LIP) of the right age (Kamo et al. 2003). When describing large igneous provinces, like the Siberian Traps, they are often depicted as slow but steady oozing lava. While this may be accurate for part of the deposits—they are flood basalts—kimberlite pipes in Kazakhstan are evidence for the more explosive type of volcano as well (Kravchinsky et al. 2002).

The type of volcano and/or lava is not all that important; more important are the gasses that were released by the volcanic activity: not only the gases that were spewed out directly by the volcanos, but also the compounds that were released indirectly as the magma penetrated thick layers of organic- and halogen-rich Neoproterozoic and Palaeozoic sediments (Polozov et al. 2016). The first process pumps large quantities of one of the main offenders (CO_2) into the atmosphere, the latter frees halogens that ended up destroying (part of) the Earth's protective ozone layer. As the time the volcanism commenced, the atmospheric CO_2-levels were already rising, as is evidenced decreased leaf stomatal density and carbonates found in palaeosols (Mora et al. 1996). The amalgamation of the continents into the supercontinent of Pangea increased continentality, which reduced the overall amount of precipitation, which in turn impeded Earth's slow but highly effective carbonate-silicate geochemical cycle. This, in combination with subduction related volcanism--which is always associated with high CO_2 release--along the northern edge of the supercontinent, caused the global CO_2 levels to rise to an estimated 2800 ppmv, compared to 403 ppmv today (September 2017) ("Earth's CO_2 Home Page" n.d.). Even at those high levels, CO_2 does not have much of a direct on life. For reference, the CO_2-level of the air on board the International Space Station varies somewhere between 3000-7000 ppm (Massa et al. 2016). The indirect effects of such high CO_2-levels include an increased greenhouse effect and ocean acidification, leading to higher global temperatures and thereby altering the global climate, ocean circulation patterns and sea level among other things (Goddéris et al. 2014). These processes obviously greatly affect life on the planet. Jurikova et al (2017) used boron isotopes from brachiopods to assess ocean acidification levels in

the Paleo-Tethys. Different ratios of boron species are incorporated into biogenic calcium carbonate, which can be used to reconstruct ancient seawater pH. Their results show that ocean acidification appears to be widespread during the End Permian.

Small quantities of certain halogens like fluorine are essential for human health. However, in the atmosphere these long-lived molecules are highly efficient at breaking down ozone, which leaves life on Earth exposed to UV radiation. While UV-A is not entirely harmless as it can also cause skin cancer, it is UV-B that causes damage at the molecular level. UV-B radiation is readily absorbed by DNA, which can lead to irreparable modifications of the genome. This disrupts cellular metabolism as gene transcription and DNA replication are blocked (Jansen et al. 1998). Through this mechanism, UV-B radiation not only affects the health of living organisms, it also has the ability of influence the next generations, particularly in plants as their gametes tend to be more exposed to the environment. UV-B radiation results in malformation of pollen grains, and experimental work by Benca et al. (2018) has demonstrated that early abortion of ovulate cones in conifers may have greatly influenced the overall reproductive health and resilience of the vegetation to environmental perturbations.

1.4 Methane clathrate hydrate (incl. sea level and temperature change)

The weaker bonds of lighter isotopes are energetically favorable and are more easily broken than those of heavier isotopes during biotic and abiotic reactions (Dawson and Brooks 2001). Shifts in ratios between heavier and lighter isotopes can therefore be indicative of environmental perturbations. When the lighter ^{12}C is released from its biotic reservoir, the $\delta^{13}C$ signal drops. The Siberian Traps in all likelihood did not release enough light carbon to create the $\delta^{13}Ccarb$ excursion found in the fossil record. Research has therefore been focused on other likely sources of relatively light carbon (^{12}C). Methane clathrate hydrate form vast reservoirs of this relatively light carbon. They form under high pressure at great depths where organic material decomposes anaerobically. Because they have a biogenic origin, the composition is light as biological processes favor ^{12}C over ^{13}C. The clathrates will remain stable, as long as the water stays below a certain threshold temperature. But as the global temperatures were rising towards the end of the Permian, and these methane hydrates like became unstable, the icy matrix of the clathrate melts, releasing large quantities of methane into the atmosphere. This also explains the jaggedness of the negative $\delta^{13}C$ excursion (Korte and Kozur 2010). Methane being a potent greenhouse gas, creates a positive feedback loop where the release of the gas, will increase the amount of gas being freed.

The melting of the clathrates can hardly be viewed without taking other changes in the marine realm into account. With the polar icecaps from the beginning of the period long gone, it seems counterintuitive to have a eustatic low (Haq and Schutter 2008). However, factors such as continental aggregation, oceanic area, sedimentation, mantle convection, superplumes, large igneous province

emplacement, and ice volume all greatly influence the global sea level (Müller et al. 2008). Newly formed oceanic floor at mid-ocean ridges sinks into the Earth's mantle as it cools. If the seafloor spreading is relatively fast, there is relatively little time for the newly formed floor to sink back into the mantle. If the spreading is slow and the floor has time to slowly sink into the Earth's mantle, it causes the whole oceanic floor to drop because the sinking process drags the whole slab down. This increases the global ocean basin depth and thus lowering sea-level. The speed of the spreading of the crust is determined by mantle convection. Evidence for mid-ocean ridges, their position, the speed at which they spread etc. is based on magnetic anomalies. As the ocean floor is constantly being subducted and almost the entire ocean floor is 200Mya or younger, the Permian – Triassic ocean floor can only be modeled.

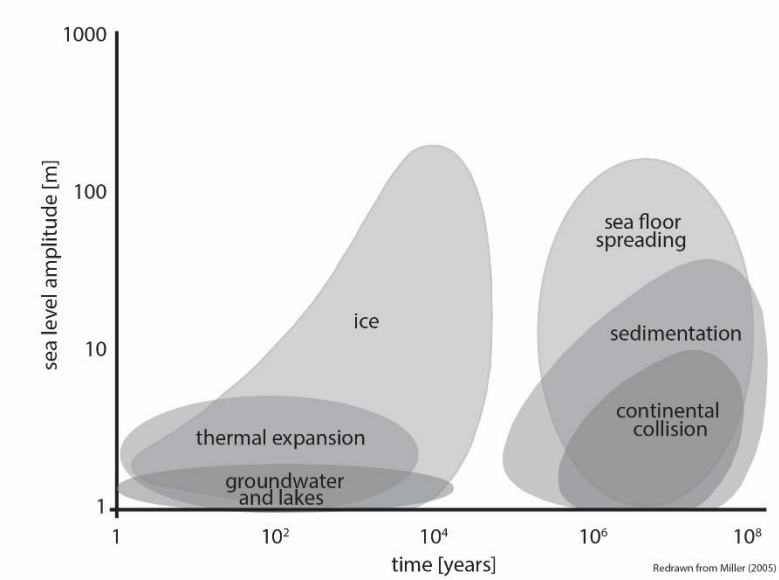

Fig 2. *Amount of years it takes various sources to change sea level. Redrawn from Miller (2005)*

Miller et al. (2005) collected data on the various processes that can influence fluctuations in global sea level and the timescale at which these processes can operate (Fig. 2). E.g. thermal expansion of water can occur relatively quickly, but it can only account for 6-7 meter sea level rise. The accumulation and or melting of ice can also happen in 10,000 years or less but can change the sea level by roughly 120 meters. Based on their estimates and considering the rate and magnitude of sea level rise towards the end of the Permian can best be explained by a change in seafloor spreading, continental collision and the building of mountains and the subsequent erosion and ensuing sedimentation.

The continental aggregation also meant that underneath the supercontinent heat could build up as the result of continental insulation. A building plume underneath a plate can lead to isostatic lift, which results in sea level drop. Continental insulation can also explain the formation of the aforementioned

Siberian Traps as well as the inevitable break-up of the supercontinents in general and Pangea in this particular case.

1.5 Oceanic anoxia and hypercapnia

Looking at the marine fossil record and specifically at the families that survive the end-Permian biotic crisis it becomes evident that the crisis was highly selective. Genera and families of organisms did not go randomly extinct: there is a clear link between the physiology of the organism and its chance surviving the biotic crisis (Knoll et al. 2007). Organisms categorized by characters such as low metabolic rate, limited or no circulatory system, and limited respiratory surfaces were hit particularly hard (Knoll et al. 1996). About 81% of the genera that fell into that category disappeared, while the organisms that did not only suffered about a 38% reduction. This selectivity, combined with other proxies such as $\delta^{13}C$ signals from marine carbonates and pedogenic carbonates, and plant stomatal density allows for a better understanding of the environmental conditions that precipitated the biotic crisis (*e.g.* Retallack 2001; Payne et al. 2007).

While whole-ocean anoxia has been disproven, there are clear indicators such as pyrite abundance and $\delta^{13}C$ signal suggest local anoxia, hypercapnia (physiological effects of elevated PCO_2), acidification, toxic sulfide and an overall shift towards a more reducing marine environment (Cui and Kump 2014; Algeo et al. 2010; Knoll et al. 2007).

With the rising global temperatures and increasing CO_2 levels towards the end of the Permian, oxygen levels in the ocean dropped and relative carbon dioxide levels rose. Higher water temperatures also lead to increased stratification and stagnation of global ocean circulation (Kiehl and Shields 2005). Modeling the combination of a stagnate ocean and warm high latitude surface air temperature shows that there was a shift in the later Paleozoic atmospheric circulation which led to an increasingly arid interior whole the coasts experienced seasonality (Tabor and Montañez 2002).

1.6 Other (under-explored) mechanisms

Another source of methane put was forward by Rothman et al (2014). They suggested that as a result of the influx of nickel into the oceans from the Siberian Traps, methanogens that were previously limited by the amount of available nickel, now flourished and developed news pathways that enabled them to efficiently convert marine organic carbon into methane (Rothman et al. 2014).

In water with a stable thermocline, oxygen levels at the bottom drop as bacteria decompose organic matter. If there is little to no mixing, sulfate reducing bacteria can produce H_2S in these anoxic waters. H_2S, which can build up in stratified waters to be released in one fell swoop into the atmosphere, has been suggested to decrease the amount of ozone in the stratosphere (Kump et al. 2005) . However, while Kaiho and Koga (2013) do not disagree the release of the H_2S itself, their calculations suggest that

the hydrogen sulfide is oxidized at a relatively high rate which would result in a very limited effect on stratospheric O_3 and therefore would not lead to an increase in UV-radiation levels near the surface (Kaiho and Koga 2013). Of course elements that cause acid rain, sulfur, and to a lesser extent nitrogen, are expected to have an effect on the ecosystem as the acid rain leaches the base cations out of the soil which are therefore lost to the vegetation. While ecosystems can recover from acidification, studies done on modern ecosystems show that this is a very slow process (Likens et al. 1996). Based on a study by Black et al. (2013), who modeled global patterns of acid rain as a result of the Siberian Traps, particularly the northern hemisphere would have experienced acidic precipitation. In that regard, it is important to remember that most of our knowledge of the fossil record comes from the northern hemisphere. This is the largely the legacy of the historical collection bias. Many older paleontological studies were carried out and written up by north-western Europeans. While researchers are working hard to resolve the discrepancy between the northern and southern hemisphere, the fact remains that the fossils records is skewed (DiMichele et al. 2008).

1.7 Conclusion: Lethal Synergy

The end-Permian biotic crisis currently cannot be seen nor explained as one single event with one single cause. Multiple systems failures, that co-occur with the onset of the lava flows and associated gas release of the Siberian Traps, may well have had a cascading downstream effect that culminated in the massive biotic crisis. The amalgamation the continents led to a change in ocean circulation which changed the global climate. While global average temperatures were higher than in the preceding period, the weathering of silicate rocks was reduced. Orogenesis that exposes unweathered rock slowed and precipitation needed for the chemical weathering was reduced by increased continentality. Reduced precipitation also limited terrestrial primary productivity. Carbon dioxide was now not only released by volcanism, it was also less readily recycled, reused and fixed. Increased CO_2 levels raised global temperatures, caused ocean acidification and oceanic anoxia. Anoxia led to the production of hydrogen sulfide which, together with the halogens released from the salt layers in Siberia, damaged the Earth's protective ozone layer, affecting the fitness of flora and fauna in the marine as well as the terrestrial realm.

PART 2 : To expect the expected – or is the Permian-Triassic (and Jurassic) plant fossil record likely to hold surprises?

2.1 Factors feeding into the (plant) fossil record

Part 1 of this this chapter not only to sketches the background of all the environmental factors in play during the end-Permian biotic crisis, but also serve to set the stage for the questions addressed in the next chapters. Most of the fossil data used in studying the end-Permian crisis is from the marine realm, but what do we know about what precipitated on land and specifically to the plants on land? While there is an unavoidable taphanomic overprint where climate zones shifted altering the preservation potential, it appears that ecosystems previously dominated by sphenopsids and glossopterids are now mainly occupied by peltasperms, ginkgophytes and cycdophytes (Rees 2002; Looy et al. 2014). Both in Northern China and in Euramerica groups such as gigantopterids and sphenopsids disappeared or declined in abundance while others such as ginkgophytes and particularly conifers increased. The apparent absence of (local) vegetation therefore seems more a results of turn-over rather than a worldwide die-off of vegetation (Retallack et al. 1996; Rees 2002). With the plant fossil record being relatively sparse as it is, the question I will address in this part of the chapter is: based on the information available from the largest paleo database, how bad is the plant fossil record really or, ***Is the Permian-Triassic plant fossil record likely to hold surprises?***

Irrespective of the ultimate cause of the end-Permian biotic crisis, the effect on life on Earth was profound as is evidenced by the fossil record. The result of the severe environmental disturbance is particularly well-recorded in marine sediments, where the fossil records tend to be more continuous, better preserved, relatively less prone to erosion and probably most important of all; the organisms that preserve well, tend to do so in great numbers. On land, the fossil record often has a much lower resolution regarding both time and (preserved) diversity. This is particularly pertinent to the situation in the Permian and the Triassic, when the world climate shifted from an ice house world to a hot house world. This hotter and drier environment is much less favorable for the preservation of fossils. That is not to say there are simply fewer organisms to fossilize per se, but that the chance of an organism living, dying, and then preserving in a generally hotter and drier world is much slimmer (Looy et al. 2014).

In the Permian, Gondwana and Laurasia merged to form the enormous supercontinent Pangaea. Where the plates collided, the Central Pangaean Mountain Range formed, creating a physical barrier between the southern and northern half of Pangaea. The increased continentality of the mega continent caused a rapid shift in the Permian towards drier conditions with significant drop in annual rainfall: an

estimated decrease of 800 mm/yr (Watson 1992). This shift took place relatively quickly and had an enormous impact on the vegetation and its preservation (Looy et al. 2014). Not only altered oceanic current and decreased precipitation but also an increased evapotranspiration as a result of rising temperatures, lead to an even greater change in water availability (Barron 1981). With a mountain range across central equatorial Pangaea and deserts flanking both sides, plants were forced to adapt and/or migrate. The hot and dry conditions pushed the vegetation towards the poles. These poles, which now formed so-called refugia, had been covered with icecaps during the Carboniferous, but had melted under the hot conditions of the Permian (Burgoyne et al. 2005). The biodiversity hotspots are thought to have shifted away from the equatorial region and sought refuge in more temperate regions. This shift poleward might have positively influenced the rate of diversification as plants explored new habitats and competed over limited resources.

Fossils offer information about past biodiversity, species origination and extinction and past climate. As the current climate is changing rapidly, the search for potential precedents and patterns is invaluable. Since the discovery of the Rhynie Chert in the early 1900s people have purposefully been collecting, studying and describing plant fossils in the hopes of expanding the knowledge about plant evolution and life on earth in general. Even though the plant fossil record around the end-Permian Biotic Crisis is sparse, it is evident that there was no mass extinction in the floral realm. In fact, none of the plant groups went extinct. There was a clear shift in the makeup of the vegetation, or turnover, but the overall diversity was hardly impacted (Knoll 1984; Willis and McElwain 2002). The changing climate spurred plant lineages to alter their *modus operandi* or rather their *modus vivendi*. Having a reproductive cycle be independent or less dependent on water availability, was advantageous. Seeds plants dominated the world flora during the Permian: the already in place Cordaitales and pteridosperms further diversified while new groups of Cycadales, Ginkgoales, Bennettitales and Glossopteridaceae emerged. Most sources seem to agree that the genus of Cordaitales does go extinct at the end of the Permian, some sources argue that it persists into the Triassic (Seward 2011).

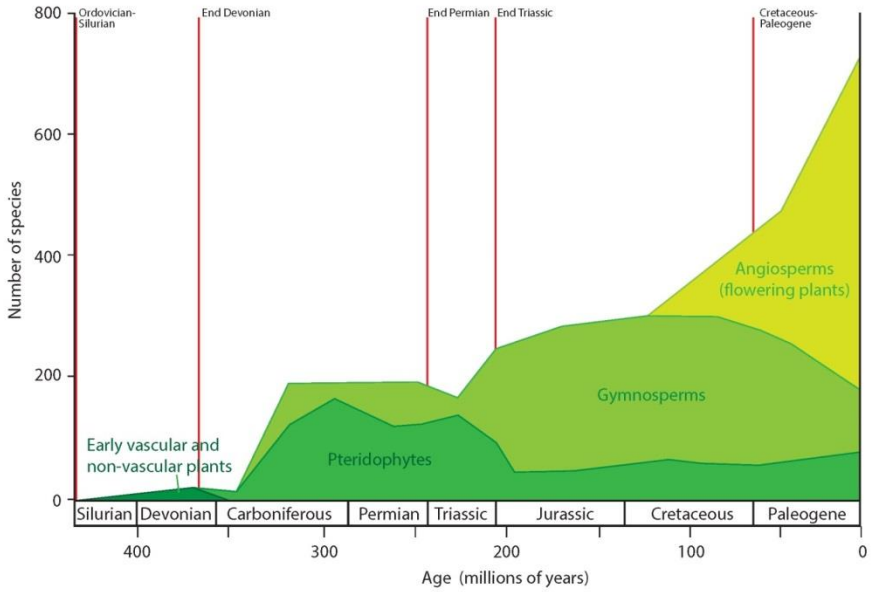

Fig. 3. *Plant diversity in the Phanerozoic, with five mass extinctions. Redrawn from Niklas et al.(1983)*

Regardless of the precise timing of the disappearance the Cordaitales, the fact remains that plants are much less affected by the end-Permian crisis. This can partially be explained by certain characteristics that only plant possess, such as simple "dietary requirements" (water, light, CO_2 and nutrients), resistant propagules, resilience to mechanical and in some cases chemical and even radiation damage, asexual reproduction (stolons or runners), and genetic flexibility (hybridizations, polyploidy and selfing) (Traverse 1988).

Even though most plants families seem to survive the end-Permian Biotic Crisis unscathed, with the terrestrial plant fossil record being as scant as it is, the question remains: does the fossil record provide us with enough and reliable enough data to make sound inferences? What are the chances that we grossly undersampled a time interval? To clarify, I will not be looking at the absolute diversity, but a relative measure of diversity based on data from the Paleobiology Database, supplemented with data from two literature searches. This data is not adjusted or corrected for the total rock surface area of a specific age, which does differ per period/epoch, but only marginally (see Fig. 4).

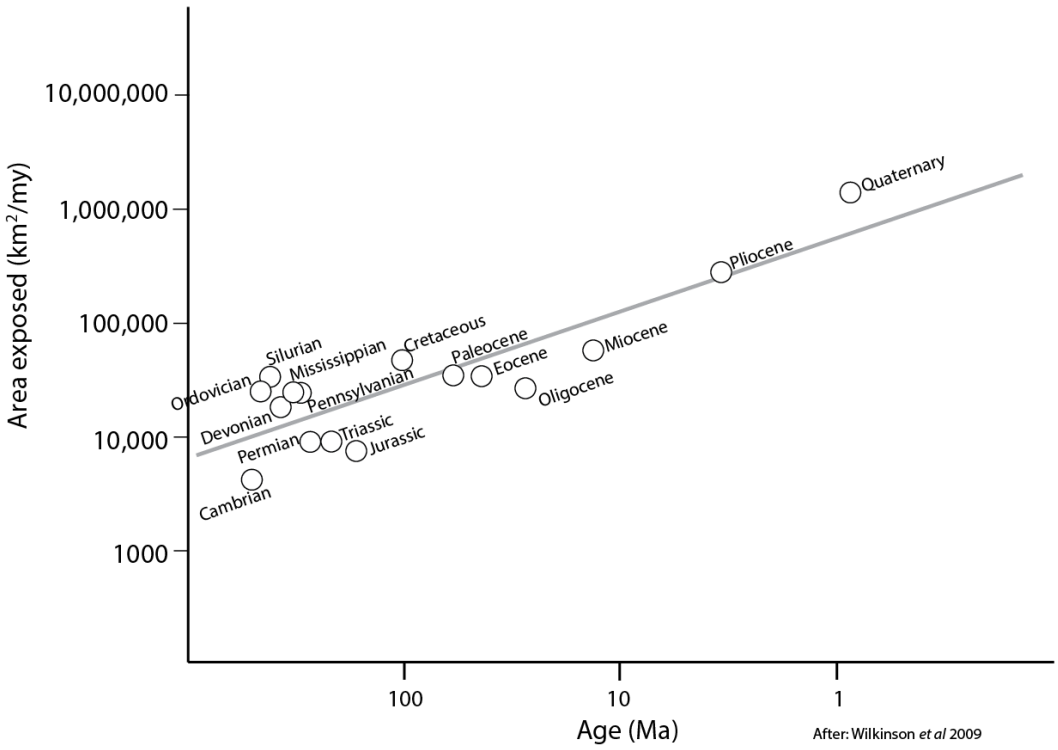

Fig 4. *Ages and areas of geologic map units exposed in North America for Phanerozoic periods and epochs (after Wilkinson et al. 2009 and Gilluly 1969).*

There is obvious sampling bias in most fossil collections. Reasons for sample bias include (but are not limited to): predilection for specific charismatic specimens aka "taxonomic favoritism"; differences in recovery effort; differences in fossilization potential; conditions needed for fossilization are relatively rare and certainly not randomly spaced; and differential exposure and exploration of fossil-bearing rocks. The number of species recovered from a locality also depends on the number of individuals sampled: the more samples you collect, the more species you will find—up to a point, particularly in a heterogeneous assemblage (high α-diversity). When sufficient samples have been collected and identified, the recorded diversity should reach an asymptote. Raw species richness is only meaningful when sampling is intensive enough for the asymptote to be reached; even then, because the fossil record is hopelessly incomplete, we cannot calculate 'true' diversity (Alroy 2003).

Diversity studies have only relatively recently begun to take into account sampling bias in quantitative ways (Miller 2000; Miller and Foote 1996; Jackson and Johnson 2001), particularly for studies of fossil plant diversity. The biases are both spatial and temporal. The position of a sample site of Permian strata and a sample taken from Jurassic rocks at the exact same modern-day location may in fact represent vastly different paleolatitudes, up to 25 degrees difference as a result of plate tectonics (Rees et al. 2002). These are important considerations because the massive shift of most continents northwards of

about 25º during the end-Paleozoic and the early Mesozoic, which also covers the Permian-Triassic boundary (PTb), now not only means a variable in time, but also in place.

To visualize plant diversity through time and space I analyzed data retrieved from the Paleobiology Database. I used rarefaction to correct for the effect of sample size on diversity (Krug and Patzkowsky 2007) and an empirical mathematical formula to approximate the resulting rarefaction curve and estimate the position of the asymptote thereby estimating the total species diversity. Rarefaction also corrects for differing area of outcrops per interval, as it correlates with number of localities However, it does not take into account the number of areas, which in itself affects the diversity counts, because more area, samples more different habitats (Barnosky et al. 2005).

This study aims to get a handle on whether the current findings—that are in the Paleobiology Database—are sufficient to make reliable estimates about the relative diversity and whether new findings will upset the status-quo. This information is based on the data that is currently available and accessible.

2.2 Methods

2.2.1 Data

I have used two data sources. The bulk of the data was retrieved from the Paleobiology Database in July 2017. Additional data was collected in two separate literature studies. One was done by Rodney Owen as part of his undergraduate research apprenticeship and another by Robin van der Ploeg as part of his master thesis work. The starting point of both their studies was a file of the original Rees data from 2002, which at that point was only partially uploaded to the Paleobiology Database. Owen and Van der Ploeg focused on cleaning the data by correcting erroneous age data, updating and correcting botanical affinities and—if applicable—adding plant organ information. They focused on finding plant fossil data not yet in the Paleobiology Database of Permian and Triassic age respectively.

Figure 5 shows the distribution of samples and genera per time bin of the data retrieved from the Paleobiology Database (in red) and the additional data that was found during the two literature studies. These studies focused exclusively on Permian and Jurassic material, hence the clear lack of extra data for the interval of 199 Ma and younger.

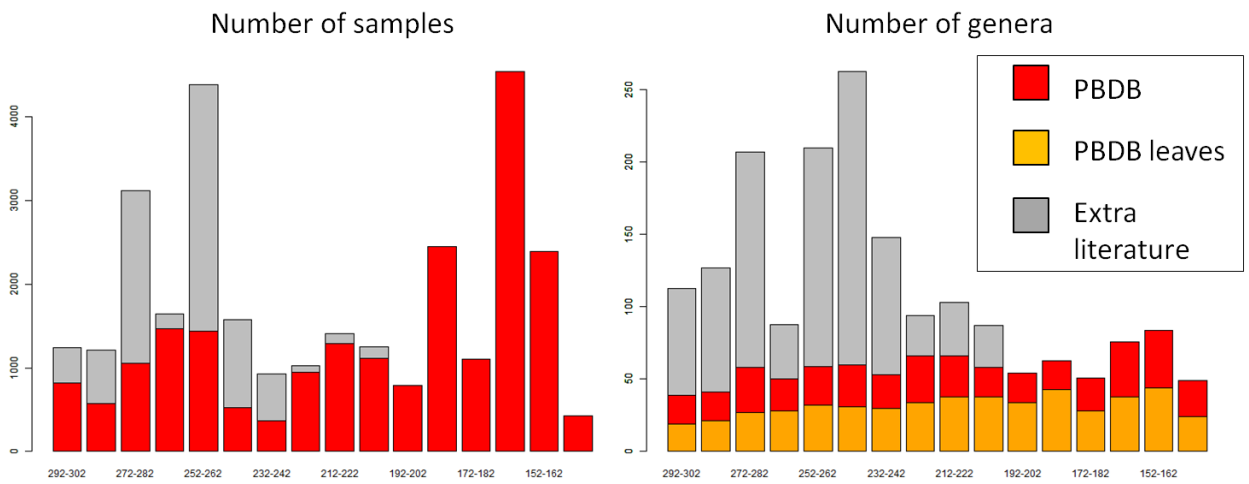

Fig 5. *The number of samples and genera compiled from the Paleobiology Database, with leaf data parsed out, and the extra data that was obtained through two separate literature studies.*

The plant data retrieved from the Paleobiology Database included all plant organs and the composite geographic range between 299 Mya and 145 Mya. The data was cleaned for ortographic errors, renamed taxa and minor inconsistencies such as switching family suffix with an order suffix and vice versa. For some of the analysis the data was split up in 10Mya time bins, which roughly corresponds with 5 intervals per period or otherwise corrected for variable epoch length is these periods. Depending on the type of analysis, splitting up the periods by epoch may lead to a skewed interpretation as some epochs cover significantly more time than others. For example, the Late Triassic is almost 7 times longer than the Early Triassic, all other things being equal, which would theoretically lead to an overinflated diversity estimate that cannot be readily compared to a shorter interval. Additionally, we know all things are not equal, and we must therefore rely on assembling and analyzing large numbers of locality-specific biotic inventories such as the data compiled in the Paleobiology Database (Alroy et al. 2001).

The dataset was retrieved from the PBDB contains a large number of non-leaf plant organ data, including fossil spores and pollen. Fossil plant remains are often found disarticulated; complete specimens, from root to shoot with reproductive structures are very rare. Plant classification systematics are based on shared features. As a result it may be possible for two fossils, of two different parts of the same plant, to have two different and apparently unrelated names. Because it is impossible to establish a measure for false diversity caused by paleobotanical taxonomy, in some case I limited the analysis to the use of fossil leaf data only. Figure 6 shows the discrepancy that arises from using all the plant entries in the database versus only the fossil leaf data. To make the leaf data visually comparable to the combined data, I had to decrease the y-axis tenfold. While the overall trend seems to hold a noticeable discrepancy

in the 282-272 bin can be explained by the additional data that was acquired during the two literature studies.

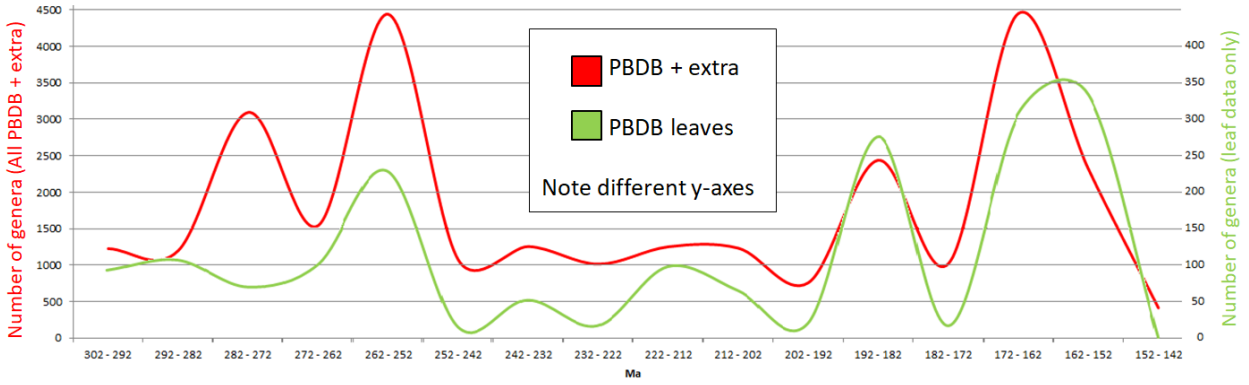

***Fig 6**. Leaf data versus all plant records.*

2.2.2 Rarefaction and diversity estimation

Rarefaction is a mathematical approach to determine the relationship between diversity and sampling intensity in order to predict the expected diversity for smaller sample sizes (Raup 1976). The rarefaction curve shows whether the diversity has reached the asymptote, given the number of samples available. Therefore I fitted an analytical approximation through the rarefaction curves to determine the position of the asymptote. The approximated diversity (f) is determined by the sample size (n), the asymptotical diversity (d), the range (r) at which the observed diversity equals half the asymptotical diversity and an empirical parameter (p) controlling the parameter (p) controlling the curvature of the function.

$$f(n) = d\left(\frac{(n/r)^p}{1 + (n/r)^p}\right)$$

The parameters (d, r and p) were fitted using a least squares objective function (O) with R the rarefaction curve and f the analytical approximation.

$$O = \sum_{i=1}^{n} \frac{(f_i - R_i)^2}{n}$$

The results of the fitting procedure were expressed as the residual error (objective function), the correlation coefficient between the rarefaction curve and the analytical approximation and the sampled diversity, being the observed diversity as a fraction of the asymptotical diversity. The rarefaction was performed using the rarefaction function written by Jacobs which is available through her website (Jacobs

2008). The rarefaction as well as the curve fitting was done in R (R-3.4.2) and R-studio (RStudio Desktop 1.0.153).

The estimated values of this asymptote parameter were used to study the relative plant diversity across the globe during the different time intervals. Specifically, I studied the relative diversity through time, and whether the additional data that became available through the aforementioned literature studies changes the pattern.

2.3 Results

2.3.1 Data

Table 1 shows the total number of locations, number of individuals and the number of unique individuals as the raw data was retrieved from the Paleobiology Database and the additional data from the two literature studies.

Table 1. *Data from Paleobiology Database, plus the additional data from two literature studies.*

	Total number of sites	Total number of individuals	Total number of unique occurrences
All Plantae	2932	29,512	567
Leaf fossils only	1695	14,454	97
Percent decrease when using leaf fossils only	42%	51%	83%

2.3.2 Plate tectonics and sampling bias

Figure 7 illustrates the directional movement the sample sites underwent since deposition of the fossils based on the present-day coordinates and the paleo latitude and longitudes associated with the sample sites. If all the samples fell onto the one to one line it would mean that none of the sample sites had shifted between the deposition of the fossil and the time it was unearthed. However, there is an upward trend which corresponds with the northerly movement of the continents. Only very few locations have moved southward, primarily the result of the rotation of Laurasia (Dietz and Holden 1970). The outlier on the paleolatitude of 0º and modern latitude of -80º is almost certainly caused by missing or erroneous data entry in the database. We also observe a lacuna in the modern latitude sampling locations between 20º and -20º, which is the result of relative little landmass at this particular latitude, but also encompasses most the worlds' rainforests, which are for practical, historical and/or geopolitical reasons understudied, undersampled and/or underreported.

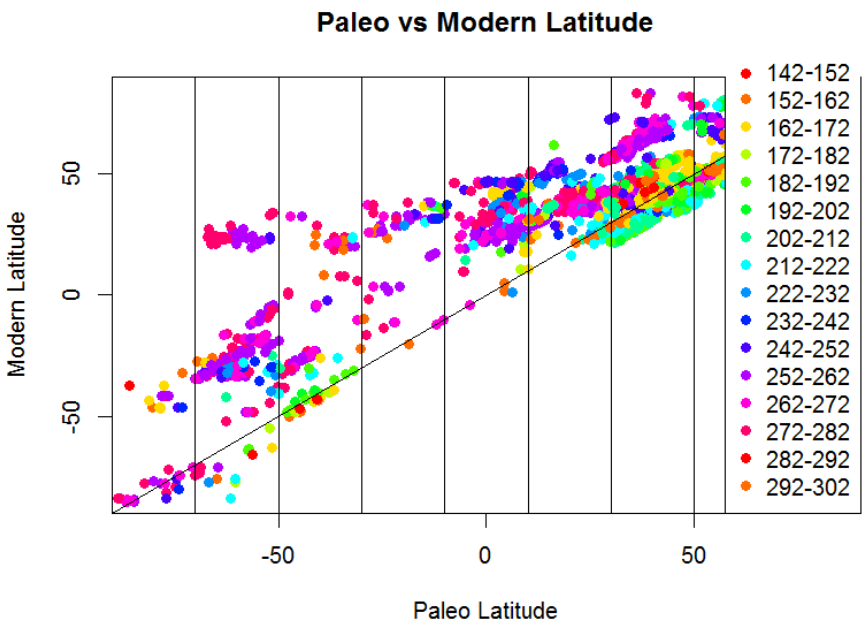

Fig 7*. The directional movement the sample sites since deposition.*

The high density of sampling locations in the modern latitudes between 20º and 60º is also—at least partly contributable to bias. Figure 8 shows the relative sample distribution where the total number is samples is divided by the size of the particular continents. We see that a relative high number of locations can be found in Europe and Asia, both of which are positioned for respectively 100% and 95% on the northern hemisphere. This is not only the result of actual sample bias regarding the physical sampling locations, but also the (original) language in which the report was written up, where and if it was published in (readily) accessible works and if those were then incorporated in the (various) databases.

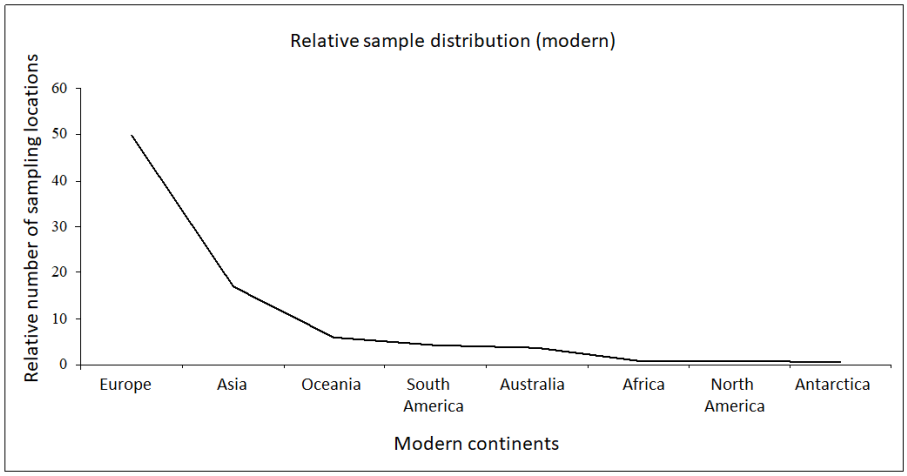

Fig 8. *The relative sample distribution where the total number is samples is divided by the size of the particular continents*

2.3.3 Origination and extinction

Figure 9 shows the total number of plant genera, the number of originations and extinctions and the survival rate from the beginning of the Permian until the end of the Jurassic based on PBDB data plus the extra data. Diagram A and C do not include singletons; diagram B and D do. This dampens the signal, but the peak at 252-242 and trough at 272-262 in diagrams A and B remains clear. The peak at 252-242 of originations and extinctions signals high turn-over and leads to the dip in the survival rate of the genera. C and D represent the survival of the different genera based on range-through, looking 3 bins ahead, hence the obvious drop towards the end the Jurassic where everything seemingly goes extinct, because that is the data ends not the genera.

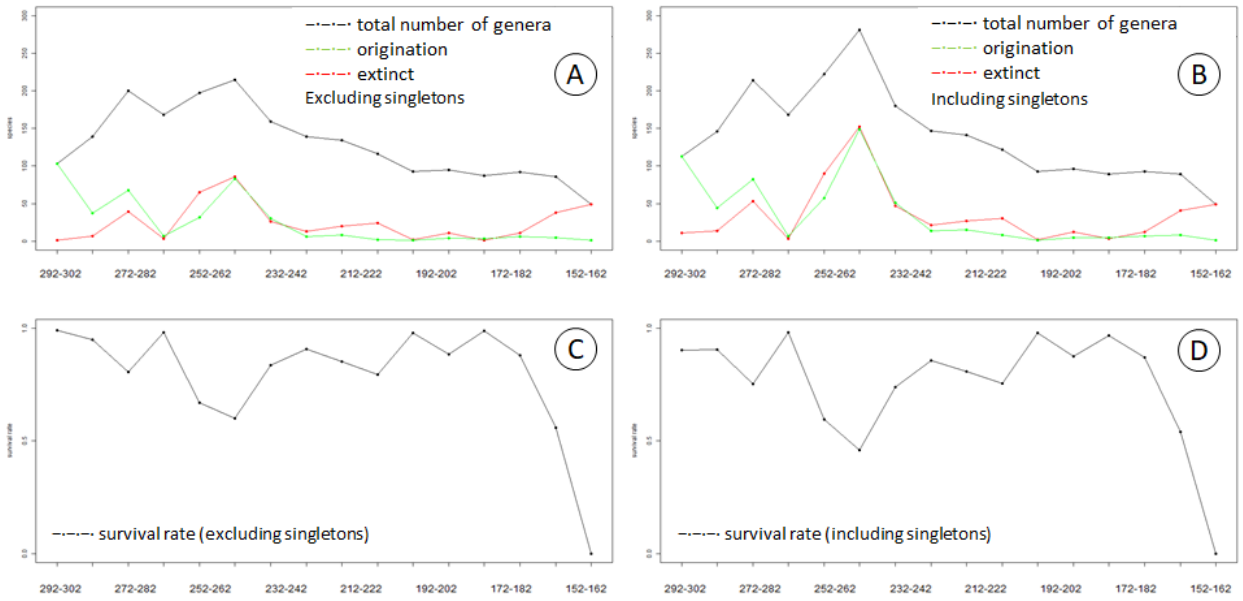

***Fig 9**. The total number of plant genera, the number of originations and extinctions and the survival rate from the beginning of the Permian until the end of the Jurassic.*

Figure 9 only provides a rough estimate of the diversity based on the number of genera appearing and disappearing from one time bin to the next. Figure 10 is another way of visualizing the same data, but it provides a better indication of the longevity of the various genera. For a more comprehensive interpretation of the data and diversity, I used a method by Alroy (2014) the results of which are in figure 11a and 11b.

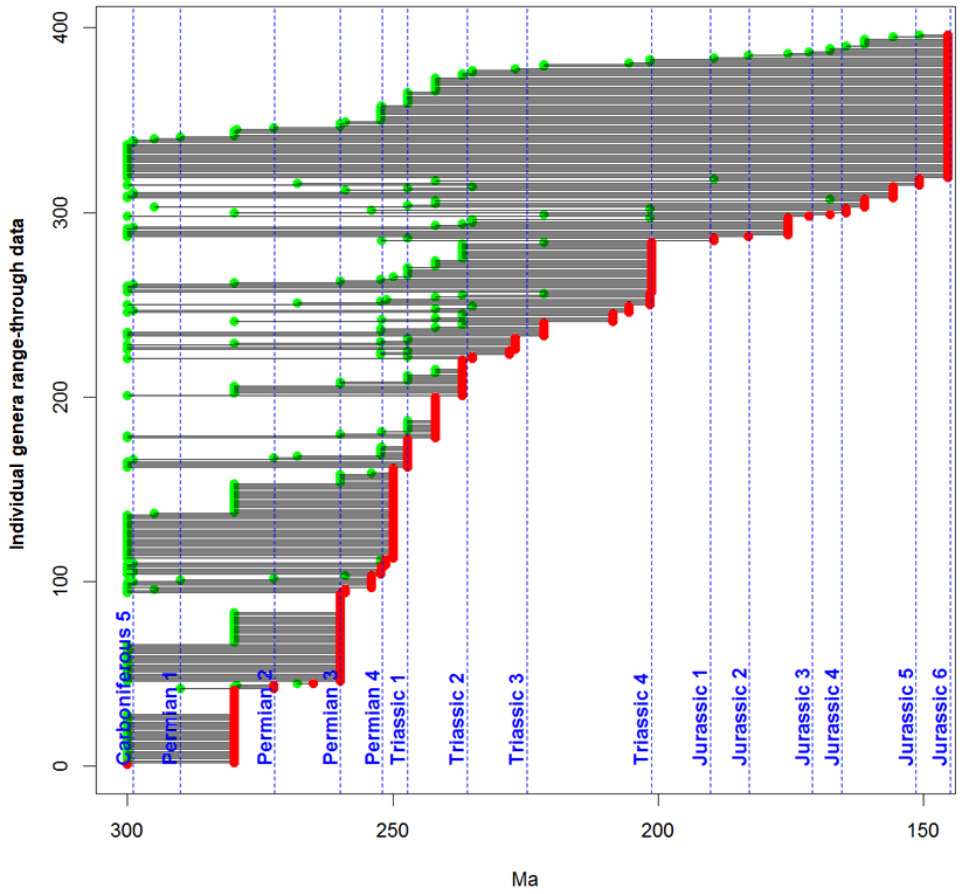

Fig 10. *Range-through data of the various plant genera from the beginning of the Permian until the end of the Jurassic. Excluding singletons. Green dots = origination. Red dots = extinction. The red dots at the end of Jurassic 6 may either be a true last occurrence, but more like the result of not looking to Cretaceous 1.*

Table 2. *Overview of period and epochs duration as used by Alroy.*

	Beginning in Ma	End in Ma	Duration in Ma
Jurassic 6	152.1	145.0	7.1
Jurassic 5	166.1	152.1	14.0
Jurassic 4	170.3	166.1	4.2
Jurassic 3	182.7	170.3	12.4
Jurassic 2	190.8	182.7	8.1
Jurassic 1	201.3	190.8	10.5
Triassic 4	227.0	201.3	25.7
Triassic 3	237.0	227.0	10.0
Triassic 2	247.2	237.0	10.2
Triassic 1	251.9	247.2	4.7
Permian 4	259.1	251.9	7.2
Permian 3	273.0	259.1	13.9
Permian 2	290.1	273.0	17.2
Permian 1	298.9	290.1	8.8

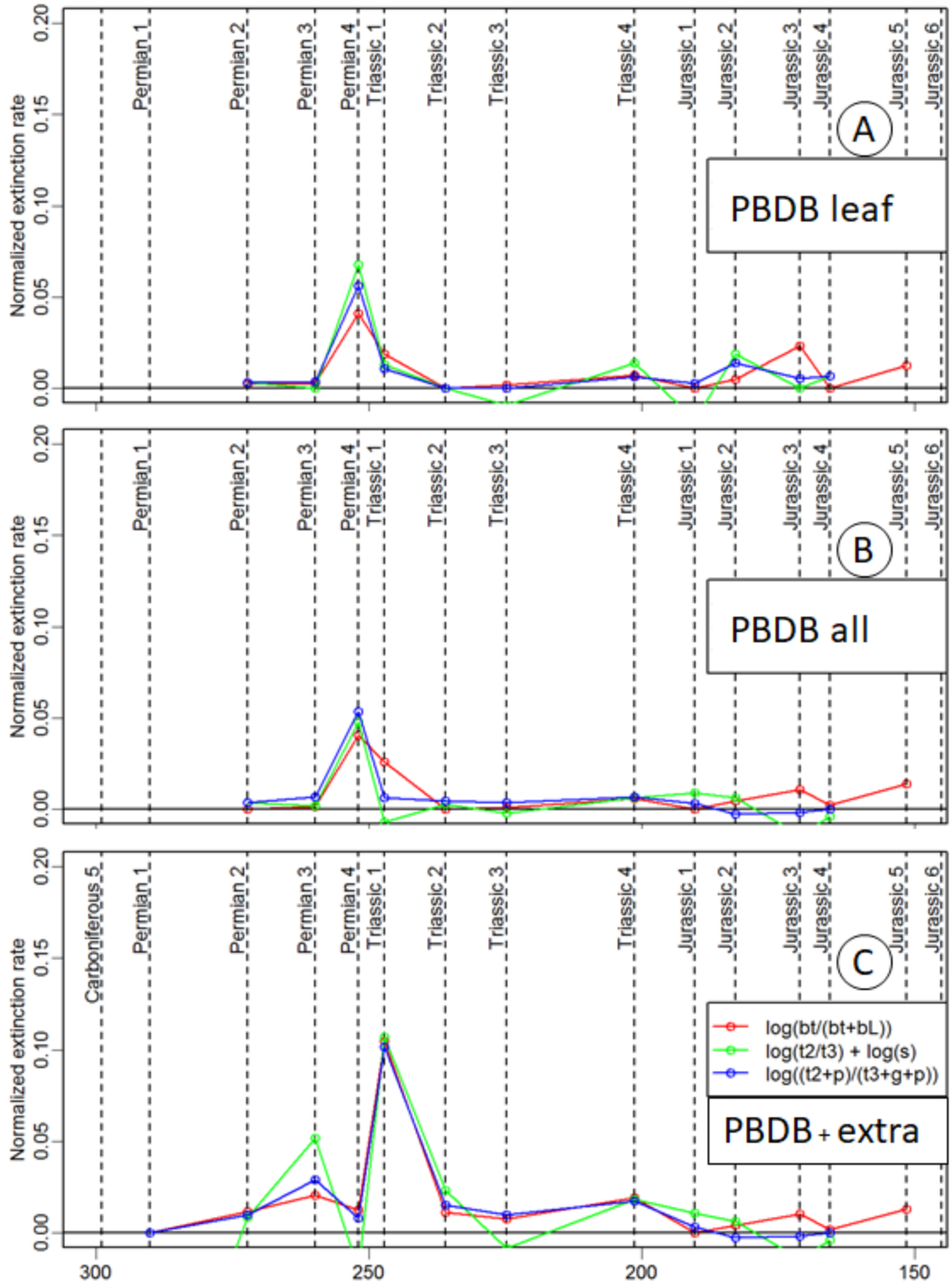

Fig 11. *Estimated extinction rates without singletons, corrected for epoch length using different equations based on Alroy (2014).*

All the lines in figure 11 show a measure of estimated extinction rate. The red line represents the difference between the origination and extinction rate of boundary crosser, corrected for the bin length. The green line is the so-called three-timer estimate which reflects boundary crossers, but focuses on a four-interval moving window as to include two successive time intervals and the genera are therefore extant at the boundary between them. The blue line uses "gap filler data" (Alroy 2014) which looks 2 bins forwards (ignoring 1 bin forward) and 1 bin back and is therefore better at assessing potential Lazarus taxa.

While there is some variation between the figure 11A and 11B, the pattern based on all the PBDB data or just the leaf data from PBDB, is comparable. A noticeable difference is while the leaf data and the PBDB data seem to hold the same trend, when including the extra data in the analysis, the different data sets do give a different estimate of the timing of the greatest extinction rate, shifting from Late Permian for both the PBDB data and the leaf data from PBDB to the Early Triassic with addition of the extra data. The extra data collected in the two literature studies showed that a portion of the genera previously deemed to be at the end of their respective ranges in the late Permian, in fact made it past the Permian-Triassic boundary. This is effect particularly important when considering data that is currently entered into the Paleobiology Database. While databases are unarguably imperative to collect, reposit and retrieve information, drawing conclusions solely based information in any particular database without considering its potential shortcomings, may lead to erroneous conclusions.

2.3.4 Rarefaction analysis

Under ideal rarefaction analysis conditions, the distribution of taxa within the studied area is even, all taxa are equally common (or rare) and all taxa had the same chance of becoming fossilized. Of course, in the real world these criteria are never met, which is among the reasons why these numbers cannot be translated into actual global or ɣ-diversity. One way to combat this inherent “sampling” error is by limiting the study area and focusing on local diversity or α-diversity as opposed to globally distributed samples (Rees 2002). However, obtaining an estimate of the global diversity is not the focus of this study.

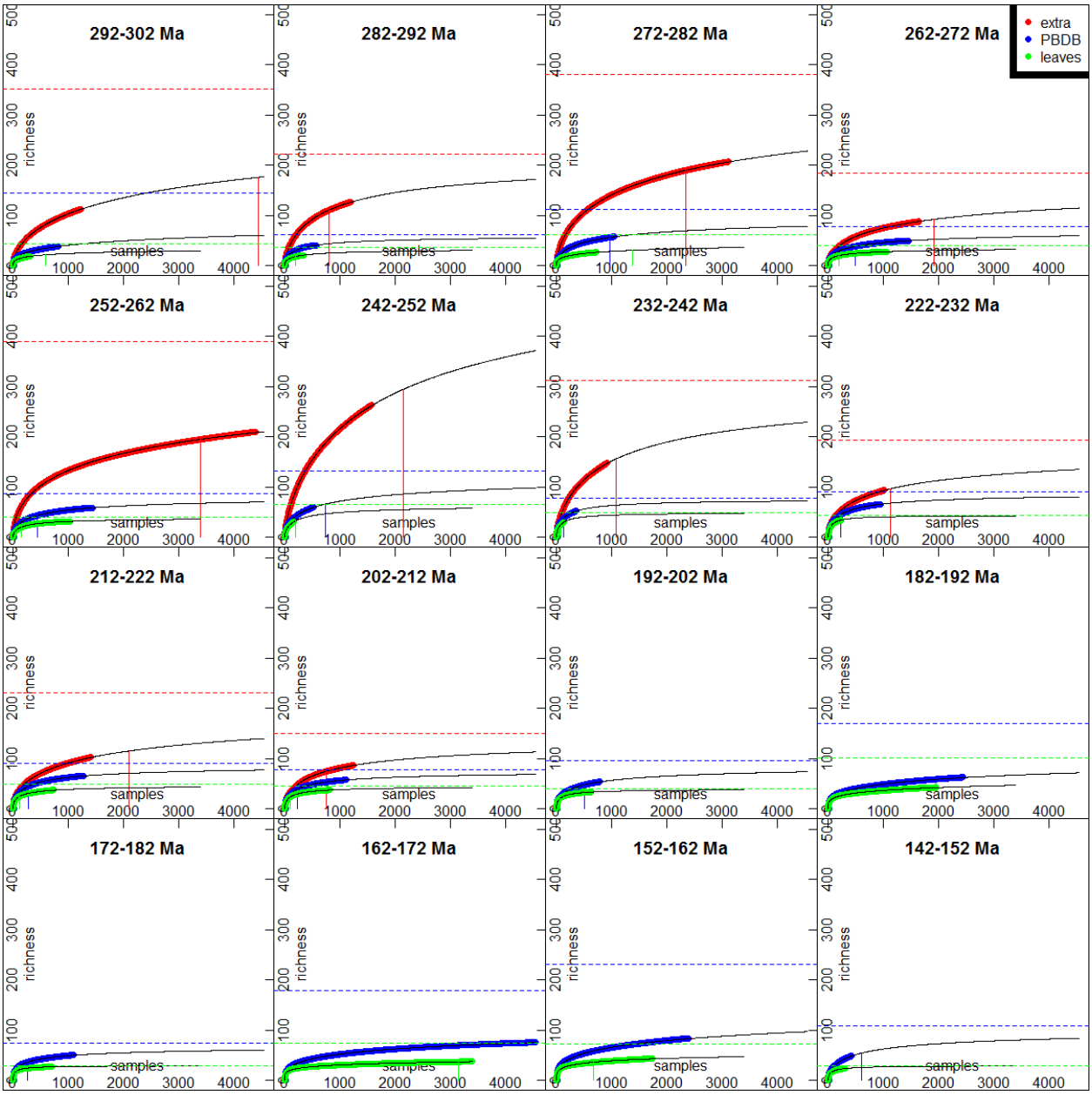

Fig 12a. *Rarefaction curves per 10MYA bins, from Permian through the end of the Jurassic. All data sets exclude singletons.*

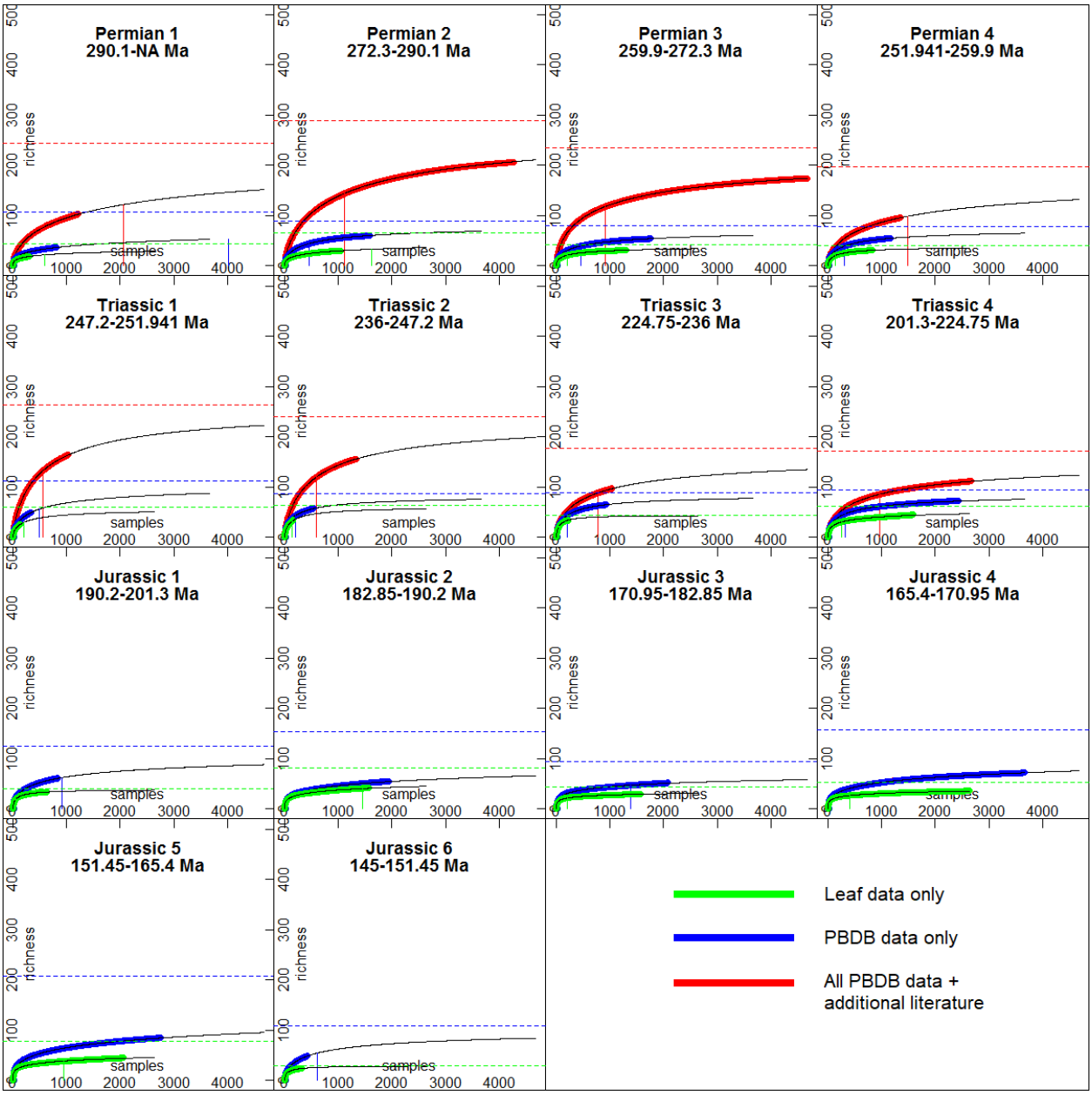

Fig 12b. *Rarefaction curves per epoch, from Permian through the end of the Jurassic, corrected for variable bin length. All data sets exclude singletons.*

Figure 12a shows 16 individual diagrams for each 10Ma time bin, from the beginning of the Permian through the end of the Jurassic. In each diagram the colored lines are the rarefaction curves based either the leaf fossils from the PBDB (green), all the PBDB data (blue) or the PBDB data plus the extra literature (red). The rarefaction curves were produced to estimate the maximum global relative diversity based on the fit through the rarefaction curve and the position of the asymptote. The asymptotes are reflected by the colored dotted horizontal lines.

Figure 12b shows the same data, but binned per epoch. Particularly when the ages of the specimens are unclear, either from unresolved ages of the strata or lack of resolution, they will—by default—end up in the middle of an epoch or period. If the data is then binned, it creates artificial data richness in the middle bins. This problem is particularly evident when looking at the 282-272 MYA bin in 12a and the Permian 2 bin in 12b. Both these bins contain the middle of the entire Permian period at around 275 Mya. Because the rarefaction curve and its asymptote in 12a is based on 10 MYA and the one in 12b on approximately 17.8 Mya, the relative diversity estimate falls from 380 to 290 genera, which is the result of data inflation around the period's midpoint.

Table 3. *The rarefaction parameters for rarefaction curve with most data and highest asymptotic diversity (see figure 12b)*

	diversity	range	power	residual	correlation	f_diversity	f_range
Permian1	244	2059	0.61	0.0262	1.0000	0.42	1.68
Permian2	288	1123	0.70	0.1826	1.0000	0.71	0.26
Permian3	235	911	0.64	0.1980	0.9999	0.74	0.19
Permian4	197	1490	0.61	0.0228	1.0000	0.49	1.10
Triassic1	264	557	0.79	0.0662	1.0000	0.62	0.54
Triassic2	241	600	0.76	0.0270	1.0000	0.65	0.45
Triassic3	177	776	0.65	0.0680	0.9999	0.55	0.75
Triassic4	171	959	0.61	0.0708	0.9999	0.65	0.36
Jurassic1	125	914	0.54	0.1742	0.9995	0.49	1.09
Jurassic2	153	10000	0.36	0.3661	0.9980	0.36	5.15
Jurassic3	95	1385	0.39	0.5482	0.9960	0.55	0.67
Jurassic4	158	5697	0.40	0.1414	0.9996	0.46	1.55
Jurassic5	208	7109	0.40	0.3525	0.9993	0.41	2.58
Jurassic6	109	612	0.60	0.0620	0.9998	0.45	1.42

In table 3 the asymptotic maximum diversity, range, power parameter, error, correlation, f_diversity and f_range are listed. F_diversity is the observed diversity as fraction of estimated asymptotic diversity. A value of 0.50 therefore means we expect the "real" diversity to be double that of the diversity based on the current findings. F_range is the number of samples as fraction of number of samples at which half of asymptotic diversity is observed. In other words, the further removed from 0 the value of f_range is, the less robust the asymptotic maximum estimate is and the more the analysis would benefit from added more samples to the data. The particular low value of 0.19 for f_range in Permian3 means that new findings are unlikely to upset the current estimates, while e.g. Permian1 would need more samples to reach the f_diversity of 0.50.

The rarefaction curve of all the PBDB data in Jurassic5 seems to fit as well as the curve of e.g. Jurassic4. However, the sampled diversity in Jurassic5 is only at 41% of the asymptotic diversity, which combined with the relative high asymptotic diversity, produces a less accurate estimate than most other intervals. Figure 13 is a visualization of the asymptotic diversity through time with error bars. The error band (ocher) flaring out both left and right of the boundary event, shows that the analysis would benefit more from additional data surrounding the extinction event window rather than adding more information about the Late Permian and Early Triassic.

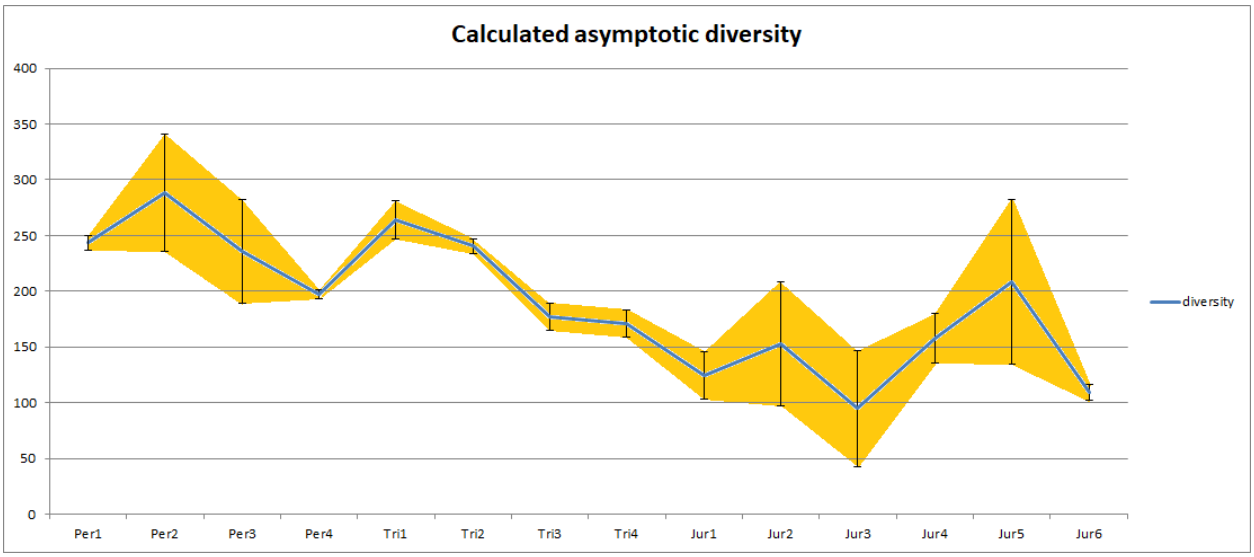

Fig 13. *Calculated asymptotic diversity from the beginning of the Permian to the end of the Jurassic, plus error bars shaded in ocher.*

All the modern geographical coordinates associated with the sample sites were converted to paleocoordinates. These paleocoordinates are plotted on paleogeographical maps in figure 14. It not only shows the disposition towards the northern hemisphere, but also the unevenness of the distribution of the samples overall. Gondwana also appears to be grossly understudied, undersampled and/or underreported,

at least regarding plant fossils. The red dots, which represent the data that was collected for the 2 additional literature studies, do not significantly contribute to a wider spatial understanding of the diversity.

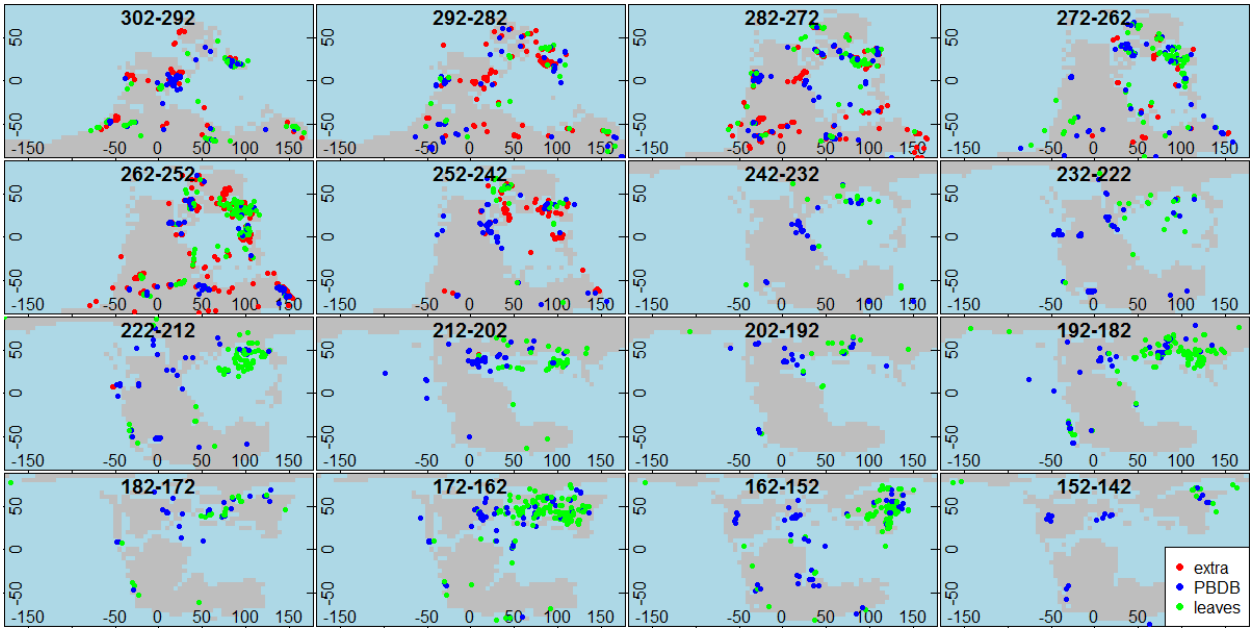

***Fig 14**. Position of the plant samples, based on converted modern coordinates, plotted on paleomaps.*

2.4. Discussion

The compiled data shows a drop in plant genera diversity around the Permian-Triassic boundary. Considering the small error margins (see Fig 13) in the end Permian through the Triassic data, this seems a robust pattern. However, the ideal conditions for a rarefaction analysis would be an even distribution of taxa within the studied area, that all taxa are equally common (or rare) and that all taxa had the same chance of becoming fossilized and an equal chance of getting correctly identified. Because real world conditions are not ideal, data can easily get skewed. For example, if for a specific data entry effort on one specific taxon for one specific time intervals is entered, it will influence the shape and height of the rarefaction curves. It would make them look as if the maximum diversity has been reached because with every "new draw", you draw the same taxon. Which would make it look like a robust, but taxon-poor reading. One way to avoid this problem is to go up in taxonomic level. A side effect of this may be the loss of finer patterns, but it does reduce the risk splitting similar taxa in different groups as a result of e.g. preservation quality and therefore identifiability. All the analyses presented here are based on genera level identification, resulting in a more homogeneous dataset that is likely to underestimate diversity levels, but gives more comparable predictions from one epoch to the next.

Selective data entry may also be the cause of the pattern seen in figure 11, where additional data extended genera range and thereby putting the peak of plant turnover in the Triassic rather than at the Permo-Triassic boundary. The Triassic-Jurassic boundary is one of the less studied (faunal) mass extinctions, not in the least because there is a lack of plant palaeoecological evidence. However, the little that we do know indicates major palaeoecological disturbance (McElwain and Punyasena 2007). The effect of this disturbance can be seen in the diversity transition from the Late Triassic to the Early Jurassic (Fig. 11). The lower diversity levels persisted through the Jurassic, not only on a global scale, but also on a more regional scale.

2.5. Conclusions

The analysis presented here provides a seemingly robust trend which shows a drop in diversity during the Permian Triassic transition. While rarefaction can give an unbiased estimate of global and regional plant diversity, it goes without saying that mathematical data analyses are only as good as the data that goes into them. While the trend itself may hold, the overall diversity estimates will most likely increase as other, hitherto un- and under explored fossil beds are discovered and recorded in publically accessible databases. Additional data will not only to resolve the extinction and turn-over patterns, but particularly to resolve the lack of spatial resolution. There are entire continents that are underrepresented in the currently available data. Based on the analyses presented here, it is likely that new data has the potential to upset the current estimated diversity.

Acknowledgements

I am most grateful to Ate Visser for the enormous help with R.

Literature cited

Algeo, Thomas J., Linda Hinnov, Jessa Moser, J. Barry Maynard, Erika Elswick, Kiyoko Kuwahara, and Hiroyoshi Sano. 2010. "Changes in Productivity and Redox Conditions in the Panthalassic Ocean during the Latest Permian." *Geology* 38 (2): 187–90. https://doi.org/10.1130/G30483.1.

Alroy, J., C. R. Marshall, R. K. Bambach, K. Bezusko, M. Foote, F. T. Fürsich, T. A. Hansen, et al. 2001. "Effects of Sampling Standardization on Estimates of Phanerozoic Marine Diversification." *Proceedings of the National Academy of Sciences* 98 (11): 6261–66. https://doi.org/10.1073/pnas.111144698.

Alroy, John. 2003. "Global Databases Will Yield Reliable Measures of Global Biodiversity." *Paleobiology* 29 (1): 26–29. https://doi.org/10.1666/0094-8373(2003)029<0026:GDWYRM>2.0.CO;2.

———. 2014. "Accurate and Precise Estimates of Origination and Extinction Rates." *Paleobiology* 40 (3): 374–97. https://doi.org/10.1666/13036.

Barnosky, Anthony D, Marc A Carrasco, and Edward B Davis. 2005. "The Impact of the Species–Area Relationship on Estimates of Paleodiversity." Edited by Simon Levin. *PLoS Biology* 3 (8): e266. https://doi.org/10.1371/journal.pbio.0030266.

Barnosky, Anthony D., Nicholas Matzke, Susumu Tomiya, Guinevere O. U. Wogan, Brian Swartz, Tiago B. Quental, Charles Marshall, et al. 2011. "Has the Earth/'s Sixth Mass Extinction Already Arrived?" *Nature* 471 (7336): 51–57. https://doi.org/10.1038/nature09678.

Barron, Eric J. 1981. "Paleogeography as a Climatic Forcing Factor." *Geologische Rundschau* 70 (2): 737–47. https://doi.org/10.1007/BF01822147.

Becker, L., R. J. Poreda, A. R. Basu, K. O. Pope, T. M. Harrison, C. Nicholson, and R. Iasky. 2004. "Bedout: A Possible End-Permian Impact Crater Offshore of Northwestern Australia." *Science* 304 (5676): 1469–76. https://doi.org/10.1126/science.1093925.

Benca, Jeffrey P., Ivo A. P. Duijnstee, and Cindy V. Looy. 2018. "UV-B–induced Forest Sterility: Implications of Ozone Shield Failure in Earth's Largest Extinction." *Science Advances* 4 (2): e1700618. https://doi.org/10.1126/sciadv.1700618.

Benson, Roger B. J., and Paul Upchurch. 2013. "Diversity Trends in the Establishment of Terrestrial Vertebrate Ecosystems: Interactions between Spatial and Temporal Sampling Biases." *Geology* 41 (1): 43–46. https://doi.org/10.1130/G33543.1.

Black, Benjamin A., Jean-François Lamarque, Christine A. Shields, Linda T. Elkins-Tanton, and Jeffrey T. Kiehl. 2013. "Acid Rain and Ozone Depletion from Pulsed Siberian Traps Magmatism." *Geology*, November, G34875.1. https://doi.org/10.1130/G34875.1.

Burgess, Seth D., Samuel Bowring, and Shu-zhong Shen. 2014. "High-Precision Timeline for Earth's Most Severe Extinction." *Proceedings of the National Academy of Sciences* 111 (9): 3316–21. https://doi.org/10.1073/pnas.1317692111.

Burgoyne, P, A Vanwyk, J Anderson, and B Schrire. 2005. "Phanerozoic Evolution of Plants on the African Plate." *Journal of African Earth Sciences* 43 (1–3): 13–52. https://doi.org/10.1016/j.jafrearsci.2005.07.015.

Ceballos, G., P. R. Ehrlich, A. D. Barnosky, A. Garcia, R. M. Pringle, and T. M. Palmer. 2015. "Accelerated Modern Human-Induced Species Losses: Entering the Sixth Mass Extinction." *Science Advances* 1 (5): e1400253–e1400253. https://doi.org/10.1126/sciadv.1400253.

Clapham, M. E., and J. L. Payne. 2011. "Acidification, Anoxia, and Extinction: A Multiple Logistic Regression Analysis of Extinction Selectivity during the Middle and Late Permian." *Geology* 39 (11): 1059–62. https://doi.org/10.1130/G32230.1.

Cui, Ying, and Lee R. Kump. 2014. "Global Warming and the End-Permian Extinction Event: Proxy and Modeling Perspectives." *Earth-Science Reviews*. https://doi.org/10.1016/j.earscirev.2014.04.007.

Dao-Yi, Xu, Ma Shu-Lan, Chai Zhi-Fang, Mao Xuo-Ying, Sun Yi-Ying, Zhang Qin-Wen, and Yang Zheng-Zhong. 1985. "Abundance Variation of Iridium and Trace Elements at the Permian/Triassic Boundary at Shangsi in China." *Nature* 314 (6007): 154. https://doi.org/10.1038/314154a0.

Dawson, Todd E., and Paul D. Brooks. 2001. “Fundamentals of Stable Isotope Chemistry and Measurement.” In *Stable Isotope Techniques in the Study of Biological Processes and Functioning of Ecosystems*, 1–18. Current Plant Science and Biotechnology in Agriculture. Springer, Dordrecht. https://doi.org/10.1007/978-94-015-9841-5_1.

Dietz, Robert S., and John C. Holden. 1970. “Reconstruction of Pangaea: Breakup and Dispersion of Continents, Permian to Present.” *Journal of Geophysical Research* 75 (26): 4939–56. https://doi.org/10.1029/JB075i026p04939.

DiMichele, W, H Kerp, N Tabor, and C Looy. 2008. “The So-Called ‘Paleophytic–Mesophytic’ Transition in Equatorial Pangea — Multiple Biomes and Vegetational Tracking of Climate Change through Geological Time.” *Palaeogeography, Palaeoclimatology, Palaeoecology* 268 (3–4): 152–63. https://doi.org/10.1016/j.palaeo.2008.06.006.

“Earth’s CO2 Home Page.” n.d. CO2.Earth. Accessed October 6, 2017. https://www.co2.earth/.

Ehmann, W.D., and P.A. Baedecker. 2015. “The Distribution of Gold and Iridium in Meteoric and Terrestrial Materials.” In *Origin and Distribution of the Elements: International Series of Monographs in Earth Sciences*, edited by L. H. Ahrens, 301–11. Elsevier.

Erwin, Douglas H. 1989. “The End-Permian Mass Extinction: What Really Happened and Did It Matter?” *Trends in Ecology & Evolution* 4 (8): 225–29. https://doi.org/10.1016/0169-5347(89)90165-1.

———. 1993. *The Great Paleozoic Crisis: Life and Death in the Permian*. Columbia University Press.

Gilluly, James. 1969. “Geological Perspective and the Completeness of the Geologic Record.” *GSA Bulletin* 80 (11): 2303–12. https://doi.org/10.1130/0016-7606(1969)80[2303:GPATCO]2.0.CO;2.

Goddéris, Yves, Yannick Donnadieu, Guillaume Le Hir, Vincent Lefebvre, and Elise Nardin. 2014. “The Role of Palaeogeography in the Phanerozoic History of Atmospheric CO2 and Climate.” *Earth-Science Reviews* 128 (January): 122–38. https://doi.org/10.1016/j.earscirev.2013.11.004.

Haq, Bilal U., and Stephen R. Schutter. 2008. “A Chronology of Paleozoic Sea-Level Changes.” *Science* 322 (5898): 64–68. https://doi.org/10.1126/science.1161648.

Jackson, Jeremy B. C., and Kenneth G. Johnson. 2001. “Measuring Past Biodiversity.” *Science* 293 (5539): 2401–4. https://doi.org/10.1126/science.1063789.

Jacobs, Joshua. 2008. *Rarefaction*. R. www.joshuajacobs.org/R/rarefaction.html.

Jansen, Marcel A. K, Victor Gaba, and Bruce M Greenberg. 1998. “Higher Plants and UV-B Radiation: Balancing Damage, Repair and Acclimation.” *Trends in Plant Science* 3 (4): 131–35. https://doi.org/10.1016/S1360-1385(98)01215-1.

Jurikova et al. 2017. “Assessing Ocean Acidification and Carbon Cycle Perturbations during the End-Permian Extinction Using Boron Isotopes.” *Permophiles*, no. 65.

Kaiho, Kunio, and Seizi Koga. 2013. “Impacts of a Massive Release of Methane and Hydrogen Sulfide on Oxygen and Ozone during the Late Permian Mass Extinction.” *Global and Planetary Change* 107 (August): 91–101. https://doi.org/10.1016/j.gloplacha.2013.04.004.

Kamo, Sandra L, Gerald K Czamanske, Yuri Amelin, Valeri A Fedorenko, D.W Davis, and V.R Trofimov. 2003. “Rapid Eruption of Siberian Flood-Volcanic Rocks and Evidence for Coincidence with the Permian–Triassic Boundary and Mass Extinction at 251 Ma.” *Earth and Planetary Science Letters* 214 (1–2): 75–91. https://doi.org/10.1016/S0012-821X(03)00347-9.

Kerr, Richard A. 2004. “Evidence of Huge, Deadly Impact Found Off Australian Coast?” *Science* 304 (5673): 941–941. https://doi.org/10.1126/science.304.5673.941a.

Kiehl, Jeffrey T., and Christine A. Shields. 2005. “Climate Simulation of the Latest Permian: Implications for Mass Extinction.” *Geology* 33 (9): 757–60. https://doi.org/10.1130/G21654.1.

Knoll, A., R. K. Bambach, D. E. Canfield, and J. P. Grotzinger. 1996. “Comparative Earth History and Late Permian Mass Extinction.” *SCIENCE-NEW YORK THEN WASHINGTON-*, 452–57.

Knoll, A.H. 1984. “Patterns of Extinction in the Fossil Record of Vascular Plants.” In *Extinctions*, edited by M.H. Nitecki, 21–68. Chicago: The University of Chicago.

Knoll, Andrew H., Richard K. Bambach, Jonathan L. Payne, Sara Pruss, and Woodward W. Fischer. 2007. “Paleophysiology and End-Permian Mass Extinction.” *Earth and Planetary Science Letters* 256 (3–4): 295–313. https://doi.org/10.1016/j.epsl.2007.02.018.

Korte, Christoph, and Heinz W. Kozur. 2010. “Carbon-Isotope Stratigraphy across the Permian–Triassic Boundary: A Review.” *Journal of Asian Earth Sciences* 39 (4): 215–35. https://doi.org/10.1016/j.jseaes.2010.01.005.

Kravchinsky, Vadim A., Konstantin M. Konstantinov, Vincent Courtillot, Jams I. Savrasov, Jean-Pierre Valet, Sergey D. Cherniy, Sergey G. Mishenin, and Boris S. Parasotka. 2002. “Palaeomagnetism of East Siberian Traps and Kimberlites: Two New Poles and Palaeogeographic Reconstructions at about 360 and 250 Ma.” *Geophysical Journal International* 148 (1): 1–33. https://doi.org/10.1046/j.0956-540x.2001.01548.x.

Krug, Andrew Z., and Mark E. Patzkowsky. 2007. “Geographic Variation in Turnover and Recovery from the Late Ordovician Mass Extinction.” *Paleobiology* 33 (3): 435–54. https://doi.org/10.1666/06039.1.

Kump, Lee R., Alexander Pavlov, and Michael A. Arthur. 2005. “Massive Release of Hydrogen Sulfide to the Surface Ocean and Atmosphere during Intervals of Oceanic Anoxia.” *Geology* 33 (5): 397. https://doi.org/10.1130/G21295.1.

Labandeira, Conrad C. 2005. “The Fossil Record of Insect Extinction: New Approaches and Future Directions.” *American Entomologist* 51 (1): 14–29. https://doi.org/10.1093/ae/51.1.14.

Likens, G. E., C. T. Driscoll, and D. C. Buso. 1996. “Long-Term Effects of Acid Rain: Response and Recovery of a Forest Ecosystem.” *Science; Washington* 272 (5259): 244.

Looy, C., H. Kerp, I. Duijnstee, and B. DiMichele. 2014. “The Late Paleozoic Ecological-Evolutionary Laboratory, a Land-Plant Fossil Record Perspective.” *The Sedimentary Record* 12 (4): 4–18.

Massa, G.D., R.M. Wheeler, R.C. Morrow, and H.G. Levine. 2016. “Growth Chambers on the International Space Station for Large Plants.Pdf.” 2016. http://ntrs.nasa.gov/archive/nasa/casi.ntrs.nasa.gov/20160006558.pdf.

McElwain, Jennifer C., and Surangi W. Punyasena. 2007. “Mass Extinction Events and the Plant Fossil Record.” *Trends in Ecology & Evolution* 22 (10): 548–57. https://doi.org/10.1016/j.tree.2007.09.003.

Miller, Arnold I. 2000. “Conversations about Phanerozoic Global Diversity.” *Paleobiology* 26 (4): 53–73.

Miller, Arnold I., and Mike Foote. 1996. “Calibrating the Ordovician Radiation of Marine Life: Implications for Phanerozoic Diversity Trends.” *Paleobiology* 22 (2): 304–9.

Miller, Kenneth G., Michelle A. Kominz, James V. Browning, James D. Wright, Gregory S. Mountain, Miriam E. Katz, Peter J. Sugarman, Benjamin S. Cramer, Nicholas Christie-Blick, and Stephen F. Pekar. 2005. “The Phanerozoic Record of Global Sea-Level Change.” *Science* 310 (5752): 1293–98. https://doi.org/10.1126/science.1116412.

Mora, Claudia I., Steven G. Driese, and Lee Ann Colarusso. 1996. “Middle to Late Paleozoic Atmospheric CO2 Levels from Soil Carbonate and Organic Matter.” *Science; Washington* 271 (5252): 1105.

Müller, R. Dietmar, Maria Sdrolias, Carmen Gaina, Bernhard Steinberger, and Christian Heine. 2008. “Long-Term Sea-Level Fluctuations Driven by Ocean Basin Dynamics.” *Science* 319 (5868): 1357–62. https://doi.org/10.1126/science.1151540.

Niklas, Karl J. 2015. “Measuring the Tempo of Plant Death and Birth.” *New Phytologist* 207 (2): 254–56. https://doi.org/10.1111/nph.13402.

Payne, Jonathan L., Daniel J. Lehrmann, David Follett, Margaret Seibel, Lee R. Kump, Anthony Riccardi, Demir Altiner, Hiroyoshi Sano, and Jiayong Wei. 2007. “Erosional Truncation of Uppermost Permian Shallow-Marine Carbonates and Implications for Permian-Triassic Boundary Events.” *GSA Bulletin* 119 (7–8): 771–84. https://doi.org/10.1130/B26091.1.

Phillips, John. 1860. *Life on the Earth: Its Origin and Succession*. Macmillan and Company.

Polozov, Alexander G., Henrik H. Svensen, Sverre Planke, Svetlana N. Grishina, Kirsten E. Fristad, and Dougal A. Jerram. 2016. “The Basalt Pipes of the Tunguska Basin (Siberia, Russia): High Temperature Processes and Volatile Degassing into the End-Permian Atmosphere.” *Palaeogeography, Palaeoclimatology, Palaeoecology*, Impact, Volcanism, Global changes and Mass Extinctions, 441, Part 1 (January): 51–64. https://doi.org/10.1016/j.palaeo.2015.06.035.

Raup, David M. 1976. “Species Diversity in the Phanerozoic: An Interpretation.” *Paleobiology* 2 (4): 289–97.
Rees, P. McAllister. 2002. “Land-Plant Diversity and the End-Permian Mass Extinction.” *Geology* 30 (9): 827–30. https://doi.org/10.1130/0091-7613(2002)030<0827:LPDATE>2.0.CO;2.
Rees, P. McAllister, Alfred M. Ziegler, Mark T. Gibbs, John E. Kutzbach, Pat J. Behling, and David B. Rowley. 2002. “Permian Phytogeographic Patterns and Climate Data/Model Comparisons.” *The Journal of Geology* 110 (1): 1–31.
Renne, Paul R, H Jay Melosh, Kenneth A Farley, W Uwe Reimold, Christian Koeberl, Michael R Rampino, Simon P Kelly, and Boris A Ivanov. 2004. “Is Bedout an Impact Crater? Take 2.” *Science* 306 (5696): 610–12.
Retallack, Gregory J. 2001. “A 300-Million-Year Record of Atmospheric Carbon Dioxide from Fossil Plant Cuticles.” *Nature* 411 (6835): 287. https://doi.org/10.1038/35077041.
Retallack, Gregory J., John J. Veevers, and Ric Morante. 1996. “Global Coal Gap between Permian–Triassic Extinction and Middle Triassic Recovery of Peat-Forming Plants.” *Geological Society of America Bulletin* 108 (2): 195–207. https://doi.org/10.1130/0016-7606(1996)108<0195:GCGBPT>2.3.CO;2.
Rothman, Daniel H., Gregory P. Fournier, Katherine L. French, Eric J. Alm, Edward A. Boyle, Changqun Cao, and Roger E. Summons. 2014. “Methanogenic Burst in the End-Permian Carbon Cycle.” *Proceedings of the National Academy of Sciences* 111 (15): 5462–67. https://doi.org/10.1073/pnas.1318106111.
Saunders, Andy, and Marc Reichow. 2009. “The Siberian Traps and the End-Permian Mass Extinction: A Critical Review.” *Chinese Science Bulletin* 54 (1): 20–37. https://doi.org/10.1007/s11434-008-0543-7.
Seward, Albert Charles. 2011. *Fossil Plants: A Text-Book for Students of Botany and Geology*. Vol. 4. Cambridge University Press.
Shen, Shu-zhong, and Samuel A. Bowring. 2014. “The End-Permian Mass Extinction: A Still Unexplained Catastrophe.” *National Science Review*, August, nwu047. https://doi.org/10.1093/nsr/nwu047.
Shen, Shu-zhong, James L. Crowley, Yue Wang, Samuel A. Bowring, Douglas H. Erwin, Peter M. Sadler, Chang-qun Cao, et al. 2011. “Calibrating the End-Permian Mass Extinction.” *Science*, November. https://doi.org/10.1126/science.1213454.
Silvestro, Daniele, Borja Cascales-Miñana, Christine D. Bacon, and Alexandre Antonelli. 2015. “Revisiting the Origin and Diversification of Vascular Plants through a Comprehensive Bayesian Analysis of the Fossil Record.” *New Phytologist* 207 (2): 425–36. https://doi.org/10.1111/nph.13247.
Song, Haijun, Paul B. Wignall, Jinnan Tong, and Hongfu Yin. 2012. “Two Pulses of Extinction during the Permian-Triassic Crisis.” *Nature Geoscience* 6 (1): 52–56. https://doi.org/10.1038/ngeo1649.
Tabor, Neil J., and Isabel P. Montañez. 2002. “Shifts in Late Paleozoic Atmospheric Circulation over Western Equatorial Pangea: Insights from Pedogenic Mineral Δ18O Compositions.” *Geology* 30 (12): 1127–30. https://doi.org/10.1130/0091-7613(2002)030<1127:SILPAC>2.0.CO;2.
Traverse, Alfred. 1988. “Plant Evolution Dances to a Different Beat: Plant and Animal Evolutionary Mechanisms Compared.” *Historical Biology* 1 (4): 277–301. https://doi.org/10.1080/08912968809386480.
Watson, A. 1992. “Desert Soils.” In *Weathering, Soils & Paleosols, Developments in Surface Processes*, 225–60. Elsevier.
Wignall, Paul, Bruce Thomas, Robbert Willink, and John Watling. 2004. “Is Bedout an Impact Crater? Take 1.” *Science* 306 (5696): 609–10. https://doi.org/10.1126/science.306.5696.609d.
Wilkinson, Bruce H., Brandon J. McElroy, Stephen E. Kesler, Shanan E. Peters, and Edward D. Rothman. 2009. “Global Geologic Maps Are Tectonic Speedometers—Rates of Rock Cycling from Area-Age Frequencies.” *Geological Society of America Bulletin* 121 (5–6): 760–79.
Willis, K. J., and J. C. McElwain. 2002. *The Evolution of Plants*. New York: Oxford University Press.

Wu, Huaichun, Shihong Zhang, Linda A. Hinnov, Ganqing Jiang, Qinglai Feng, Haiyan Li, and Tianshui Yang. 2013. “Time-Calibrated Milankovitch Cycles for the Late Permian.” *Nature Communications* 4 (September). https://doi.org/10.1038/ncomms3452.

Yabushita, Shin, and Shin-Ichi Kawakami. 2007. “Measurement of Iridium in the Fullerene-Rich Layer in Central Japan by the Neutron Activation Method.” *Fullerenes, Nanotubes and Carbon Nanostructures* 15 (2): 127–33. https://doi.org/10.1080/15363830601179731.

Zajzon, N., Zs. Molnár, and T. G. Weiszburg. 2012. “Ppt Range Iridium Determination by RNAA and Application of That Method on a Permian/Triassic Boundary Section, Bálvány, Bükk Mts., Hungary.” *Journal of Radioanalytical and Nuclear Chemistry* 291 (3): 579–86. https://doi.org/10.1007/s10967-011-1562-4.

Chapter 2: Silica in plants – main act or sideshow?

– a review of the role of silica in plants –

Abstract

Silicon (Si) is the second most abundant element in the Earth's crust. As the minerals containing silicon weather, they can form monosilicic acid. In this form, it can be taken up by the roots of land plants to either remain in solution or to be deposited in plant tissue as phytoliths. The uptake of monosilicic acid was initially thought to be entirely passive process. More recently, however, it has become clear that many plants have developed several pathways to actively absorb silica. Incorporating silicon in plant tissues has a multitude of benefits ranging from structural support to defenses against a myriad environmental stresses, herbivory and pathogenic invasion. On a molecular level the role of silicon remains unclear. It is however evident that plants, particularly under stress conditions, benefit from bio-available silica.

1. Introduction

Phytoliths, microscopic structures made of silica (SiO_2), are commonly studied plant micro-remains. Phytoliths are small yet robust silica particles produced by many plants. As the dissolved silica precipitates inside the various tissues, the phytoliths take on the shape of the cell, which can—depending on the specific plant lineage—be diagnostic acting as indicators of their past presence. In the last decade, approximately 500 papers and abstracts were published that mention the word phytoliths in the title and another roughly 6,700 refer to phytoliths in the main text (source: Google Scholar, search term ‘phytolith’, downloaded July 3, 2017). Most of these publications deal with archeological questions, paleoenvironmental studies or geochemical investigations. As such, the majority of those papers sidesteps the function of biogenic silica or briefly list the most commonly acknowledged properties. To better understand the role of phytoliths and silica in plant function and their potential advantages and disadvantages, this review provides a summary of studies on the importance of silica in plants. This review discusses the history of phytolith research, the mechanisms of silica uptake by plants and phytolith formation, the importance of dissolved silica in biochemical pathways and the benefit of phytoliths to plants. Silica plays a role in the core biochemical cycling of ethylene (C_2H_4) and it aids plants in the protection against abiotic stress factors (climate, salinity, radiation) as well as biotic stress factors (pathogens, herbivores). Reported and suggested benefits of silica and phytoliths are critically reviewed and further research directions are listed.

2. A short history of phytolith research

Phytoliths were first described in living plants by the German Gustav A. Struve in 1835 (Figure 1; Struve, 1835). A decade later, Christian G. Ehrenberg, a biologist who specialized in micro-organisms, published a more systematic approach in the form of a thesis titled "Passatstaub und Blutregen" (*Trade Wind Dust and Blood Rain;* Ehrenberg, 1849). He also analyzed the dust samples collected by Charles Darwin during his voyages on the Beagle (Darwin 1909). Darwin had noted the copious amounts of dust raining down onto the ship while sailing to Cape Verde, off the coast of Senegal (Darwin 1909). Prior to Ehrenberg's work, it was assumed that trade wind dust consisted of volcanic ash or mineral particles blown into the atmosphere from deserts (e.g. (Murray and Irvine 1892). However, the specimens that Darwin collected between 1834 and 1838 and sent to Ehrenberg for examination contained a variety of *infusoria* (aquatic microorganisms) and phytoliths (Ehrenberg, 1849).

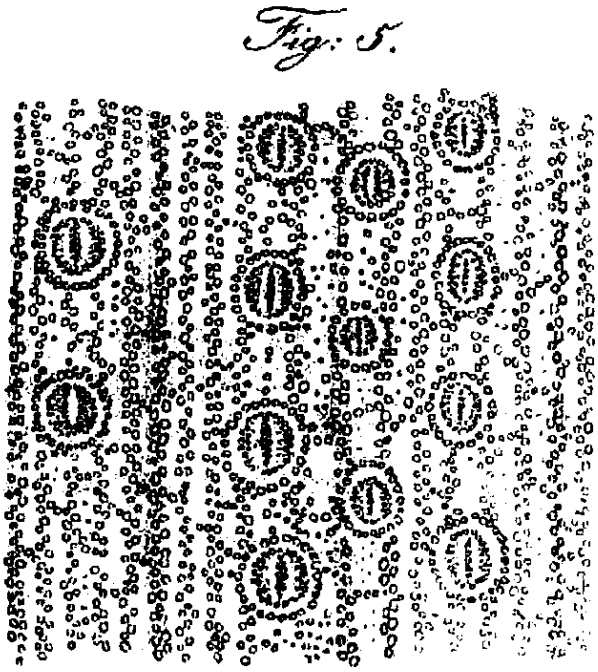

Fig 1. *A reproduction of one of Stuve's original drawings of Equisetum from 1835.*

In the early 1900s, the fifty years that followed Ehrenberg's work, most phytolith publications were focused on morphology and taxonomy. At the turn of the 19th century, Schellenberg in 1904 was the first to use phytoliths to identify wheat and barley residues on archeological artifacts of aeneolithic age (6000-5100 B.C.) (Pumpelly 1908). Prior to the using phytoliths as an archeological tool, the benefit of silica to plant growth was known and described. Publications dating as far back as 1848 mention the benefits of fertilizing crops with silica-rich materials such as the ashes of burnt left-overs from previous harvest or

pozzolan, a silica-rich volcanic deposit (Morfit 1848). Especially for silica accumulators (>1% Si dry weight) like wheat, maize and rice, silica is a critical element.

3. Silica uptake and phytolith production

Before discussing the functions of the silica inclusions in plants, it is important to understand the mechanism by which the silica is absorbed and where it is deposited. Silicon is the second most abundant element in of the Earth's crust, mostly bound in silicate minerals (mainly silica (SiO_2) (Kump et al. 2010). Silica dissolves, generally at slow rates, to form monosilicic acid or orthosilicic acid (H_4SiO_4):

$$SiO_{2(\alpha\text{-quartz})} + 2H_2O \leftrightarrow H_4SiO_{4\,(aq)}$$

Though from a structural standpoint it is better to write:

$$SiO_{2(\alpha\text{-quartz})} + 2H_2O \leftrightarrow Si(OH)_{4\,(aq)}$$

Plants take up water, together with dissolved silica and other minerals, through their roots. The cohesion of the water, combined with the osmotic pressure, which may or may not be the result of evaporation, leads to an inward flow of water and the dissolved minerals. The solution passes through the epidermis, endodermis and vascular tissue before it is pulled in the xylem vessels by tension, and transported to the other plant organs (Sperry et al. 2003)

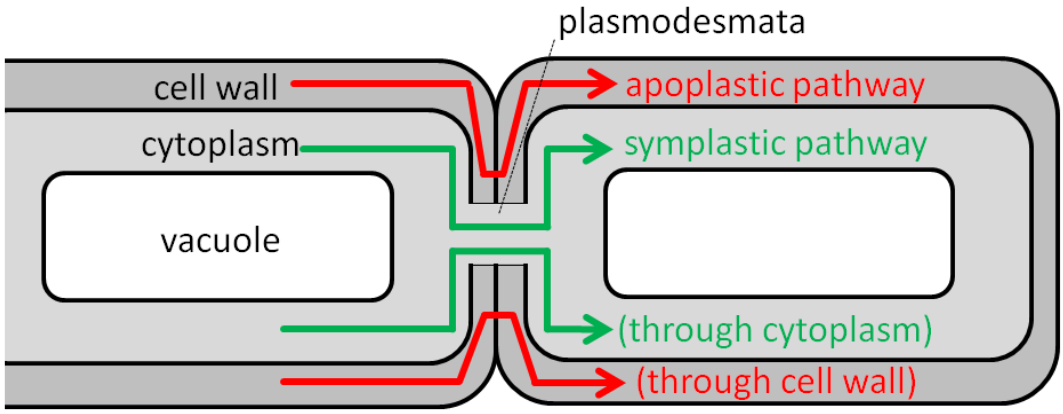

Fig 2. *Water transport in plant cells. Modified after Reece et al. (2014)*

Within the plant water flows through apoplastic (a continuum of cell walls), and cell-to-cell pathways (see Fig 2, after Reece et al.). The cell-to-cell pathways comprise of the symplastic and transcellular paths. The symplastic path is the continuum of cytoplasm interconnected by plasmodesmata, while the transcellular path includes the cell walls, cytoplasm, and vacuoles of the cells. Because in practice the

transcellular and symplastic paths are difficult to separate, they are often combined together as the cell-to-cell pathway.

Aquaporins are integral membrane proteins that mediate the transport of water and/or small neutral solutes (Maurel et al. 2008) and part of the transcellular path (Delseny and Kader 2007). They connect all the cells and allow for selective water transport. Aquaporins can be found in all plant organs, but they are particularly abundant in the plasma membranes of root tissue and xylem parenchema cells (Otto and Kaldenhoff 2000). The type of aquaporin determines the size of the pore and charge, which in turn demines the size of the molecules and charge that are capable of passing though these water channels. Aquaporins are members of the Nodulin 26-like Intrinsic Proteins (NIPs) which are part of the larger Major Intrinsic Proteins (MIPs) family (Wallace et al. 2006). MIPs are found in most organisms, but more commonly so in plants. In plants, the majority of MIPs function as water channels (Johansson et al 2000). Molecular data indicates an adaptive radiation of the NIPs that are responsible for the transport of silicic acid amongst other elements, early within land plant lineages (Trembath-Reichert et al. 2015). Trembath-Reichert et al. organized the NIPs responsible for silica biomineralization with their associated plant divisions. The way the NIPs fall onto the phylogenetic tree, suggests horizontal gene transfer from bacteria into early terrestrial plants.

Members of the eusporangiate fern orders Equisetales and Marattiales contain up to 10% silica dry weight and are prolific phytolith producers (see Figure 3) (Sapei et al. 2007).

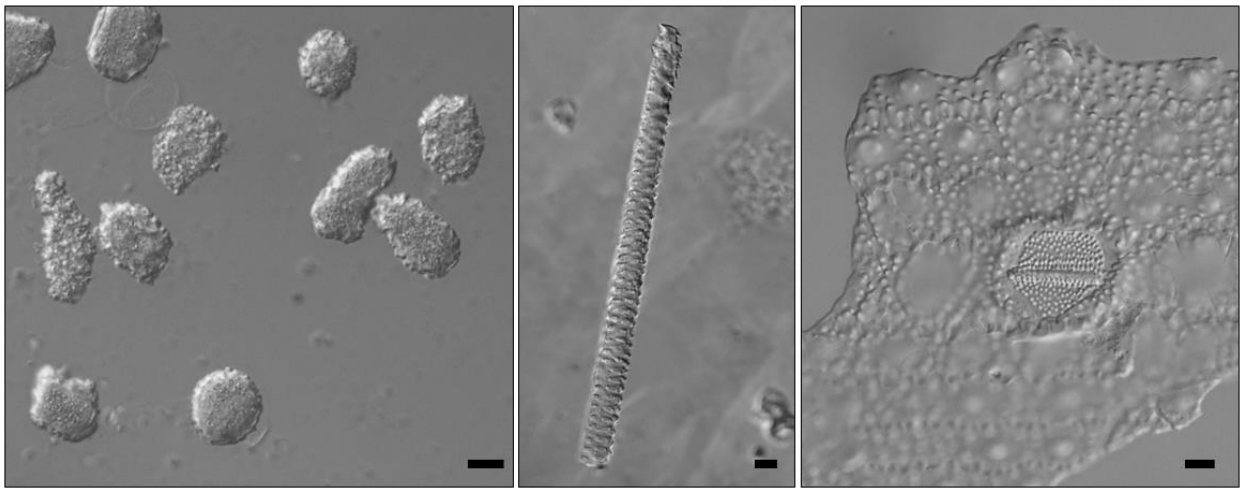

Fig. 3. *Phytoliths extracted from plants. Examples of eusporangiate ferns Marattiaceae and Psilotaceae and sister group Equisetum (Knie et al., 2015). All of which are identified as silica accumulators, but the Si transporter has only been identified in the latter. left to right: Angiopteris evecta, ovate to globular granulate; Psilotum nudum, vascular element, cylindrical striate; Equisetum telmateia, epidermal element, long cells with papillae features. Scale bars 10μm.*

The silica transporter in the eusporangiate ferns is, however, is still unknown (Trembath-Reichert et al. 2015). This suggests that besides the silica transporting NIPs there must be another pathway to absorb silicic acid. Leptosporangiate ferns do not accumulate silica at the same rate and have a silica content of less than 1% of dry matter. The families within this group do produce morphologically diverse phytoliths (Figure 4).

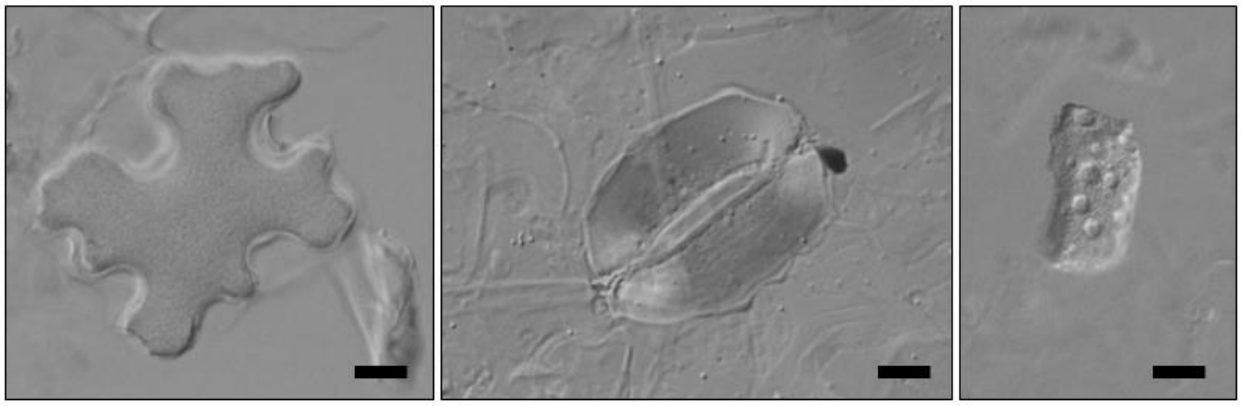

Fig. 4. *Phytoliths extracted from Leptosporangiate ferns. From left to right: Blechnum gibbum, an epidermal element; Osmunda japonica, stomatal guard elements; Lonchitis hirsuta, a trapeziform morphotype with irregular pitting. Scale bars 10μm.*

The type of aquaporins determines the size of the elements passing through; they are essentially the gatekeeper of purity. The variety and distribution of specific porins also explain why the silica is not evenly and not randomly deposited throughout the plant. To investigate the internal distribution of silica inside plants, Ma et al (2004) grew two varieties of rice; a wild rice, which is a natural silica accumulator, and a low-silicon rice mutant in the same medium. Both varieties showed an equal increase in silicon concentrations in the root symplastic solution with an increased concentration of silica in the medium. The crucial difference in the silicon concentration, however, was found in the xylem sap. The concentration in the wild rice variety was roughly five times higher than that of the mutant. This is evidence that there is not only selectivity in the epidermis/cortex (SIT1, fig. 5) but also evidence for active transport from the cortical cells (SIT2, fig. 5) to the plants' xylem.

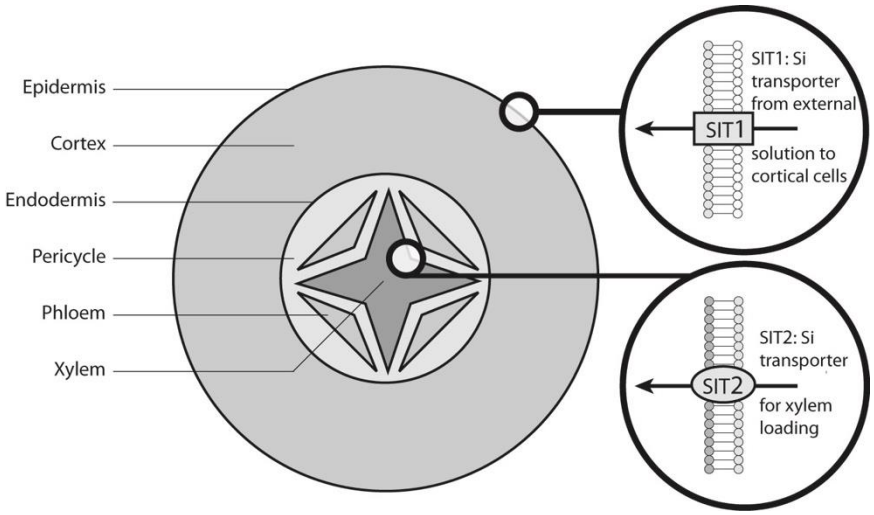

Fig. 5. *Diagram of the root structure, showing two sites of silica transporters. Modified after Ma (2004)*

Silica accumulation is determined by the rate of silica uptake and the longevity of a plant and its organs. There are multiple studies published that will attest to the fact that over time plants will sequester more silica (*e.g.* Motomura, Hikosaka, and Suzuki 2007; Lewin and Reimann 1969; Blackman 1968; Hodson and Sangster 1998). Taxa with high accumulation rates will have high amounts of silica in young tissue, while other taxa will have long-lived leaves that are not rich in phytoliths. *Equisetum arvense*, which in most climates only has annual above-ground growth, accumulates more than 10% silica dry weight (Piperno 2006) and is an example of a high silica accumulation rate. In contrast, 82 conifer species (Pinales) studied, where the ages of the leaves is well over one year old, have an average silica dry weight content of 0.8% (Trembath-Reichert et al. 2015). There are also plants that actively exclude silicon like tomatoes (Takahashi et al. 1990).

3.1. Silica deposition as phytoliths

In most plants the majority of the taxonomically significant shaped silica is deposited in their aerial parts where evaporation occurs (Hodson et al. 2008). Here the undersaturated solution of silicic acid [$Si(OH)_4$] or its ionized form, $Si(OH)_3O^-$ changes to a supersaturated solution as a result of the removal of water. The silica in the supersaturated solution (~100ppm) will change phase and polymerize in a controlled fashion and crystallize (Currie and Perry 2007; Jones and Handreck 1967). The crystallization can take place anywhere where there is xylem or phloem sap; the cell lumen – partially or completely, the cell walls, intercellular spaces in root or shoot tissue or in an extracellular (e.g. cuticle) layer (Piperno 2006). Though most silica accumulation takes place in actively transpiring areas, phytoliths are also formed in xylem, parenchyma and sclerenchyma cells (Honaine, Zucol, and Osterrieth 2009). The cellular

morphology is the mold for the silica bodies; hence a uniquely shaped space with sufficient silica deposition may yield morphologically distinct phytoliths. To be useful in answering (paleo-)ecological and/or (ethno-)botanical questions, the silica has to be deposited in loci that produce phytoliths that are both sturdy enough to survive in the soil record and morphologically distinctive. Some plants, for example oaks, produce a very morphologically distinct single-layer honeycomb-like structure in its leaves that unfortunately does not hold up under pressure and therefore does not preserve in de soil record (Bremond 2004; Kirchholtes et al 2015).

4. Benefits of dissolved silica and phytoliths

Until the 1960s, silica absorption and phytolith production was believed to be a passive affair - the side effect of evaporation of water that happened to have dissolved silica in it. It was not until the mid-sixties that Okuda and Takahashi(Okuda and Takahashi 1965) proved using *Oryza sativa* (Asian rice) that this does not hold true in all plants. Their experimental work showed that, in contrast to tomato plants (*Solanum lycopersicum*), rice can absorb silica from their growth medium, against the gradient. The silica concentration in the rice plants was several hundred times higher than their medium, indicating an active transport mechanism. Silica is critical for optimal growth in rice plants. But even for a non-silica accumulator like tomato, a little available silica is essential during its reproductive stage (Takahashi and Miyake 1977). Takahashi and Miyake firmly established that plants actively absorb silica, and showed plant silica has a multitude of functions and benefits (see Figure 6 for a schematic overview of the various roles of silica in plant functioning). Silica plays a role in the core biochemical cycling of ethylene and it aids plants in the protection against abiotic stress factors (climate, salinity, radiation) as well as biotic stress factors (pathogens, herbivores). The roles of silica and examples of studies describing these attributes are listed in Table 1. In general, silica benefits plants in two distinct ways: 1) Dissolved silica plays an important role in a number of biochemical functions, and 2) Phytoliths provide physical rigidity to plant tissue, improving light interception and gas exchange potential, and making circumstances less favorable for infections that benefit from constant ambient moisture such as mildew. In specific cases, the formation of phytoliths benefit the plants chemically by incorporating toxins into the amorphous form. The rest of this chapter will address these benefits in more detail.

Table 1. *An overview of reported benefits of silica to plants.*

Benefit	Benefit	Reference (*i.a.*)	Mechanism, process
Structural support			
	Increase photosynthetic capability	Yoshida et al. (1969); Takahashi and Miyake (1977)	More erect stature
	Rigidity	Toresano-Sánchez, Valverde-García, and Camacho-Ferre 2012; Takahashi et al. (1990)	Reducing/regulating ambient moisture which reduces susceptibility to infections such as mildew
	Relatively "cheap building blocks"	Raven (1983)	Energetically, it is less costly for a plant to incorporate Si than to synthesize lignin
Reduce Abiotic Stress			
	Heavy Metals	Hodson and Evans (1995); Neumann and Zur Nieden (2001)	co-deposition and adsorption
	Heavy Metals	Wang, Stass, and Horst (2004)	Incorporation of heavy metals in the silica matrix
	Salt	Liang et al. (2007); Liang et al. (2006)	changes the charge of the root plasma membrane which results in a decrease of Na^+ absorption
	Drought, reduced evaporation	Keutman et al. (2015); Kaufman et al. (1971); Sangster (1970)	Sheets of silica in the upper epidermal cells
	Drought, reduced evaporation	Kaufman et al. (1985); Yoshida, Ohnishi, and Kitagishi (1962)	release of water from the silica gel
	Drought, reduced evaporation	Liang et al. (2008)	accumulation of polar monosilicic acid and/or polymerized silicic acid in the epidermal cell walls
	Drought, Increased root/shoot biomass	Pei et al. (2010)	More roots to compensate for water loss
	Anti-freeze	Larcher (1991)	Reduced freezing point of sap w/o the deleterious effects of a salt like Na^+
	UV-protection	Goto (2003)	Physical and increase anti-oxidant production
Reduce biotic stress			
	Protection against pathogens	Van Brockhaven (2015); Yin (2016)	Increased production of anti-oxidants, stimulated by Si
	Physical protection against herbivory	Massey et al. (2009)	Silica provides a physical barrier
	Chemical protection against herbivory	Moore (1984)	Slower growth rates of insects feeding on Si-rich plant sap

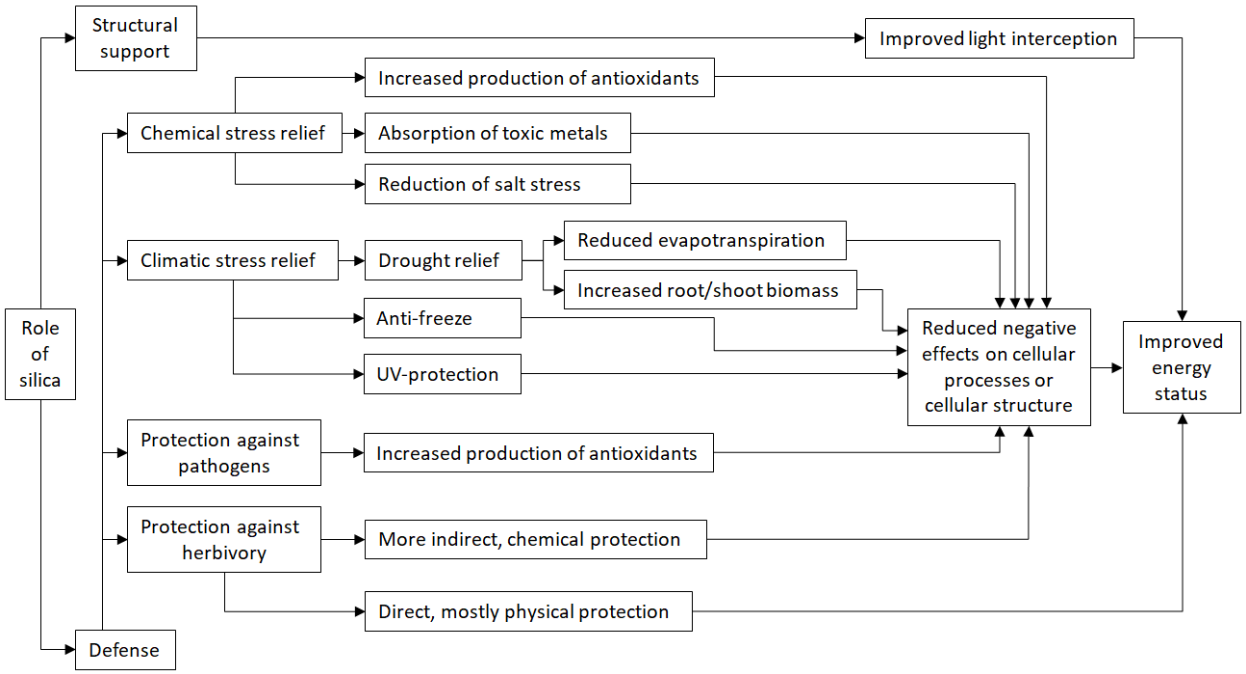

Fig. 6. *A schematic overview of the various ways silica plays a role in plant functioning.*

4.1. The role of silica in the ethylene and polyamine pathway

The ancient Egyptians knew that scarring certain fruits promoted ripening. What they did not know was that this scarring triggered a chemical response that promotes the ripening process (Galil 1968). It was Neljubow who—roughly 5000 years later—worked out that the gas involved in this process was ethylene (Neljubow 1902). The list of plant responses to ethylene is long and—by now—well-established (Bleecker and Kende 2000). Among other things, ethylene stimulates the synthesis of several different enzymes, it signals and regulates seed germination, the production of Reactive Oxygen Species ($^{\cdot}O_2^-$) and with that the spread of (programmed) cell death and organ senescence (Overmyer et al. 2000; Steffens and Sauter 2009).

Because ethylene influences many aspects of a plants' life, it is considered to be one of the most important biochemical pathways and silica plays a pivotal role in ethylene production (see figure 7). S-adenosyl-l-methionine (SAM) is the precursor of both ethylene and polyamines (polyvalent cation compounds; PAs). Their pathways are therefore often considered to be in competition with each other (Pandey et al. 2000). However, even though PAs and ethylene are based on the same substrate, their pathways can operate simultaneously and through complex feed-back systems, do not seem to exhaust the supply of SAM (fig. 7) (Steffens and Sauter 2009; Van de Poel et al. 2013). In fig. 7a simplified pathway illustrates the production of the volatile signaling hormone ethylene on one side, and the production of PAs which are essential for abiotic and biotic stress responses, various antiaging and developmental

processes in plants on the other. The balance between the production of ethylene and PA is critical as an overproduction of either, or underproduction of one, can lead to irreparable damage of plant tissue. In a healthy, unstressed plant the ethylene and PA production is stable, though the balance may shift through the plant's life and its reproductive stages. Particularly under (drought) stress, PA synthesis is up-regulated by silicon, ultimately protecting the plants photosynthetic capabilities (Kazemi et al 2012; Yin et al. 2016).

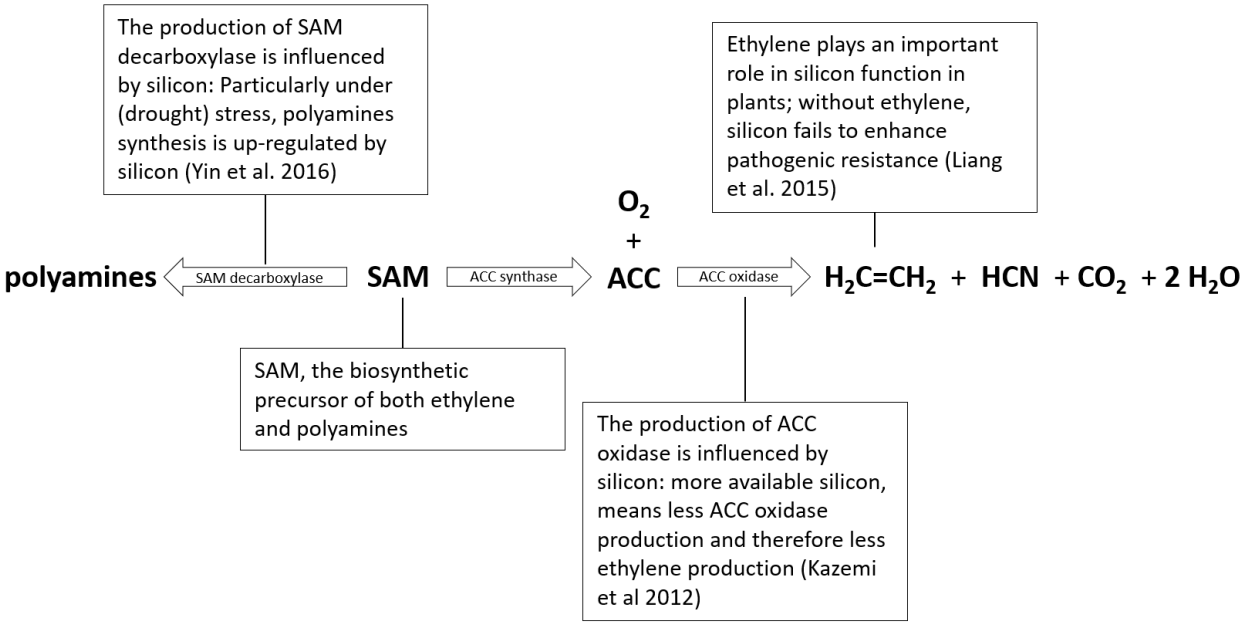

Fig. 7*. A simplified overview of the ethylene and polyamines forming pathways from SAM and the importance of silicon.*

Silica is known to bind hydroxyl groups (Fauteux et al. 2005). As such, silica gel could bind ·OH very effectively and thus protect the cell from oxidative damage. Bioavailable silica that is absorbed by the plant increases antioxidant enzyme activity which has the ability to detoxify the surplus of reactive oxygen species that are produced under stress (Pei et al. 2010). Silica also reduces membrane damage by preventing lipid peroxidation, and silica deposits in epidermal cell and the cuticular surface protect the plant against water loss and improves the overall water balance (see *5.2.2. & 5.2.3. Drought Resistance*). It needs to be noted that the exact role of silica in the various plant pathways is at a molecular level is as of yet rather unclear. For instance, Liang et al. (2015) discovered that there is feedback between silicon and ethylene signaling; without ethylene, silicon fails to enhance pathogenic resistance and might even induce cell death processes in certain plants. This is just an example of how intricately connected and complex these pathways are.

4.2. Silica as protector against environmental stress

4.2.1. Drought Resistance: Reduced evaporation

The deposition of biogenic silica in epidermal plant tissue is often invoked as protectant against drought. Sheets of silica in the upper epidermal cells of the leaves form a physical barrier against evaporation in addition to the cuticle (Keutman et al. 2015; Kaufman et al. 1971; Sangster 1970). Another form of drought stress relief that has been suggested is the slow release of water from the silica gel in the plant (Kaufman et al. 1985). Depending on the amount of silica dissolved in the sap of the plant, it can form a gel. A shift in the water balance can lead to either resorption of water out of the gel-like solution, or it can add more water to the gel making it more viscous (Kaufman et al. 1985; Yoshida, Ohnishi, and Kitagishi 1962). Liang and others(2008) have suggested that plants are able to reduce their evapotranspiration rate because the accumulation of polar monosilicic acid and/or polymerized silicic acid in the epidermal cell walls. They suggested the hydrogen bonds between water and $SiO_2 \bullet H_2O$ prevent water loss even when the stomata are open.

4.2.2. Drought Resistance: Increased root/shoot biomass

Multiple studies have investigated improved drought tolerance by increased cavitation resistance of vessels and/or improved hydraulic conductivity under drought stress. It has been suggested that silica would reinforce the vessels and keep them open, like a stent, under negative pressure (Coughenour 1985) however, solid proof for this has not been found yet (Pei et al. 2010; Sonobe et al. 2009). Silica does alleviate biotic and abiotic stress by improving the plants' hydration status (Pei et al. 2010). This has two benefits; adequate hydration levels support optimal nutrient delivery and waste product removal, and additional less cellular dehydration results in less reactive oxygen species are being produced (also see *5.3.1. Pathogen protection*).

Much research on how silica alleviates drought stress was focused on evaporation modulation. However, Yin and colleagues (Yin et al. 2014) found that the improved relative water content—the water content of a given amount of leaf relative to its fully hydrated or fully turgid state—is regulated literally from the other end of the plant; the roots. An increased root to shoot biomass, stimulated by silica, would not directly protect the above-ground plant mass from drought stress necessarily, but instead indirectly alleviate the water shortage by an improved ability to absorb water from the soil. In contrast to what Yin and colleagues found earlier in Maize, stomatal conductivity in silica-fertilized *Sorghum* (Poaceae) was just as high as in the control plants (Yin et al. 2013). In their previous studies, they determined that it was not an increased amount of polyamines that was responsible for the higher relative water content. PAs are associated with stomatal opening and closure in plants (Liu et al. 2000). As the polyamine levels between

the silicon-treated plants and the control group were similar, Yin et al. concluded that the source of the improved water balance was not the result of improved stomatal regulation but the effect of the silica on the roots. Depending on the surface, anatomy and hydraulic conductivity of the roots, water is absorbed as a result of a combination of the hydrostatic pressure gradient and osmotic gradient. The osmotic potential of the roots was not increased under the influence of additional silica, but the root/shoot ratio was higher in the silicon-treated plants (Yin et al. 2013). The higher root mass was linked to higher polyamine levels and lower aminocyclopropane-1-carboxylic acid (ACC) concentrations in the root tissue, which suggests that silicon may alter the physical anatomy and thereby the surface area of the roots (Yin et al. 2014).

4.2.3. Silica as anti-freeze

Silica will, like any other solute, lower the water's freezing point, allowing for super-cooling of these solutions. As a result, even when the internal temperature of the plant drops below 0°C, the sap in the cells, xylem and phloem will not freeze, protecting the tissues from the potentially damaging effects of the growth of ice crystals (Larcher et al. 1991). Other elements can have a similar effect, but some have particularly deleterious effects (e.g. sodium (Na^+)) because they hamper cellular metabolic processes and alter the plant's osmotic equilibrium (Flowers et al. 2015).

4.2.4. Silica as sunscreen

Rice plants (*Oryza sativa*), supplemented with silica, reflect more radiation in the UV-B spectrum (280 - 320 nm) than control plants (Goto et al. 2003). The silica forms a ~2.5 µm thin layer underneath the cuticle and reduces the transmission of the UV-B ration to the underlying tissues (Ma and Yamaji 2006). The protective role of silica may not be solely mechanically; promoted by the presence of silica, UV-B radiation may also trigger the synthesis of UV-absorbing compounds such as phenolic acids and flavonoids which protect the plants against damage (Datnoff, Snyder, and Korndörfer 2001).

4.2.5. Chemical stress – salinity

Salt (NaCl), though essential to a degree, can be extremely detrimental to plant growth. To keep adequate cell turgor, some taxa synthesize sufficient organic compounds (sugars, organic acids) to draw in enough water to equalize the concentrations between the interstitial water and the plant itself (Campbell and Reece 2005). Increasing the osmotic value in their tissues using organic compounds comes at a cost; a loss of energy that otherwise could have been directed at growth and/or reproduction. Silica mediates tolerance to high salinity levels in several ways. It inhibits evapotranspiration, it increases root activity, and changes the charge of the root plasma membrane which results in a decrease of Na^+ absorption (Y. Liang et al. 2007, 2006; See also *5.2.2. Drought Resistance: Increased root/shoot biomass*).

4.2.6. Chemical stress – heavy metals

Silica in plants has the ability to moderate and modify the amount of heavy metals that is circulating in the plant sap. High heavy metal concentrations have direct and indirect deleterious effects on plants. It affects the plants directly by inhibiting cytoplasmatic enzymes as the metals bind with the enzymes' sulfhydryl groups which affects the enzymes' structural integrity and function (Van Assche and Clijsters 1990). Under the influence of light, copper also catalyzes a Fenton-type reaction, where free radicals formed from H_2O_2, destabilize the thylakoid membrane inside chloroplasts (Pospíšil 2009). Because the light-dependent reactions of photosynthesis taking place directly in the membrane, the integrity of the membrane is critical to the plants' ability to fix CO_2 (Clijsters and Van Assche 1985). Due to their charge, heavy metals can inhibit electron transport, thereby reducing CO_2 fixation (Malčovská et al. 2014). Another direct deleterious effect of (heavy) metal absorption is the accumulation of metal ions also disturbs cellular ionic homeostasis, which is critical to solute flow and/or signal transfer (Dubyak 2004).

High metal concentrations indirectly affect the plants in at least two ways. The metals bind tightly at cation exchange sites of soil that otherwise would have been taken up by elements that are beneficial for the plant (Giller, Witter, and McGrath 1998). For example, Pb^{2+} and Cu^{2+} are more readily adsorbed than iron, zinc, copper and manganese, because it is energetically more favorable (McBride 1989). Another indirect effect is the toxic effect of metals to the soil microorganism, which leads to a slower and/or less effective organic matter turnover (Giller, Witter, and McGrath 1998).

There are several studies that suggest that silica alleviates the stress caused by high levels of heavy metal (density $\geq$ 5 g/cm^3) concentrations in soils. Some metals, e.g., cobalt, copper, iron, manganese, molybdenum, nickel and zinc, are essential micro-nutrients for plants and play an important role in photosynthesis, respiration, and nitrogen assimilation (Shah et al. 2010), while others, such as cadmium, chromium, lead and mercury, have no role in a plants' functioning (Nagajyoti, Lee, and Sreekanth 2010). Shi et al. (2005) described how toxic quantities of manganese resulted in increased amounts of hydrogen peroxide which can lead to oxidative stress in plants. Silica has been shown to alleviate the stress of these elements by incorporating and/or binding them, a process also called co-deposition (Hodson and Evans 1995; Neumann and Zur Nieden 2001). By incorporating the metals into the apoplastic silica matrix, the silica precipitate prevents the metals from interfering with cellular processes (Wang, Stass, and Horst 2004).

4.3. Silica as protector against biotic stress

4.3.1. Pathogen protection

Incorporating silica in its tissues increases the plants' defense against pathological fungi (Van Bockhaven et al. 2015; Massey, Ennos, and Hartley 2006; Keeping and Kvedaras 2008). For a long time, it was believed that the incorporated silica protected against pathogens simply because it forms a physical barrier. The hyphae were assumed to be incapable of penetrating the plant cells successfully and therefore the fungus would not succeed at infecting the plant. Though this might hold up in some plant groups, Samuels et al. (1991) demonstrated that this is not an accurate interpretation of the processes in cucumber plants (*Cucumis sativus*). In silica fertilization experiments, the leaves showed rapid silicification of leafy tissue, primarily in the trichome bases, with an increased resistance to powdery mildew infections as a result. However, after silica supplements were no longer administered, and even though the silicified cells were still in place, the plants became susceptible again to fungal infection. While the silica incorporated the epidermal and mesophyll cells plays an important role in preventing infections, the dissolved silica helps in fighting off infections once they have entered the plant. Once polymerized into phytoliths, silica fails to induce defense responses (Chérif et al. 1992). This could imply that the defense mechanism is associated with the process of phytolith production; once the silica is polymerized, thermodynamic considerations dictate that the silica is unlikely to redissolve (Iler 1979). Keeping the silica in solution may therefore be beneficial to the plants. This could explain why, for example non-silica accumulators/non-excluders like cucumber plants, still benefit hugely from silicate treatment in nutrient solutions (Samuels et al. 1991).

The course of an infection of a plant by a pathogen has three stages:1) the infected cells trigger a primary response, 2) the adjacent cells are signaled by elicitors, and 3) a systemic response signaling all the tissues of the plant (Hutcheson 1998). It has been suggested that silica plays a role in the primary response; the production of phytoalexins and other antimicrobial antioxidative substances such as chitinases, peroxidases and polyphenoloxydases, increases under the influence of silica (Chérif et al. 1994). Whether the silica serves as an activator or a modulator is not quite clear. Some suggest that it aids in pathogen resistance through an activation of a gene regulation system which stimulates the production of phenolics and lignin-like materials (Chérif et al. 1992). Others propose that silica helps by preventing pathogens from hijacking the ethylene pathway which would inhibit ethylene production (Van Bockhaven et al. 2015). The role of this plant hormone is critical to plant functioning, and includes fruit ripening, signaling, senescence and abscission as well as stem elongation, promotion of stem thickening and horizontal growth (Bleecker and Kende, 2000).

4.3.2. Herbivore defense

Plants have evolved various strategies to protect themselves against herbivory, mechanical defense being one of them. While these structural defenses discourage herbivory, they also come at a cost. Using silica instead of carbon-based alternatives, e.g. lignin, is estimated to be between 10 to 20 times more energy efficient (Raven 1983). It is interesting to note that while epidermal pubescence and prickles are often silicified, large spines are typically reinforced by lignin instead of silica (Sangster et al. 2001; Piperno 2006; Hanley et al. 2007).

Herbivores come in different shapes and sizes including the larger grazing vertebrates and the often smaller, invertebrate herbivores. While smaller animals are able to actively select plants with lower silica content, the larger grazers cannot (Massey et al. 2009). The dental wear in grazers has long been attributed to the relative high concentration of silica in grasses (e.g. MacFadden 2000; McNaughton et al. 1985). This is counterintuitive because the enamel of mammalian teeth is considerably harder than phytoliths, 51–211 versus 257–397 on the Vickers Hardness scale (Sanson et al. 2007). The bulk of the damage in grazers is done by the inorganic soil matrix that is inadvertently consumed while feeding (Strömberg et al. 2016). Still, microwear by silica cannot be ruled out (Lucas et al. 2013). The density, hardness, solubility and viscosity of biogenic silica varies considerably with the hydration level (Mann and Perry 1986), and fracture toughness and scratch angle also play a role. The softer dentin and cementum, which makes up much of the surface area of teeth once the cusps are breached, i.e., through most of the life of the animal, can be worn by phytoliths (Erickson 2014). A series of simulations regarding the wear of mammalian herbivore teeth as a result of mastication showed that tooth morphology also determines the amount of expected wear (Kaiser et al. 2016)

For smaller sized herbivores, the silica content of plant tissues matters much more. Massey et al. (2007) measured a 400% increase in foliar silica content in two different grass species in response to damage by voles or locusts. To demonstrate that the increased silica levels also functions as a defense mechanism, the researchers fed the affected plant material back to the animals. Both groups favored the control plants over the feed with higher silica concentrations. The elevated silica concentrations affected the palatability of the food, and had a deterring effect on both types of herbivores.

How silica protects plants physically from herbivorous insects is more straightforward. To successfully gain access to the cell contents, an insect first has to break through or break up the cell walls. Cell walls that are reinforced with silica may prevent an insect from penetrating the cell entirely, or it may hinder feeding. Silica fortification has also been shown to wear down irreversible mandible damage in insects (Massey and Hartley 2009).

While the direct silica protection in herbivory defense stems from providing a physical barrier, the indirect role is the result of chemical processes. For example, the colonization of stem-boring insects such as Grass flies (Chloropidae), whose larvae develop inside the vegetative or reproductive parts of Poales (which include grasses), can be hampered by silica in several ways (Massey et al. 2006). A number of factors contribute to the reduced intensity of an infestation. Firstly, a silicified surface may turn off the female fly, as surface texture plays an important role in determining a suitable site for oviposition. Fewer eggs results in a decreased total pupal mass. Secondly, the larvae that do find their way into the host plant are limited in their movement as the silicified parts form barriers and thereby limiting the larvae damaging effect. Thirdly, the larvae that feed on plants with higher silica content tend to grow slower, leaving them more vulnerable to predators and other compromising factors. And fourthly, with increased silica encrusted/filled tissue there is simply less edible plant tissue for the larvae to feed on (Moore 1984; Massey et al. 2006).

4.4. Structural support

Plants can gain structural support by strategically distributing the silica throughout their tissue ((Takahashi and Miyake 1977). Rice, a natural silica accumulator, is estimated to provide 20 percent of the world's dietary energy (FAO 2016). Intensive farming practices along with extensive fertilization use are needed to keep up with crop demands. Fertilizing rice with nitrogen alone, however, makes the leaves droopy, which reduces its photosynthetic capabilities (Yoshida et al. 1969). Adding bio-available silica provides the rice plant with the necessary rigidity which allows it to stand more erect; a trait that is directly and positively correlated with the dry-matter content of the plant. Improved leaf rigidity following silica fertilization has been observed in many other agricultural plants, e.g. cucumber and lettuce (*Lactuca sativa*) (Toresano-Sánchez et al., 2012; Takahashi et al., 1990). This improved stature, more robust foliage, may be particularly advantageous to plants when competing for light (Quigley and Anderson 2014). All this said, even heavy accumulators like rice and wheat, can be grown to maturity with nutrient solutions without added silicon, particularly in the absence of biotic or abiotic stress (Epstein 2009). Besides the effect of silica on the structural integrity of the leaves, there is also reduced lodging, a bending of the plants at the roots or the stems, as a result of climatic stress (Wang et al. 2001)

5. Conclusion

Incorporating silica has a multitude of benefits for plants that leads to improved fitness. Some of these benefits have been extensively studied and proven, while others have merely been suggested without much evidence. These benefits range from providing the plants with physical support, to a (passive) toxin

absorber and chemically, as a catalyst in reactions that enhance plant resistance and/or tolerance to various biotic (pathogens, herbivores) and abiotic (climate, salinity, radiation) stresses. Silica also plays a role in the core biochemical cycling of ethylene, a gas that influences many aspects of a plants' life. While it is clear that plants, particularly under environmental stress, benefit from available silica, at the molecular level, the exact role of silica is as of yet unclear. Future research should therefore be aimed at studying the proposed benefits as, particularly considering anticipated future climate change combined with human population growth, will put more pressure on the food chain under increasingly deterioration conditions. Crops that are more resilient to environmental stress will be essential to food security. A greater understanding of interplay between phytolith production in plant health will aid in the interpretation of phytoliths as micro-fossils and possibly expand the application of phytoliths as indicators for environmental conditions or biotic stress factors.

WORK CITED

Blackman, Elizabeth. 1968. “The Pattern and Sequence of Opaline Silica Deposition in Rye (Secale Cereale L.).” *Annals of Botany* 32 (1):207–18.

Bleecker, Anthony B., and Hans Kende. 2000. “Ethylene: A Gaseous Signal Molecule in Plants.” *Annual Review of Cell and Developmental Biology* 16 (1):1–18. https://doi.org/10.1146/annurev.cellbio.16.1.1.

Bremond, L. 2004. “Advantages and Disadvantages of Phytolith Analysis for the Reconstruction of Mediterranean Vegetation: An Assessment Based on Modern Phytolith, Pollen and Botanical Data (Luberon, France).” *Review of Palaeobotany and Palynology* 129 (4):213–28. https://doi.org/10.1016/j.revpalbo.2004.02.002.

Campbell, Neil A, and Jane B Reece. 2005. “Biology.” In *Biology*, 738–51. San Francisco: Pearson, Benjamin Cummings.

Chérif, M., A. Asselin, and R.R. Bélanger. 1994. “Defense Responses Induced by Soluble Silicon in Cucumber Roots Infected by Pythium Spp.” *Phytopathology* 84 (3):236–42.

Chérif, M., N. Benhamou, J. G. Menzies, and R. R. Bélanger. 1992. “Silicon Induced Resistance in Cucumber Plants against Pythium Ultimum.” *Physiological and Molecular Plant Pathology* 41 (6):411–25. https://doi.org/10.1016/0885-5765(92)90053-X.

Clijsters, H., and F. Van Assche. 1985. “Inhibition of Photosynthesis by Heavy Metals.” *Photosynthesis Research* 7 (1):31–40. https://doi.org/10.1007/BF00032920.

Coughenour, Michael B. 1985. “Graminoid Responses to Grazing by Large Herbivores: Adaptations, Exaptations, and Interacting Processes.” *Annals of the Missouri Botanical Garden* 72 (4):852. https://doi.org/10.2307/2399227.

Currie, Heather A., and Carole C. Perry. 2007. “Silica in Plants: Biological, Biochemical and Chemical Studies.” *Annals of Botany* 100 (7):1383–89. https://doi.org/10.1093/aob/mcm247.

Darwin, Charles. 1909a. *The Voyage of the Beagle*. P.F. Collier.

———. 1909b. *The Voyage of the Beagle*. New York: P.F. Collier.

Datnoff, L. E., George H. Snyder, and G. H. Korndörfer, eds. 2001. *Silicon in Agriculture*. 1st ed. Studies in Plant Science 8. New York: Elsevier.

Delseny, Michel, and Jean-Claude Kader. 2007. *Advances in Botanical Research. Volume 46, Volume 46,*. Boston; Amsterdam: Elsevier. http://site.ebrary.com/id/10216734.

Dubyak, George R. 2004. “Ion Homeostasis, Channels, and Transporters: An Update on Cellular Mechanisms.” *Advances in Physiology Education* 28 (4):143–54. https://doi.org/10.1152/advan.00046.2004.

Ehrenberg, Christian Gottfried. 1849. *Passat-Staub und Blut-Regen: Ein grosses organisches unsichtbares Wirken und Leben in der Athmosphäre: mehrere Vorträge*.

Epstein, E. 2009. “Silicon: Its Manifold Roles in Plants.” *Annals of Applied Biology* 155 (2):155–60. https://doi.org/10.1111/j.1744-7348.2009.00343.x.

Erickson, Kayley L. 2014. “Prairie Grass Phytolith Hardness and the Evolution of Ungulate Hypsodonty.” *Historical Biology* 26 (6):737–44. https://doi.org/10.1080/08912963.2013.841155.

FAO. 2016. *Save and Grow: Maize, Rice and Wheat.* Rome: Food & Agriculture Org.

Fauteux, François, Wilfried Rémus-Borel, James G. Menzies, and Richard R. Bélanger. 2005. “Silicon and Plant Disease Resistance against Pathogenic Fungi.” *FEMS Microbiology Letters* 249 (1):1–6. https://doi.org/10.1016/j.femsle.2005.06.034.

Flowers, Timothy J., Rana Munns, and Timothy D. Colmer. 2015. “Sodium Chloride Toxicity and the Cellular Basis of Salt Tolerance in Halophytes.” *Annals of Botany* 115 (3):419–31. https://doi.org/10.1093/aob/mcu217.

Galil, J. 1968. “An Ancient Technique for Ripening Sycomore Fruit in East-Mediterranean Countries.” *Economic Botany* 22 (2):178–90. https://doi.org/10.1007/BF02860561.

Giller, Ken E, Ernst Witter, and Steve P Mcgrath. 1998. “Toxicity of Heavy Metals to Microorganisms and Microbial Processes in Agricultural Soils: A Review.” *Soil Biology and Biochemistry* 30 (10–11):1389–1414. https://doi.org/10.1016/S0038-0717(97)00270-8.

Goto, Masakazu, Hiroshi Ehara, Shyuichi Karita, Keiji Takabe, Natsumi Ogawa, Yutaka Yamada, Satoru Ogawa, Mohammed Sani Yahaya, and Osamu Morita. 2003. “Protective Effect of Silicon on Phenolic Biosynthesis and Ultraviolet Spectral Stress in Rice Crop.” *Plant Science* 164 (3):349–56. https://doi.org/10.1016/S0168-9452(02)00419-3.

Hanley, Mick E., Byron B. Lamont, Meredith M. Fairbanks, and Christine M. Rafferty. 2007. “Plant Structural Traits and Their Role in Anti-Herbivore Defence.” *Perspectives in Plant Ecology, Evolution and Systematics* 8 (4):157–78. https://doi.org/10.1016/j.ppees.2007.01.001.

Hodson, M. J., and D.E. Evans. 1995. “Aluminium/Silicon Interactions in Higher Plants.” *Journal of Experimental Botany* 46 (2):161–71. https://doi.org/10.1093/jxb/46.2.161.

Hodson, M. J., and A. G. Sangster. 1998. “Mineral Deposition in the Needles of White Spruce [Picea Glauca(Moench.) Voss].” *Annals of Botany* 82 (3):375–85. https://doi.org/10.1006/anbo.1998.0694.

Hodson, Martin J., Adrian G. Parker, Melanie J. Leng, and Hilary J. Sloane. 2008. “Silicon, Oxygen and Carbon Isotope Composition of Wheat (Triticum Aestivum L.) Phytoliths: Implications for Palaeoecology and Archaeology.” *Journal of Quaternary Science* 23 (4):331–39. https://doi.org/10.1002/jqs.1176.

Honaine, M.F., A.F. Zucol, and M.L. Osterrieth. 2009. “Phytolith Analysis of Cyperaceae from the Pampean Region, Argentina.” *Australian Journal of Botany* 57 (6):512–23.

Hutcheson, Steven W. 1998. “Current Concepts of Active Defense in Plants.” *Annual Review of Phytopathology* 36 (1):59–90. https://doi.org/10.1146/annurev.phyto.36.1.59.

Iler, Ralph K. 1979. *The Chemistry of Silica: Solubility, Polymerization, Colloid and Surface Properties, and Biochemistry*. Canada: John Wiley &Sons Inc.

Jones, L.H.P., and K. A. Handreck. 1967. “Silica in Soils, Plants and Animals.” In *Advances in Agronomy. Vol. 19 Vol. 19*, edited by A. G Norman, 107–49. New York: Academic Press. http://site.ebrary.com/id/10235536.

Kaiser, Thomas M., Marcus Clauss, and Ellen Schulz-Kornas. 2016. “A Set of Hypotheses on Tribology of Mammalian Herbivore Teeth.” *Surface Topography: Metrology and Properties* 4 (1):014003. https://doi.org/10.1088/2051-672X/4/1/014003.

Kaufman, Wilbur C. Bigelow, Rudolf Schmid, and Najati S. Ghosheh. 1971. “Electron Microprobe Analysis of Silica in Epidermal Cells of Equisetum.” *American Journal of Botany* 58 (4):309–16. https://doi.org/10.2307/2441411.

Kaufman, P.B., P. Dayanandan, C. I. Franklin, and Y. Takeoka. 1985. “Structure and Function of Silica Bodies in the Epidermal System of Grass Shoots.” *Annals of Botany* 55 (4):487–507.

Kazemi, M., M. GHolami, and F. Bahmanipou. 2012. “Effect of Silicon and Acetylsalicylic Acid on Antioxidant Activity, Membrane Stability and ACC-Oxidase Activity in Relation to Vase Life of Carnation Cut Flowers.” *Biotechnology(Faisalabad)* 11 (2):87–90. https://doi.org/10.3923/biotech.2012.87.90.

Keeping, Malcolm G., and Olivia L. Kvedaras. 2008. “Silicon as a Plant Defence against Insect Herbivory: Response to Massey, Ennos and Hartley.” *Journal of Animal Ecology* 77 (3):631–33. https://doi.org/10.1111/j.1365-2656.2008.01380.x.

Keutman, I.C., B. Melzer, R. Seidel, R. Thomann, and T. Speck. 2015. “Review: The Functions of Phytoliths in Land Plants.” In *Evolution of Lightweight Structures: Analyses and Technical Applications*, edited by Christian Hamm, 157–69. Biologically-Inspired Systems, Volume 6. Dordrecht ;Heidelberg ;New York ;London: Springer.

Kirchholtes, Renske P. J., J. M. van Mourik, and B. R. Johnson. 2015. “Phytoliths as Indicators of Plant Community Change: A Case Study of the Reconstruction of the Historical Extent of the Oak Savanna in the Willamette Valley Oregon, USA.” *CATENA* 132 (September):89–96. https://doi.org/10.1016/j.catena.2014.11.004.

Kump, Lee R., James F. Kasting, and Robert G. Crane. 2010. *The Earth System*. 3rd ed. San Francisco: Prentice Hall.

Larcher, Walter, Ursula Meindl, Elisabeth Ralser, and Masaya Ishikawa. 1991. "Persistent Supercooling and Silica Deposition in Cell Walls of Palm Leaves." *Journal of Plant Physiology* 139 (2):146–54. https://doi.org/10.1016/S0176-1617(11)80599-7.

Lewin, J, and B E F Reimann. 1969. "Silicon and Plant Growth." *Annual Review of Plant Physiology* 20 (1):289–304. https://doi.org/10.1146/annurev.pp.20.060169.001445.

Liang, Xiaolei, Huahua Wang, Yanfeng Hu, Lina Mao, Lili Sun, Tian Dong, Wenbin Nan, and Yurong Bi. 2015. "Silicon Does Not Mitigate Cell Death in Cultured Tobacco BY-2 Cells Subjected to Salinity without Ethylene Emission." *Plant Cell Reports* 34 (2):331–43. https://doi.org/10.1007/s00299-014-1712-6.

Liang, Yongchao, Wanchun Sun, Yong-Guan Zhu, and Peter Christie. 2007. "Mechanisms of Silicon-Mediated Alleviation of Abiotic Stresses in Higher Plants: A Review." *Environmental Pollution* 147 (2):422–28. https://doi.org/10.1016/j.envpol.2006.06.008.

Liang, Yongchao, Wenhua Zhang, Qin Chen, Youliang Liu, and Ruixing Ding. 2006. "Effect of Exogenous Silicon (Si) on H+-ATPase Activity, Phospholipids and Fluidity of Plasma Membrane in Leaves of Salt-Stressed Barley (Hordeum Vulgare L.)." *Environmental and Experimental Botany* 57 (3):212–19. https://doi.org/10.1016/j.envexpbot.2005.05.012.

Liang, Yongchao, Jia Zhu, Zhaojun Li, Guixin Chu, Yanfang Ding, Jie Zhang, and Wanchun Sun. 2008. "Role of Silicon in Enhancing Resistance to Freezing Stress in Two Contrasting Winter Wheat Cultivars." *Environmental and Experimental Botany* 64 (3):286–94. https://doi.org/10.1016/j.envexpbot.2008.06.005.

Liu, Kun, Huihua Fu, Qixin Bei, and Sheng Luan. 2000. "Inward Potassium Channel in Guard Cells As a Target for Polyamine Regulation of Stomatal Movements." *Plant Physiology* 124 (3):1315–26. https://doi.org/10.1104/pp.124.3.1315.

Lucas, P. W., R. Omar, K. Al-Fadhalah, A. S. Almusallam, A. G. Henry, S. Michael, L. A. Thai, J. Watzke, D. S. Strait, and A. G. Atkins. 2013. "Mechanisms and Causes of Wear in Tooth Enamel: Implications for Hominin Diets." *Journal of The Royal Society Interface* 10 (80):20120923–20120923. https://doi.org/10.1098/rsif.2012.0923.

Ma, Jian Feng, and Naoki Yamaji. 2006. "Silicon Uptake and Accumulation in Higher Plants." *Trends in Plant Science* 11 (8):392–97. https://doi.org/10.1016/j.tplants.2006.06.007.

MacFadden, B.J. 2000. "Cenozoic Mammalian Herbivores from the Americas: Reconstructing Ancient Diets and Terrestrial Communities." *Annual Review of Ecology and Systematics* 31:33–59.

Malčovská, Silvia Mihaličová, Zuzana Dučaiová, Ivana Maslaňáková, and Martin Bačkor. 2014. "Effect of Silicon on Growth, Photosynthesis, Oxidative Status and Phenolic Compounds of Maize (Zea Mays L.) Grown in Cadmium Excess." *Water, Air, & Soil Pollution* 225 (8):2056. https://doi.org/10.1007/s11270-014-2056-0.

Mann, S., and Carole C. Perry. 1986. "Structural Aspects of Biogenic Silica." In *Silicon Biochemistry*, edited by David Evered and Maeve O'Connor, 40–58. Ciba Foundation Symposium 121. Chichester [West Sussex] ; New York: Wiley.

Massey, Fergus P., A. Roland Ennos, and Sue E. Hartley. 2006. "Silica in Grasses as a Defence against Insect Herbivores: Contrasting Effects on Folivores and a Phloem Feeder: Antiherbivore Effects of Silica in Grasses." *Journal of Animal Ecology* 75 (2):595–603. https://doi.org/10.1111/j.1365-2656.2006.01082.x.

Massey, Fergus P., and Sue E. Hartley. 2009. "Physical Defences Wear You down: Progressive and Irreversible Impacts of Silica on Insect Herbivores." *Journal of Animal Ecology* 78 (1):281–91. https://doi.org/10.1111/j.1365-2656.2008.01472.x.

Massey, Fergus P., Kate Massey, A. Roland Ennos, and Sue E. Hartley. 2009. "Impacts of Silica-Based Defences in Grasses on the Feeding Preferences of Sheep." *Basic and Applied Ecology* 10 (7):622–30. https://doi.org/10.1016/j.baae.2009.04.004.

Massey, Fergus P., A. Roland Ennos, and Sue E. Hartley. 2007. “Herbivore Specific Induction of Silica-Based Plant Defences.” *Oecologia* 152 (4):677–83. https://doi.org/10.1007/s00442-007-0703-5.
Maurel, Christophe, Lionel Verdoucq, Doan-Trung Luu, and Véronique Santoni. 2008. “Plant Aquaporins: Membrane Channels with Multiple Integrated Functions.” *Annual Review of Plant Biology* 59 (1):595–624. https://doi.org/10.1146/annurev.arplant.59.032607.092734.
McBride, M.B. 1989. “Reactions Controlling Heavy Metal Solubility in Soils.” In *Advances in Soil Science*, 10:1–56. Advances in Soil Science. New York, NY: Springer New York. http://link.springer.com/10.1007/978-1-4613-8847-0.
McNaughton, S. J., J. L. Tarrants, M. M. McNaughton, and R. D. Davis. 1985. “Silica as a Defense against Herbivory and a Growth Promotor in African Grasses.” *Ecology* 66 (2):528–35. https://doi.org/10.2307/1940401.
Moore, D. 1984. “The Role of Silica in Protecting Italian Ryegrass (Lolium Multiflorum) from Attack by Dipterous Stem-Boring Larvae (Oscinellafiit and Other Related Species).” *Annals of Applied Biology* 104 (1):161–66. https://doi.org/10.1111/j.1744-7348.1984.tb05598.x.
Morfit, Campbell. 1848. *Manures, Their Composition, Preparation, and Action Upon Soils: With the Quantities to Be Applied. Being a Field Companion for the Farmer. From the French of Standard Authorities*. Lindsay and Blakiston.
Motomura, H., K. Hikosaka, and M. Suzuki. 2007. “Relationships Between Photosynthetic Activity and Silica Accumulation with Ages of Leaf in Sasa Veitchii (Poaceae, Bambusoideae).” *Annals of Botany* 101 (3):463–68. https://doi.org/10.1093/aob/mcm301.
Murray, John, and Robert Irvine. 1892. “On Silica and the Siliceous Remains of Organisms in Modern Seas.” *Proceedings of the Royal Society of Edinburgh* 18:229–50. https://doi.org/10.1017/S0370164600007392.
Nagajyoti, P. C., K. D. Lee, and T. V. M. Sreekanth. 2010. “Heavy Metals, Occurrence and Toxicity for Plants: A Review.” *Environmental Chemistry Letters* 8 (3):199–216. https://doi.org/10.1007/s10311-010-0297-8.
Neljubow, D. 1902. “Über Die Horizontale Nutation Der Stengel von Pisum Sativum Und Einiger Anderen Pflanzen.” *Zeitschrift Für Pflanzenkrankheiten* 12 (1/2):65 (12pgs total).
Neumann, D., and U. zur Nieden. 2001. “Silicon and Heavy Metal Tolerance of Higher Plants.” *Phytochemistry* 56 (7):685–92. https://doi.org/10.1016/S0031-9422(00)00472-6.
Okuda, Azuma, and Eiichi Takahashi. 1965. “The Role of Silicon - The Mineral Nutrition of the Rice Plant.”
Otto, B., and R. Kaldenhoff. 2000. “Cell-Specific Expression of the Mercury-Insensitive Plasma-Membrane Aquaporin NtAQP1 from Nicotiana Tabacum.” *Planta* 211 (2):167–72. https://doi.org/10.1007/s004250000275.
Overmyer, Kirk, Hannele Tuominen, Reetta Kettunen, Christian Betz, Christian Langebartels, Heinrich Sandermann, and Jaakko Kangasjärvi. 2000. “Ozone-Sensitive Arabidopsis Rcd1 Mutant Reveals Opposite Roles for Ethylene and Jasmonate Signaling Pathways in Regulating Superoxide-Dependent Cell Death.” *The Plant Cell* 12 (10):1849–62. https://doi.org/10.1105/tpc.12.10.1849.
Pandey, S., S A Ranade, P K Nagar, and Nikhil Kumar. 2000. “Role of Polyamines and Ethylene as Modulators of Plant Senescence.” *Journal of Biosciences* 25 (3):291–99. https://doi.org/10.1007/BF02703938.
Pei, Z. F., D. F. Ming, D. Liu, G. L. Wan, X. X. Geng, H. J. Gong, and W. J. Zhou. 2010. “Silicon Improves the Tolerance to Water-Deficit Stress Induced by Polyethylene Glycol in Wheat (Triticum Aestivum L.) Seedlings.” *Journal of Plant Growth Regulation* 29 (1):106–15. https://doi.org/10.1007/s00344-009-9120-9.
Piperno, Dolores R. 2006. *Phytoliths : A Comprehensive Guide for Archaeologists and Paleoecologists*. Lanham, Md.: AltaMira.
Pospíšil, Pavel. 2009. “Production of Reactive Oxygen Species by Photosystem II.” *Biochimica et Biophysica Acta (BBA) - Bioenergetics* 1787 (10):1151–60. https://doi.org/10.1016/j.bbabio.2009.05.005.

Pumpelly, Raphael. 1908. *Explorations in Turkestan - Expedition of 1904*. Carnegie institution of Washington.
Quigley, Kathleen M., and T. M. Anderson. 2014. "Leaf Silica Concentration in Serengeti Grasses Increases with Watering but Not Clipping: Insights from a Common Garden Study and Literature Review." *Functional Plant Ecology* 5:568. https://doi.org/10.3389/fpls.2014.00568.
Raven, John A. 1983. "The Transport and Function of Silicon in Plants." *Biological Reviews* 58 (2):179–207. https://doi.org/10.1111/j.1469-185X.1983.tb00385.x.
Samuels, A. L., A. D. M. Glass, D. L. Ehret, and J. G. Menzies. 1991. "Mobility and Deposition of Silicon in Cucumber Plants." *Plant, Cell & Environment* 14 (5):485–92. https://doi.org/10.1111/j.1365-3040.1991.tb01518.x.
Sangster, A. G. 1970. "Intracellular Silica Deposition in Immature Leaves in Three Species of the Gramineae." *Annals of Botany* 34 (1):245–57.
Sangster, A.G., M. J. Hodson, and H.J. Tubb. 2001. "Silicon Deposition in Higher Plants." In *Silicon in Agriculture*, edited by L. E. Datnoff, George H. Snyder, and G. H. Korndörfer, 1st ed, 85–104. Studies in Plant Science 8. New York: Elsevier.
Sanson, Gordon D., Stuart A. Kerr, and Karlis A. Gross. 2007. "Do Silica Phytoliths Really Wear Mammalian Teeth?" *Journal of Archaeological Science* 34 (4):526–31. https://doi.org/10.1016/j.jas.2006.06.009.
Sapei, Lanny, Notburga Gierlinger, Jürgen Hartmann, Robert Nöske, Peter Strauch, and Oskar Paris. 2007. "Structural and Analytical Studies of Silica Accumulations in Equisetum Hyemale." *Analytical and Bioanalytical Chemistry* 389 (4):1249–57. https://doi.org/10.1007/s00216-007-1522-6.
Shah, Fazal Ur Rehman, Nasir Ahmad, Khan Rass Masood, Jose R. Peralta-Videa, and Firoz ud Din Ahmad. 2010. "Heavy Metal Toxicity in Plants." In *Plant Adaptation and Phytoremediation*, edited by M. Ashraf, M. Ozturk, and M. S. A. Ahmad, 71–97. Dordrecht: Springer Netherlands. http://link.springer.com/10.1007/978-90-481-9370-7_4.
Shi, Qinghua, Zhiyi Bao, Zhujun Zhu, Yong He, Qiongqiu Qian, and Jingquan Yu. 2005. "Silicon-Mediated Alleviation of Mn Toxicity in Cucumis Sativus in Relation to Activities of Superoxide Dismutase and Ascorbate Peroxidase." *Phytochemistry* 66 (13):1551–59. https://doi.org/10.1016/j.phytochem.2005.05.006.
Sonobe, Kaori, Taiichiro Hattori, Ping An, Wataru Tsuji, Egrinya Eneji, Kiyoshi Tanaka, and Shinobu Inanaga. 2009. "Diurnal Variations in Photosynthesis, Stomatal Conductance and Leaf Water Relation in Sorghum Grown with or without Silicon under Water Stress." *Journal of Plant Nutrition* 32 (3):433–42. https://doi.org/10.1080/01904160802660743.
Sperry, John S., Volker Stiller, and Uwe G. Hacke. 2003. "Xylem Hydraulics and the Soil–Plant–Atmosphere Continuum." *Agronomy Journal* 95 (6):1362–70. https://doi.org/10.2134/agronj2003.1362.
Steffens, Bianka, and Margret Sauter. 2009. "Epidermal Cell Death in Rice Is Confined to Cells with a Distinct Molecular Identity and Is Mediated by Ethylene and H2O2 through an Autoamplified Signal Pathway." *The Plant Cell* 21 (1):184–96. https://doi.org/10.1105/tpc.108.061887.
Strömberg, Caroline A.E., Verónica S. Di Stilio, and Zhaoliang Song. 2016. "Functions of Phytoliths in Vascular Plants: An Evolutionary Perspective." *Functional Ecology*, May. https://doi.org/10.1111/1365-2435.12692.
Struve, G.A. 1835. "Silica in plantis nonnullis." Thesis, Universitate Litteraria Friderica Guilelma.
Takahashi, E., J. F. Ma, and Y. Miyake. 1990. "The Possibility of Silicon as an Essential Element for Higher Plants." *Comments on Agricultural and Food Chemistry* 2 (2):99–102.
Takahashi, Eiichi, and Yasuto Miyake. 1977. "Silica and Plant Growth." *Proceedings of the International Seminar on Soil Environment and Fertility Management in Intensive Agriculture*.
Toresano-Sánchez, Fernando, Antonio Valverde-García, and Francisco Camacho-Ferre. 2012. "Effect of the Application of Silicon Hydroxide on Yield and Quality of Cherry Tomato." *Journal of Plant Nutrition* 35 (4):567–90. https://doi.org/10.1080/01904167.2012.644375.

Trembath-Reichert, Elizabeth, Jonathan Paul Wilson, Shawn E. McGlynn, and Woodward W. Fischer. 2015. “Four Hundred Million Years of Silica Biomineralization in Land Plants.” *Proceedings of the National Academy of Sciences*, March, 201500289. https://doi.org/10.1073/pnas.1500289112.

Van Assche, F., and H. Clijsters. 1990. “Effects of Metals on Enzyme Activity in Plants.” *Plant, Cell & Environment* 13 (3):195–206. https://doi.org/10.1111/j.1365-3040.1990.tb01304.x.

Van Bockhaven, Jonas, Lukáš Spíchal, Ondřej Novák, Miroslav Strnad, Takayuki Asano, Shoshi Kikuchi, Monica Höfte, and David De Vleesschauwer. 2015. “Silicon Induces Resistance to the Brown Spot Fungus *Cochliobolus Miyabeanus* by Preventing the Pathogen from Hijacking the Rice Ethylene Pathway.” *New Phytologist* 206 (2):761–73. https://doi.org/10.1111/nph.13270.

Van de Poel, Bram, Inge Bulens, Yasmin Oppermann, Marten L. A. T. M. Hertog, Bart M. Nicolai, Margret Sauter, and Annemie H. Geeraerd. 2013. “S-Adenosyl-l-Methionine Usage during Climacteric Ripening of Tomato in Relation to Ethylene and Polyamine Biosynthesis and Transmethylation Capacity.” *Physiologia Plantarum* 148 (2):176–88. https://doi.org/10.1111/j.1399-3054.2012.01703.x.

Wallace, Ian S., Won-Gyu Choi, and Daniel M. Roberts. 2006. “The Structure, Function and Regulation of the Nodulin 26-like Intrinsic Protein Family of Plant Aquaglyceroporins.” *Biochimica et Biophysica Acta (BBA) - Biomembranes* 1758 (8):1165–75. https://doi.org/10.1016/j.bbamem.2006.03.024.

Wang, Li, and Liang. 2001. “Agricultural Utilization of Silicon in China.” In *Silicon in Agriculture*, 343–58. Elsevier Science B.V.

Wang, Yunxia, Angelika Stass, and Walter J. Horst. 2004. “Apoplastic Binding of Aluminum Is Involved in Silicon-Induced Amelioration of Aluminum Toxicity in Maize.” *Plant Physiology* 136 (3):3762–70. https://doi.org/10.1104/pp.104.045005.

Yin, Lina, Shiwen Wang, Jianye Li, Kiyoshi Tanaka, and Mariko Oka. 2013. “Application of Silicon Improves Salt Tolerance through Ameliorating Osmotic and Ionic Stresses in the Seedling of Sorghum Bicolor.” *Acta Physiologiae Plantarum* 35 (11):3099–3107. https://doi.org/10.1007/s11738-013-1343-5.

Yin, Lina, Shiwen Wang, Peng Liu, Wenhua Wang, Dan Cao, Xiping Deng, and Suiqi Zhang. 2014. “Silicon-Mediated Changes in Polyamine and 1-Aminocyclopropane-1-Carboxylic Acid Are Involved in Silicon-Induced Drought Resistance in Sorghum Bicolor L.” *Plant Physiology and Biochemistry* 80 (July):268–77. https://doi.org/10.1016/j.plaphy.2014.04.014.

Yin, Lina, Shiwen Wang, Kiyoshi Tanaka, Shinsuke Fujihara, Akihiro Itai, Xiping Den, and Suiqi Zhang. 2016. “Silicon-Mediated Changes in Polyamines Participate in Silicon-Induced Salt Tolerance in Sorghum Bicolor L.” *Plant, Cell & Environment* 39 (2):245–58. https://doi.org/10.1111/pce.12521.

Yoshida, S., S. A. Navasero, and E. A. Ramirez. 1969. “Effects of Silica and Nitrogen Supply on Some Leaf Characters of the Rice Plant.” *Plant and Soil* 31 (1):48–56. https://doi.org/10.1007/BF01373025.

Yoshida, S., Y. Ohnishi, and K. Kitagishi. 1962. “Chemical Forms, Mobility and Deposition of Silicon in Rice Plant.” *Soil Science and Plant Nutrition* 8 (3):15–21. https://doi.org/10.1080/00380768.1962.10430992.

Chapter 3: First phytoliths in Permian and Triassic redbeds in Texas USA

Abstract

The end-Permian biotic crisis (251.9 Million years ago (Ma) is long known for its profound reorganization of marine ecosystems. What happened on land, particularly to the vegetation, is less well understood. Here we focus on the paleo-environmental and vegetation changes of the western and central part of equatorial Pangea during that time period. We tested if phytolith assemblages can be used to support biostratigraphy of Permian and Triassic strata. While phytolith-based biostratigraphy has been unsuccessful in this study, we demonstrated that phytoliths of Permian and Triassic age can serve as evidence of plant life at the western portion of the supercontinent Pangea, a region previously believed to be barren.

1 Introduction

1.1 A global catastrophe: The end Permian biotic crisis

The end-Permian biotic crisis (251.9 Million years ago (Ma) is long known for its profound reorganization of marine ecosystems (Erwin 2006; Burgess and Bowring 2015). Of the known invertebrate genera, 286 disappeared entirely, contributing to the ~81% overall loss of marine species (Stanley 2016). On land, the fauna was hit similarly hard; insects experience the only mass extinction ever recorded and approximately 89% of terrestrial vertebrate genera, but these numbers are based on relatively few localities (Labandeira and Sepkoski 1993; Benton and Newell 2014). The extinction of marine invertebrate taxa is correlated with a marked negative shift in $\delta^{13}C$ of marine carbonates and terrestrial organic matter, which is indicative of a major disturbance in carbon cycle (Cui et al. 2017). This suggests that a large amount of carbon was added to the atmosphere and oceans (e.g., Payne 2004). There is still animated discussion about the ultimate cause of the crisis, specifically with respect to source and the rate at which the event unfolded, but most of the evidence seems to be pointing to the effects of the Siberian Trap volcanism (for review, see Payne and Clapham 2012; Black et al. 2014).

As a result of preservation bias in the geological record in general, the marine fossil record tend to be more comprehensive than the terrestrial fossil record, which is also the case for the end Permian biotic crisis (Padian 2018). While the record of terrestrial plant is nowhere near as comprehensive as invertebrate records, it does appear that the plants seem to have escaped a fate similar to that of the marine invertebrates. The floral records around the Permian-Triassic boundary are marked by a community turn-over rather than a sudden mass extinction (Knoll 1984; Schneebeli-Hermann, Hochuli, and Bucher 2017). This means that

while there is an observable change in community composition going from the Permian to the Triassic, only very few families disappear completely and are never seen in the fossil record again (McElwain and Punyasena 2007; Rees 2002; Xiong and Wang 2011). Most families are only gone temporarily from the record, to return once either the actual plant returns to the locality or the preservation window is in place again. Shifting continents, an ever changing climate, rising and falling of sea levels, results in an ever changing landscape and its preservational window may catch, or miss the ecological events accordingly (Rees 2002; Looy et al. 2014). That is not to say that diversity did not take a hit at the end of the Permian, because it did; ~50% of all species went extinct. However, it is important to note that taxonomic diversity does not equal ecosystem health per se (McElwain and Punyasena 2007).

At the end of the latest Permian stage (Changhsingian; 254.14 to 251.902 (Gradstein et al 2005), the dieback of woody vegetation dramatically affected terrestrial ecosystems (e.g., Visscher et al. 1996; McElwain and Punyasena 2007). The loss of Cordaitaleans in the northern and Glossopterids in southern humid climatic zones of the supercontinent Pangaea, resulted in the widespread disappearance of coal forming peat forests (Veevers 1994; Retallack 1995). In the semi-arid equatorial region, several conifer taxa (members of the Walchiaceae and Majonicaceae) of the Late Permian Euramerican floral realm became extinct during the Permian-Triassic transition (Poort et al. 1997). Among the surviving plants were lycopsids and seed ferns, which played a central role in the survival phase (e.g. (Looy et al. 2001; Grauvogel-Stamm and Ash 2005). Palynological records from eastern Euramerica indicate that ecosystem recovery to pre-crisis levels of structure and function did not occur before the transition between the Early and Middle Triassic 4–5 Ma later (Looy et al. 1999). The conifers, that do not appear in the Late Permian megaflora and palynological records, seem to be immigrants that invaded eastern Euramerica habitats after surviving or origination elsewhere (Looy et al. 1999). Hitherto, no direct evidence of where the refugional source areas of the immigrants have been located. The western and central part of equatorial Pangea (modern day USA) could be a potential source area for the Euramerican Triassic conifers and other taxa, but there are no palynological and macrofossil plant records known from that region from mid-Guadalupian to mid-Triassic age (DiMichele et al. 2008). As a result, little is known about the paleo-environmental and vegetation changes that occurred over this vast area. A third type of fossil plant remains that have not yet been utilized to reconstruct vegetation and paleoenvironments during this time interval are phytoliths.

Phytoliths are microscopically small concretions of hydrated silica that are produced by plants (e.g. Chave 1984). Phytoliths production varies among different taxonomic groups; in some groups, like the grasses, about 10% of the dry weight consists of silica, while others, e.g. the nightshades, accumulate virtually no silica (e.g., Piperno, 2006; Trembath-Reichert et al., 2015). Phytoliths have been studied and used for applied research for a long time dating back to around 1830s (e.g. Struve 1835). Most of the applications

have been for archaeological research, as many of our crops are prolific phytolith producers (e.g. wheat, rice and maize (Piperno 2006). More recently, phytoliths have been studied for paleobotanical and paleoecological purposes (e.g. Prasad et al. 2005).

Until now, phytoliths have not been used in pre-Cretaceous studies (Strömberg 2004; Piperno and Sues 2005), and we are venturing in unchartered territory. There are four caveats. First, because most studies have been focused on angiosperms. Therefore, phytoliths morphotypes indicative for spore plants and gymnosperms are not well known. Second, according to Trembath-Reichert et al. (2015) several modern spore plant and gymnosperm lineages do not accumulate silica, such as the leptosporangiate ferns, cycads, ginkgoes, and several conifer taxa. Third, the further we go back in time, the more difficult it will be to establish the botanical affinity of certain phytolith morphotypes, which makes reconstructing paleovegetation difficult. And forth, another complicating factor is that it is not always clear whether recovered silica bodies are the result of primary biomineralization or secondary diagenetic processes (Trembath-Reichert et al. 2015). Whether the morphotypes are the result of primary or secondary deposition, while potentially confusing, is not really a problem because it is still evidence of former (plant) life, which is the definition of a fossil.

The aim of this study is threefold: (1) Describe phytolith morphotype and their patterns from latest Permian and earliest Triassic sediments from the Palo Duro Basin, north-central Texas, (2) discuss the potential botanical affinities of the fossil morphotypes, and the evidence for conifer refugia (3) test the potential of phytolith assemblages to support biostratigraphy of Permian and Triassic strata.

2 Material and Methods

2.1 Permian and Triassic rock outcrops: Field sites in Texas

In eastern New Mexico and western Texas, the Permian-Triassic transition is recorded within the sediments of the Ochoan Series. Exposure and preservation of sediment of this age are rare in this region as western Euramerica landscape was subject to erosion due to regression in the Early Triassic (Lucas and Anderson 1993). The Ochoan series consists of a regressive sequence of shallow marine deposits, going to sediments rich in evaporites, to terrestrial redbeds (Tabor et al. 2011). The Ochoan Series are preserved in several basins, including the Palo Duro Basin located in the Texan panhandle. The sediment packages include the Whitehorse Group (known as the Alibates Formation when found in the subsurface; Table 1) which is conformably overlain by the Quartemaster Formation. The Whitehorse Group consists of gypsiferous red sandstones, mudstones, gypsum and dolomites (Gustavson et al. 1982). The beds contain flow ripples and cross lamination, which are mostly intertidal and supratidal deposits and have been interpreted to have been deposited in a perimarine setting. The interfingering layers of evaporites and carbonate deposits with

siliciclastic material are indicative of a warming climate (Nance 1988). While the average temperature worldwide went up, there were major regional climatic differences. For example, data from the Chinese peninsula shows the climate was getting wetter or staying equally humid. The strata in Texas on the other hand show not just a warming climate, but are also indicative of increasingly dry conditions (Tabor and Poulsen 2008). In the Palo Duro Basin the Quartermaster Formation is represented by a 40-75 m thick sediment package, with the lower part consisting of intertidal and supratidal calcareous mudstones and sandstones. The transition to redbed mud- and sandstones is interpreted as fluvial channel deposits (Lehman et al. 1999; Tabor et al. 2011). The late Triassic Dockum Group unconformably overlies the Quartermaster Formation

Table 1. *An overview of the sediments relevant to this study that surface in Caprock Canyon State Park, Palo Duro State Park and the Dickens section.*

Name of formation/group when exposed at surface	Name of formation/group when in subsurface	Age of formation/group
Dockum	Chinle	Upper Triassic
Quartermaster	Dewey Lake	Triassic
Whitehorse	Alibates	Approximately upper 20m is Triassic, rest is of Permian age

younger

older

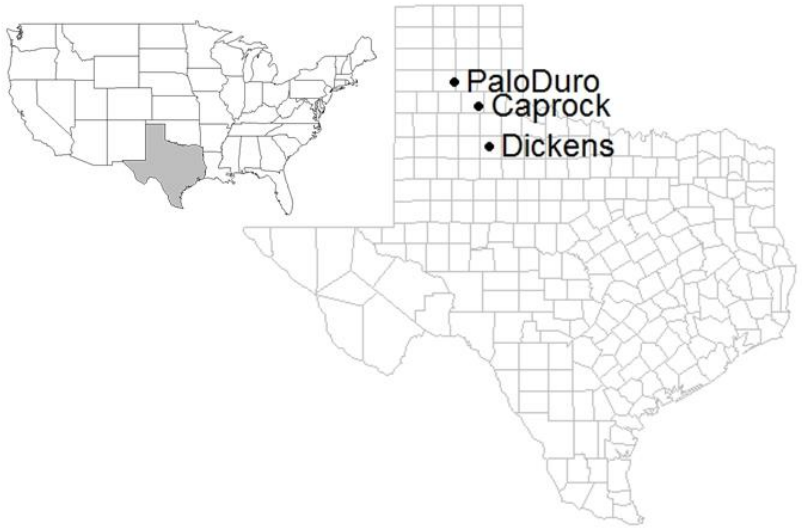

Fig 1. *Location of the sampling sites as positioned in the state of Texas and Texas itself highlighted in grey within the lower 48 of the United States of America.*

Here we focus on three different sites in the Palo Duro Basin: Palo Duro State Park, Caprock Canyon State Park, and Dickens (see Fig. 1). These sections are respectively 65 m, 100 m and 40 m thick, and include

the upper part of the Whitehorse Group, the complete Quartermaster Formation, and the base of the Dockum Group. Based on lithologic, chemostratigraphic, geochronologic and magnetostratigraphic data, the sections appear to be continuous without observable hiatuses (Tabor et al. in prep.). Exposure and preservation of this boundary layer is rare as the western Euramerica landscape was subject to erosion due to regression in the Early Triassic (Lucas and Anderson 1993).

Tephra or volcanic ash layers are deposited simultaneously over large areas at the same time and can therefore be used as marker beds. Two tephra (volcanic ash) horizons, approximately 20 meters apart, were preserved in the lower Quartermaster formation at the Caprock Canyon and Dickens localities. The physical separation in an undeformed depositional environment, rules out that these two layers are the result of the weathering of synclines or anticlines, and therefore represent two separate volcanic events. The chemical comparison by Chang (2008) allows us to correlate the ashes in the lower Quartermaster formation of these two localities, which are approximately 95 km apart as the crow flies. A single ash is known from the Palo Duro locality.

The samples of tephra layer were collected at the field sites by Renne and Mitchell (Berkeley Geochronology Center). The samples were chemically analyzed and U-Pb dated using annealed zircons (for methods, see Mitchell, 2014). Unfortunately, the isotopically determined ages show overlap (see Fig. 2).

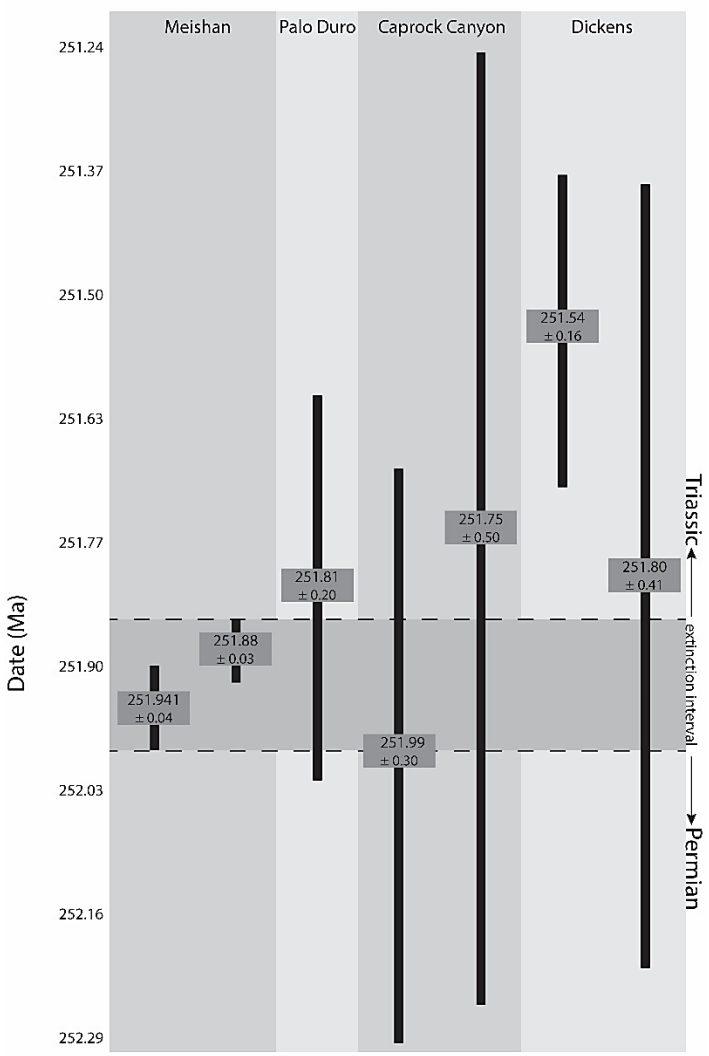

Fig 2. *The radio-isotopically determined ages (and error bars) of ash layers from four sections within the Whitehorse Group, Texas (dates from Mitchell, 2014). For comparison the start of the extinction interval from the type section in Meishan, China, is included (*by (Burgess et al. 2014). *All dates based on U-Pb dating.*

The radioisotopically determined ages of the Palo Duro Basin sections overlap (Fig. 2), and fall within the range of the extinction horizon (bed 25) of the type section in Meishan, China (Burgess et al. 2014). The Permian-Triassic boundary (251.9) is defined by the first appearance of the conodont *Hindeodus parvus* (Burgess et al. 2014), which is associated with marine deposits. Due to the terrestrial nature of the deposits studied in Texas, we cannot depend on the occurrence of a marine organism, but we have to rely ash dating and magnetostratigraphy to approximate the position of the P-Tr boundary. It is also important to note that end Permian biotic crisis takes place before the actual Permian-Triassic boundary, so depending on the local sedimentation rates, the exact position of the boundary itself is of secondary importance seeing that

this study focuses on the end Permian biotic crisis. All but one of the ash layers found at the three Texan field sites potentially fall within the extinction interval (Fig. 2)

For a more continuous, and therefore precise method, the oxygen and carbon stable isotope records can be more informative. Negative carbon isotope trends can be indicative of environmental perturbations where ^{12}C that was locked up is freed, thereby shifting the ^{13}C : ^{12}C ratio, resulting in a shift towards more negative $\delta^{13}C$ values. A marked negative shift in $\delta^{13}C$ of marine carbonates ($\delta^{13}C_{carb}$) and terrestrial organic matter ($\delta^{13}C_{org}$) is associated with the end Permian biotic crisis (e.g., Burgess et al, 2014). Due to movement and displacement of carbon-rich sources in the subsurface as the result of synorogenic processes in terrestrial sediments, or absence of organic carbon in oxidized sediments such as redbeds, it can be challenging to find an organic carbon source that that is reliably be correlated to the sedimentary layer it is found in (De Wit et al. 2002). For a $\delta^{13}C$ analysis of the Texas sediments in Tabor at al. (in prep), we have used carbon inclusions in phytoliths and are therefore certain of its floral origin. Following HF (30%)/HCl (40%) digestion the kerogen of 16 Caprock Canyon State Park samples were analyzed by Neil Tabor (Figure 3, Tabor et al., in prep.).

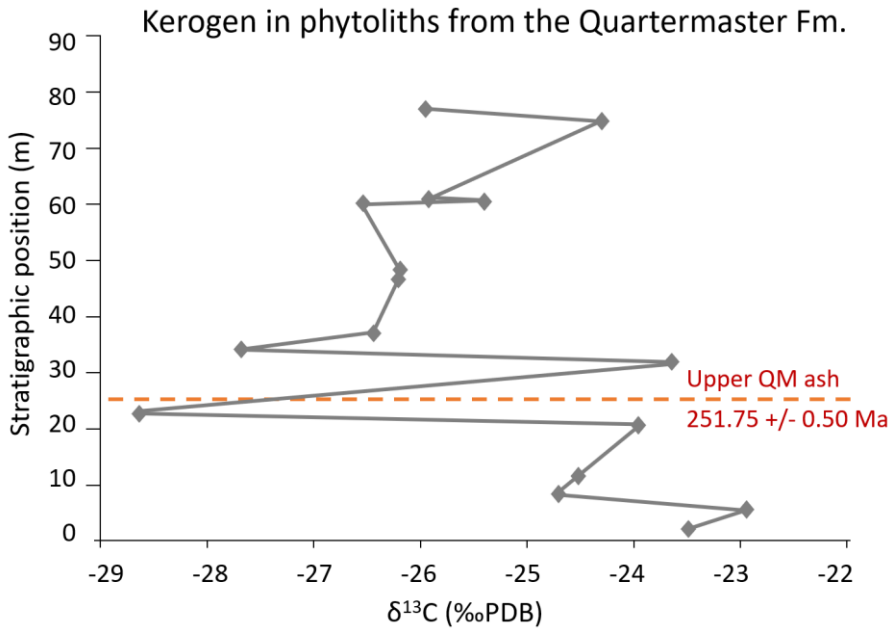

Fig 3. *Plot showing stratigraphic position versus the $\delta^{13}C$ value of organic matter (grey diamonds) among 16 different phytolith-bearing samples collected from the Quartermaster fm. in Caprock Canyons State Park, TX, U.S.A. Red dashed lines are accurately dated reference points derived from $^{40}Ar/^{39}Ar$ and U/Pb analysis of volcanic ash.*

The minute quantities of organic matter enclosed in phytoliths preserves chemostratigraphic $\delta^{13}C$ trends that are expected to occur during the end-Permian crisis. Specifically, the older samples have by values ~-

24‰, followed by a stratigraphically short (~10 m) double negative isotope shift to values of ~-28‰, and stratigraphically long (~40 m) trend toward less negative values of ~-24‰ (Figure 3). Values between 22-29‰ are consistent with those of plant matter. It is possible that these negative shifts record the excursion associated with the end Permian biotic crisis but given that most ash bed age averages indicate a younger age, and the standard deviations of these ash dates are relatively large, we cannot be sure they are.

Other chemostratigraphic, geochronologic, and magnetic polarity data indicate that the Permian-Triassic transition is present in continental strata of the Whitehorse Group in the Palo Duro Basin and that the Quartermaster Formation in northern Texas, previously considered to be Upper Permian, is entirely Lower Triassic (Tabor, in prep).

In addition to sedimentology, geochemistry and paleomagnetic analysis, biostratigraphy has the potential to elucidate hitherto undetected trends which is why I studied the same strata for phytoliths.

2.2 Using phytoliths as biostratigraphic indicators

Biostratigraphy, correlating similar sections in different locations together based on similar fossil finds, is an important component of stratigraphy. Many of the biostratigraphic techniques depended on having a particular depositional environment. If the fossils are not deposited or preserved, or if they are subsequently eroded, deformed and/or unrecognizable, they cannot be successfully used in biostratigraphic studies. Because most of the Permian and Triassic sediments in the study site consist of well-oxidized redbeds, it is hardly surprising that microfossils which are commonly used in biostratigraphy, namely pollen and spores, were not preserved in the sediments. Even if the depositional environment had been favorable, the preservational environment was not. Microfossils that are rarely used in biostratigraphy, but which are highly resistant to oxidation, are phytoliths.

2.3 Building a phytolith reference collection

There is a substantial body of work on the application of phytolith research as well as the distribution and morphology of phytoliths in various plant groups (e.g. Piperno, 1988). However, most of this research is focused on archeological and agricultural applications and limited to a specific number of plant groups such as maize, rice and sorghum.

Representatives of clades that evolved in the Paleozoic were processed (Figure 4; Table 2) to obtain information about the various morphotypes of the phytoliths that might be encountered in the Permian and Triassic sediments. The morphology of intracellular, intercellular and/or cell lumen form a mold in which, or against which the silica starts to accumulate and thus ultimately determines the phytolith's shape. The deposition of the silica is a gradual process and sometimes results in a coating rather than a complete infilling of a space. The presence of lignin promotes the deposition of silica (Fang and Ma 2006). Some of

the gymnosperm species examined for this study have lignin contents between 15 to 36% [dry weight] and therefore present many deposition sites (Campbell and Sederoff 1996).

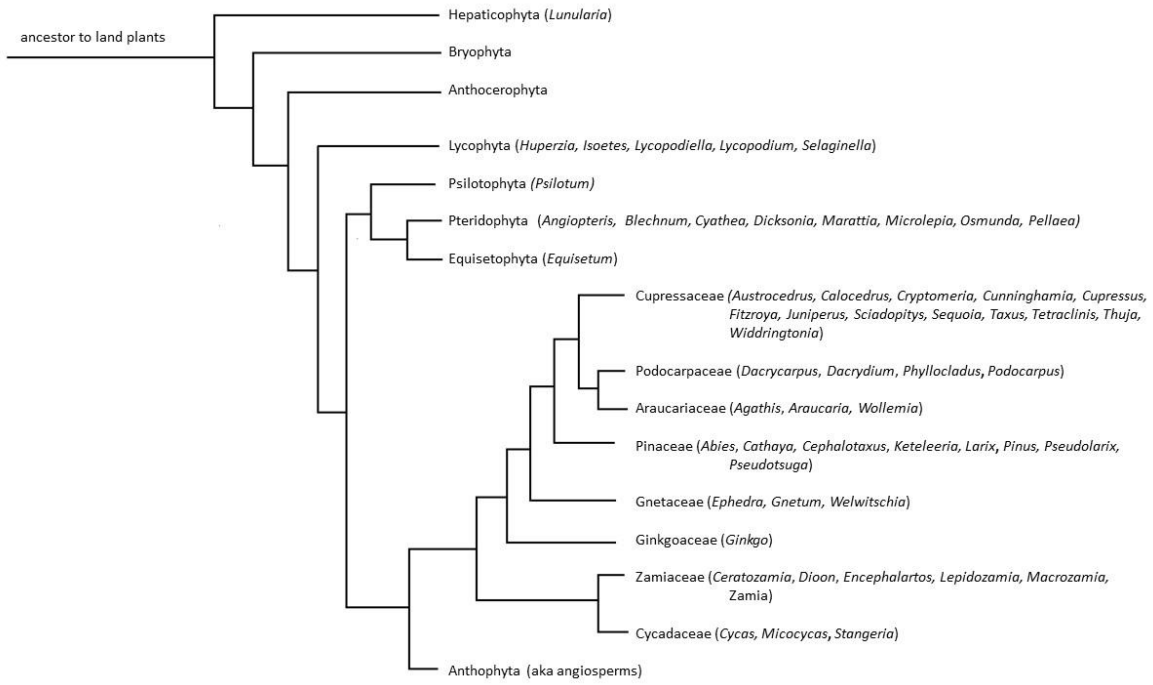

Fig. 4. *A cladogram of all land plant lineages and in brackets and italicized the names of the genera sampled for this study. Cladogram based on Crisp and Cook (2011) and Ran et al. (2010). For the list of species and their higher order taxonomic affinity see Appendix AA.*

Table 2. *Overview of the different taxonomic groups that I have sampled (see Fig AB) and the earliest evidence of plants that belong to their family of higher order taxonomic group (Taxonomy based on Taylor et al., 2009).*

Taxonomic group	**Earliest fossil finding**	**Reference**
Pteridophyta	Early Carboniferous	Metzgar et al. (2008)
Equisetophyta	Devonian	Wellman, Osterloff, and Mohiuddin (2003)
Cupressaceae	Middle Triassic	Yang, Ran, and Wang (2012)
Podocarpaceae	Early Triassic	Brodribb and Hill (2004)
Araucariaceae	Late Permian	Kunzmann (2007)
Pinaceae	Late Jurassic	LePage (2003)
Gnetaceae	Early Cretaceous	Rydin et al. (2006)
Ginkgoaceae	Permian	Zhou (2009)
Zamiaceae	Middle Triassic	Klavins et al. (2005)
Cycadaceae	Late Permian	Wang, He, and Shao (2011)

2.3.1 Extraction of phytoliths from modern plant material

Various protocols to extract phytoliths from modern plants were used over the course of this project. The protocols are all adapted from Piperno (2006), Pearsall (2000) and Blinnikov (1999). To oxidize the organic component of the samples, some samples were treated with hydrogen peroxide (H_2O_2) while others (most) received a nitric acid (HNO_3) treatment. The nitric acid was preferred over the hydrogen peroxide because the latter has the tendency to foam and bubble. While this can mostly be prevented from being problematic by adding the hydrogen peroxide slowly, the relatively violent reaction (compared to the nitric acid) can compromise the integrity of to the sample and sample matrix. If one is looking for a more in-situ, phytoliths in the plant tissue matrix, we find that nitric acid plus a little potassium chloride ($KClO_3$) to work best. Most of the samples were prepared using pressurized vessels; approximately two dozen were digested at ambient pressure.

All the plant material was collected at the UC Botanical garden. After collection, the plant samples were washed dried at 70°C for at least 48hrs to prevent any mold from growing on the plant tissue. Between 0.2 and 0.5 gram, depending in the nature of the material was weighed in and added to a test tube.

For the hydrogen peroxide treatment, the samples were placed in a hot water bath at 70°C and H_2O_2 was added until there was no longer a detectable reaction. After the organic material was digested, the samples were washed twice with deionized water.

The unpressurized nitric acid treatment also involved a hot water bath, and a visual inspection based on the color of the liquid in the test tube (changing from clear to yellow) and absence of undigested material signaled the completion of the process. A pinch of $KClO_3$ together with nitric acid forms Schultze's solution, which speeds up the digestion process. After the organic material was digested, the samples were washed twice using deionized water.

For the pressurized digestion a combination of 2mL of hydrogen peroxide and 3mL of nitric acid was used in Teflon vessels. The liquids were added to the plant material in small increments; especially the hydrogen peroxide has the tendency to produce bubbles, which—if unchecked—can lead to a loss of sample material. The vessels were sealed and loaded in a Mars 6 industrial microwave and heated to 180°C for 60 minutes. After cooling down the contents were transferred to regular test tubes for 3 rinses with deionized water. The test tubes were spun at 3000 RPM for 3 minutes and the supernatant carefully decanted.

The remaining pellets were permanently mounted using either Permount or Eukitt. These media have similar refractive indexes but Eukitt tend to maintain a lower viscosity, which makes it easier to use because the medium tends to distribute itself more readily, thinly and evenly on the slide. Eukitt is also specifically marketed as non-yellowing over time, a process that we have not witnessed with either mounting medium.

2.4 Collecting rock samples

The rock sampling was done over the course of multiple field seasons from 2010 to 2014. Figure 5 shows the stratigraphic columns of the three different sites and the various sampling intervals per site (labeled A through G). Under the assumption that the two ash layers in the lower Quartermaster formation at Dickens and Caprock Canyon are correlated, some of the samples in the different sections overlap in age. As can be seen in Figure 5 the sampling strategy was devised such that there would a spatial and temporal overlap between the different sites.

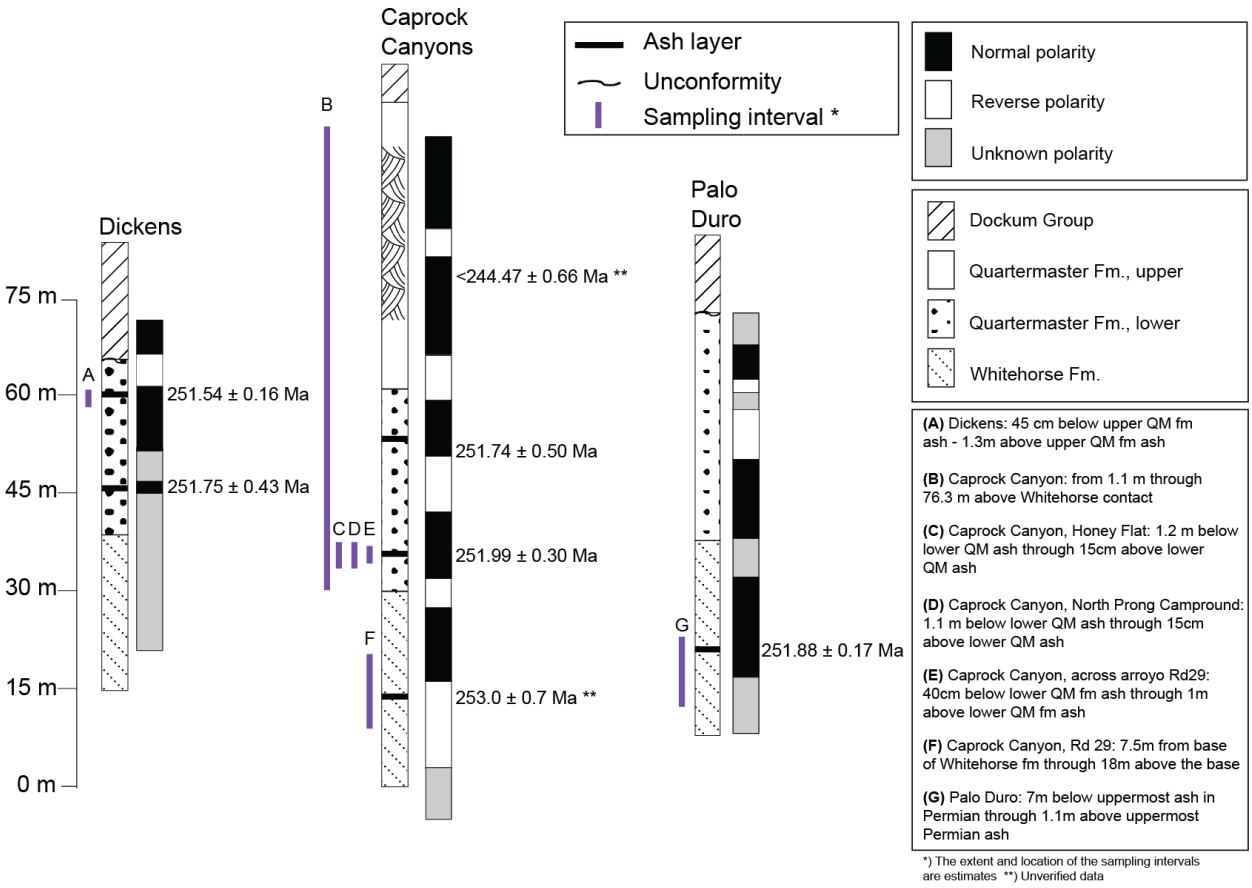

Fig 5. *Generalized stratigraphic columns of the field sites at Dickens, Caprock Canyon State Park and Palo Duro State Park, Palo Duro Basin, Texas, combined with their magnetostratigraphic signal, ash layers and sampling interval. Ash dates from Mitchell (2014).*

Under ideal circumstances there would be little to no spatial heterogeneity, which would permit us to correlate the spatially removed sites. While the sediments in these outcrops are predominantly depositional coastal and fluvial deposits, based on modern analogous landscapes, it would hardly be surprising that, even though some of these sites are spatially no more than 2km apart from one another, the original landscape was quite heterogeneous. A more detailed description of the three sections can be found below.

Dickens

The Dickens outcrop (33° 37.504' N, 100° 48.970' W) is a road cut along U.S. Route 82 consists of 20m Quartermaster formation, with limited access to any of the underlying Whitehorse. The Quartermaster is unconformably overlain by the Late Triassic Dockum formation. There are two ash layers present in the Quartermaster fm., both of which were sampled and dated by Mitchell (2014). The lower ash is dated at 251.75 ±0.43 Ma and the upper ash at 251.54 ± 0.16 Ma and this can be correlated to the upper ash layer found in the Quartermaster formation at Caprock Canyon. Sediment samples were collected close to the upper ash layer, which potentially corresponds with the sample set B from the Caprock Canyon locality (labeled B in figure 5). This overlap is expected around the ~26m above the base of the Quartermaster mark. The Caprock Canyon site and the Dickens site are approximately 95km from each other; the comparison of the two sites has the potential to provide insight in the spatial heterogeneity of the landscape.

All the Dickens samples are labeled as follows: *State – Location - Distance from base[m] – Sampling detail*. For example: TX - D – 25.55 – 0.45 BUA means the sample is from Texas, at the Dickens site, 25.55 meters from the Whitehorse contact, and Below Upper Ash (for examples, see table 3). Some carry the label AUA, which stands for Above Upper Ash.

Caprock Canyon

In Caprock Canyon we sampled five different transects. First there is the Quartermaster North Prong section (NPQM; 34°26'50.65"N, 101° 5'3.07"W) which consists of samples 1 through 51.6, where the number is the height in meters as measured in the field the base of the Quartermaster/Whitehorse contact. Because the best location to sample the lower section of this outcrop did not go up as high as desired, another nearby location that did give access to the younger layers of the Quartermaster formation was samples. As a result, the samples 52.5 through 76.3 carry the South Prong Quartermaster (SPQM; 34° 26.318' N, 101° 5.611' W) earmark. These two sites are about 2km from each other.

The lower Quartermaster ash is exposed at the Honey Flat Campground (34°25'43.59"N, 101° 3'11.16"W), the North Prong Campground, and on the eastern side of the park along Road 29 that skirts the eastern boundary of the state park.

The F section (labeled F in Fig. 5) is also located in Caprock Canyon State Park, just off Road 29 down an arroyo at approximately 34°26'1.77"N, 101° 1'6.88"W). This section exposed 17 meter of the Whitehorse formation, and the base of the section is used as reference point (with the base set at zero). An ash layer at 9 meter from the base of the section was dated at 253.0 ± 0.7 Ma (Renne in NSF project proposal, 2008). However, it is unclear who did this analysis, what method they used and therefore how reliable and accurate

this date is. Based on the stratigraphic position, this layer appears to be the same as the one found at Palo Duro state park as they are approximately at the same distance from the base of the Whitehorse formation. The ash layer at Palo Duro was dated at 251.88 ± 0.17 M which falls well in the range of the dates that Burgess et al (2014) published for the age of the Permian-Triassic boundary layer. The sample range from 7.5 meter to 14.5 meters from the base of the Whitehorse formation.

Table 3. *Example of the codes used for the phytolith sample labels in this study.*

Example transect label	Explanation of labeling
32.9 NPQM	32.9 meter from Whitehorse contact, North Prong QuarterMaster
TX-CCH-70cm_BLQMA	Texas, Caprock Canyon Honeyflat, 70cm Below Lower QuarterMaster Ash, taken at the Honey Flat Campground
TX-CCC-15cm_ALQMA	Texas, Caprock Canyon Campground, 15cm Above Lower QuarterMaster Ash, taken at the North Prong Campground
TX-CC29-50cm_ALQMA	Texas, Caprock Canyon Road 29, 50cm Above Lower QuarterMaster Ash, taken at Road 29
TX - CC - 11.0 AWh - arroyo	Texas, Caprock Canyon Campground, 11m Above Whitehorse, take in the arroyo just west of Road 29.

Palo Duro

At Palo Duro State Park, which lies approximately 70 km north/northwest of Caprock Canyon State Park, the aforementioned ash layer can be found at the base of an arroyo (34° 57.072' N, 101° 39.801' W). Here, a series of samples were taken in close proximity of the ash layer. The labeling of the samples is based on height above the base of the section and range from 2 to 10.1 meters above the base.

Based on the most current ash dates from Mitchell (2014) it is likely that only the sediments that were sampled at the arroyo along Road 29 in Caprock Canyon State Park (section F) and the samples that were taken at Palo Duro State Park (section G) represent Permian age samples. The other sections sampled at Caprock Canyon (sections B-E) and Dickens (section A) are almost certainly Triassic.

Tabor et al (in prep.) have determined that all of the Quartermaster formation is Lower Triassic (Induan). Even the top 15-20 meters of the Whitehouse Group is also Triassic, which the Permian-Triassic transition at around 9 meters from the base of the Whitehorse.

All the Palo Duro samples are labeled as follows: *State – Location - Distance from base[m] detail*. For example: TX - PD - 9.15 AWh means the sample is from Texas, taken at the Palo Duro site and—in this case—was taken at 9.15 meter Above the base of the Whitehorse.

2.4.1 Extracting phytoliths from rocks

The method used to extract the phytoliths from rocks is loosely based on Piperno's soil extraction protocol as described in her book (Piperno 2006). All the rock samples are first cleaned with a metal brush and water and then dried overnight at 65°C. Some of the samples disintegrated when manual pressure was applied. For the ones with more structural integrity, they are crushed using a mortar and pestle and, in some cases, if needed, transferred to a mechanical crusher which reduces the material to about half a mm in size. Approximately 10g of the dried and crushed sample is placed in a 50 ml centrifuge test tube to which 5% deflocculant solution is added. The samples are placed in a shaker for 12 hours. To remove the clay, the samples are centrifuged with demineralized water for 2 minutes at 3000 rpm twice. Depending on the clay content of the samples this step may need to be repeated until the supernatant is clear after centrifuging.

The samples are transferred to 400ml beakers to which 10ml of HCl (30%) is added. To speed up this process the beakers are placed on a hotplate. After this step, nitric acid (HNO_3) and a little potassium chlorate $KClO_3$ is added to remove organic material. In some of the samples H_2O_2 was used for the removal of organic material, which yielded comparable results. In that case ~15 ml of H_2O_2 is added, 5 mL at a time because a strong reaction can cause the beakers to overflow. H_2O_2 is added until reaction ceases. The beakers are filled with demineralized water and the suspension is allowed to settle for at least 24 hours. After decantation the samples are transferred to 50 ml test tubes and centrifuged twice with demineralized water to remove excess acid.

For the heavy liquid flotation step, a sodium polytungstate solution with a specific gravity of 2.40 was prepared. This is deliberately a little more dense than is common in phytolith extractions, to make sure that even if phytoliths have lost some water from their matrix which would lead to an had increased density, they would still float to the top of the sodium polytungstate solution. Approximately 15 ml of the heavy liquid solution is added to the samples in the 50 ml test tubes. After the samples are vortexed, they are centrifuged for 5 minutes at 3000 rpm. The supernatant is decanted into another 50 ml tube and diluted with demineralized water. This will cause the phytoliths to sink to the bottom of the test tube. In some samples, the sediment does not collect well at the bottom of the test tube, and decantation disturbs the sample. In these cases, another 10 to 15 ml of heavy liquid is added to the original test tube, which is vortexed again, centrifuged and decanted into the same test tube that holds the diluted supernatant.

The diluted supernatant and remaining phytoliths are centrifuged twice for 10 minutes at 3000 rpm. The phytoliths can now be mounted onto slides. Sedimentation trays are filled with demineralized water, covering the cover slips. The suspension is then evenly distributed over the cover slips and allowed to settle for two hours. After two hours the water is drained and a drop of mounting medium is added onto each

cover slip. The first set of samples was mounted using Naphrax, which needs to be cured at 140°C for ~90 minutes. The other mounting media used, Permount and Eukitt, do not require any additional curing step.

2.5 Counting phytoliths

All the slides were counted using a Leica DM2500 microscope equipped with differential interference contrast (DIC). DIC helps to highlight relief in the specimens which increases contrast and aids in the identification of the particles. All the photos were taken with a Leica MC170 and a Nikon DS-Vi1 Digital Camera. Every slide was counted in its entirety and every phytolith was recorded.

2.6 Testing the potential of phytolith assemblages to support biostratigraphy of Permian and Triassic strata

Recovered phytolith abundances in samples are a function of phytolith production, transport, preservation, sample size, preparation and identification (Piperno 2006). Different plants species can produce different morphotypes and different combinations of more than one morphotype (multiplicity). The robustness of these different phytoliths can vary due to their chemical make-up (the degree of polymerization), the physical make-up of the phytoliths (e.g. long and thin versus short and stout) or a combination of both, resulting in an assemblage that does not directly reflect plant composition. Preservation can also vary in time, so phytolith abundances not necessarily reflect total plant abundances. However, the temporal variation of phytolith preservation is assumed to apply to all forms and species. This means that the total number of phytoliths in the assemblage may go down, but the proportion of each morphotype is assumed to remain the same. Therefore, changes in relative abundance can be studied to reconstruct changes in plant communities and also cross-correlate samples if absolute dating of the geological material is not feasible.

To evaluate the ability of phytolith compositions to be used as a stratigraphic tool, phytolith proportional occurrence from six profiles were compared using a heuristic dissimilarity metric that is described in detail below. The approach was tested by comparing (aggregated) samples from sections A, C, D and E to aggregated samples from section B. The samples had to be aggregated because the phytolith content was too low to draw any reliable conclusions. This obviously came at the cost of loss of temporal detail.

Since section B encompasses the time periods that the samples from sections A, C, D and E represent, it is a good test to verify if the similarity between phytolith assemblages can be used as a tool to correlate samples in space. The approach was also tested on samples from sections F and G, both straddling the Permian-Triassic transition. Samples from sections F and G were aggregated into a Permian and a Triassic sample for F and G. Then the similarity between the four aggregate samples was calculated aiming to verify that the samples from the same time period were indeed most similar.

2.6.1 Data aggregation

The proportions of phytoliths counted in one sample are subject to statistical uncertainty (Strömberg 2009). The confidence interval around a proportion of (for example) 30% is narrower if the proportion was based on 300 phytoliths out of 1000 total phytoliths, than when it is based on 3 phytoliths out of 10. The confidence interval, also known as the normal approximation interval, of the proportion can be calculated as follows:

$$\hat{p} \pm z\sqrt{\frac{\hat{p}\,(1-\hat{p})}{n}} \qquad \text{[Eq 1]}$$

Where $\hat{p}$ is the calculated proportion, z is the 95-percentile of a standard normal distribution (z=1.96), and n is the total number of phytoliths. Figure 6 shows the confidence intervals (thin lines) around calculated proportions (bold lines) of 20% (orange), 50% (green) and 90% (blue), for a total number of identified phytoliths ranging from 5 to 50.

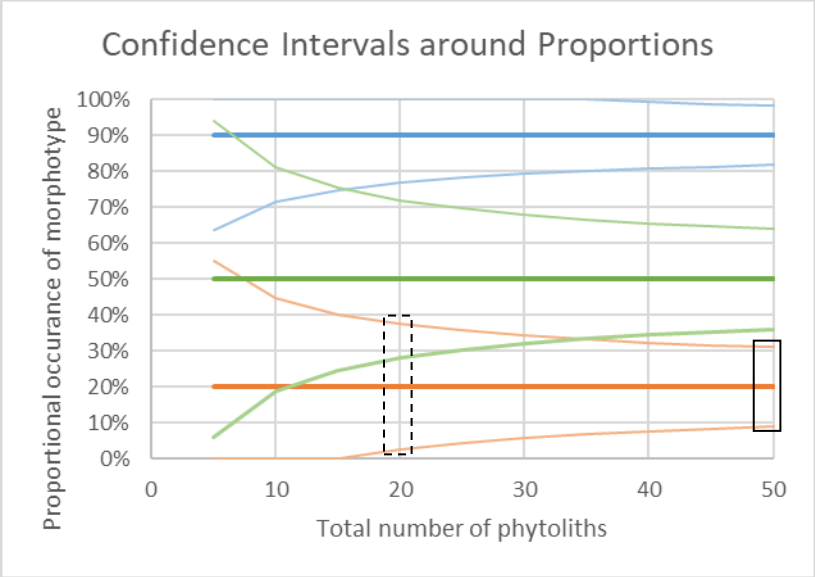

Fig 6. *The confidence intervals (thin lines) around calculated proportions (bold lines) of 20% (orange), 50% (green) and 90% (blue), for a total number of identified phytoliths ranging from 5 to 50.*

The confidence interval of a calculated proportion of 20% narrows to 10%-30% only after more than 50 phytoliths have been identified (solid box). If only 20 phytoliths have been identified, four of which are of a certain type (20%), the confidence interval around the true proportion ranges from 2% to 38% (dashed box).

Given this statistical uncertainty, it is not feasible to correlate samples across locations based on proportions calculated from samples with few identifiable phytoliths. To resolve this, phytolith morphotypes and samples were aggregated to achieve a larger number of counts and more reliable calculated proportions.

To gain sufficient counts to calculate proportions with narrower confidence intervals, neighboring samples in profile B were aggregated together to obtain aggregate samples with 45 or more phytolith detections (Table 4). One sample (collected 10.9 m above the White Horse Formation) containing 55 phytoliths was not aggregated. This reduced the number of 37 samples to 8 aggregated samples. The aggregate samples span depth intervals from 0.9 to 16.5 meters. While this greatly reduces the spatial and temporal resolution, it is – in absence of much higher phytolith counts – the only available approach to compare compositions across sampling locations.

Table 4. *Phytolith morphotypes extracted from three latest Permian to Early Triassic sections from the Palo Duro Basin, Texas. Eight phytolith morphotype categories were distinguished.*

	Morphological descriptor	***Description***	***Examples***
1	Orbicular ornamented	This category is a combination of all the rounded morphotypes, with surface ornamentation. The ornamentation appears to be dependent on preservation quality. In less preserved specimen the distinction between e.g. castelate and echinate is impossible to make.	Plate 1a-f.
2	Carbon core orbicular	A clearly distinguishable morphotype; round with a dark round center.	Plate 1g-j.
3	Carbon core square	A clearly distinguishable morphotype; parallelepipedal to trapezoidal with rectangular dark depression, with the depression sometimes showing striations.	Plate 1k-n.
4	Circular bordered pits (uniseriate)	A clearly distinguishable morphotype; a vessel element with a single row of circular bordered pits.	Plate 2a-f; 3a-d, 4a-e.
5	Clavate	Drop or club-like shaped morphotype; some with a clear crest over the length, in others not clear. Both types were lumped into one.	Plate 5a-p.
6	Cuneiform	Saddle shaped; the flatter ones (2D) are lumped with the more filled out ones (3D).	Plate 5g-h.
7	Perforated strands	All these are longer than they are wide. Perforations very from small to large, and regular to irregular. In some, the transition from one type to another was observed, demonstrating that a distinction between the types may not be warranted.	Plate 4-fg.
8	Reniform	A clearly distinguishable morphotype; kidney-shaped (3D).	Plate 6e-h.

Every slide was counted in its entirety and every phytolith was recorded. However, for the numerical analysis the groups were used, because incredibly rare morphotypes, while potentially botanically informative, can as of yet not be used in numerical and stratigraphical analysis.

2.6.2 Dissimilarity metric

A heuristic metric, similar to the root mean squared error, was used to evaluate similarity of phytolith compositions across samples. For each of the eight morphotype categories, the relative abundance (proportion) within the aggregated samples was calculated as $\hat{p}$ = i/n with i the number of phytoliths of a certain morphotype and n the total number of identified phytoliths in the aggregated sample. The similarity between aggregated samples was based on the sum of squared differences between the proportions of the two samples:

$$\text{Dissimilarity Metric} = \sqrt{\frac{\sum_{i=1}^{8}\left(\hat{p}_{i,B} - \hat{p}_{i,A}\right)^2}{8}} \qquad \text{[Eq 2]}$$

With $\hat{p}$i,A and $\hat{p}$i,B the proportion of phytolith morphotype i in sample A and B. The metric resembles the root mean squared error. Since the metric represents the error, lower numbers indicate higher similarity.

3 Results

3.1 Phytoliths from rocks

Photo plates 1 through 10 show a selection of the phytoliths from rock samples. For collection and processing details, refer to section *2.4 Collecting rock samples* and *2.4.1 Extracting phytoliths from rock* of this chapter.

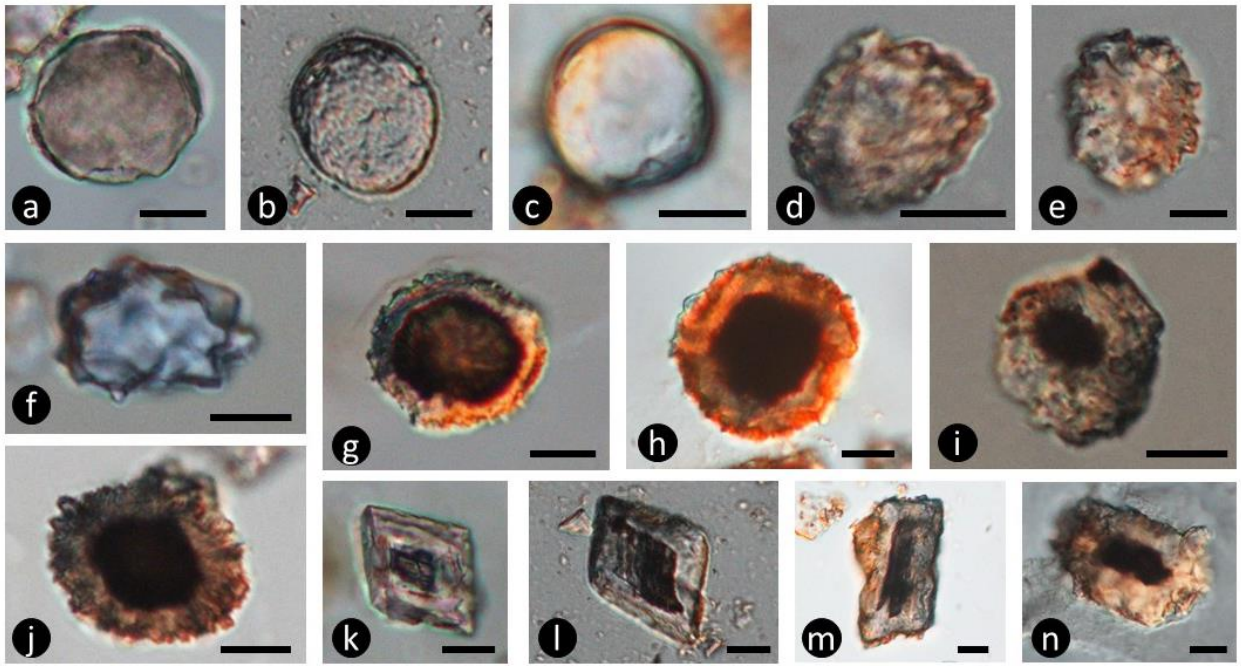

Plate 1. *Phytoliths extracted from rock. Sample ID in brackets.* ***a:*** *Orbicular 2D (NPQM 7.4);* ***b****: Orbicular 2D (CCC15CM);* ***c****: Globular (TX-CC-14.5AWh);* ***d - f****: Globular echinate (d: 45.9 NPQM; e: PD9AWHC; f: 25.0 NPQM);* ***g – j :*** *Carbon core round: globular with echinate ornamentation, with dark, carbon-rich occlusion in the center (g: 15.8 NPQM; h: TX-D25_4-060BUA; i: 51.0 SPQM; j: PD69AWHB);* ***k – n*** *: Carbon core rectangular: parallelepipedal to trapezoidal with rectangular dark depression (k: 7.4m NPQM; l – m: CCC15CM; n: TX-CC-14.5AWh. Scale bar 10µm.*

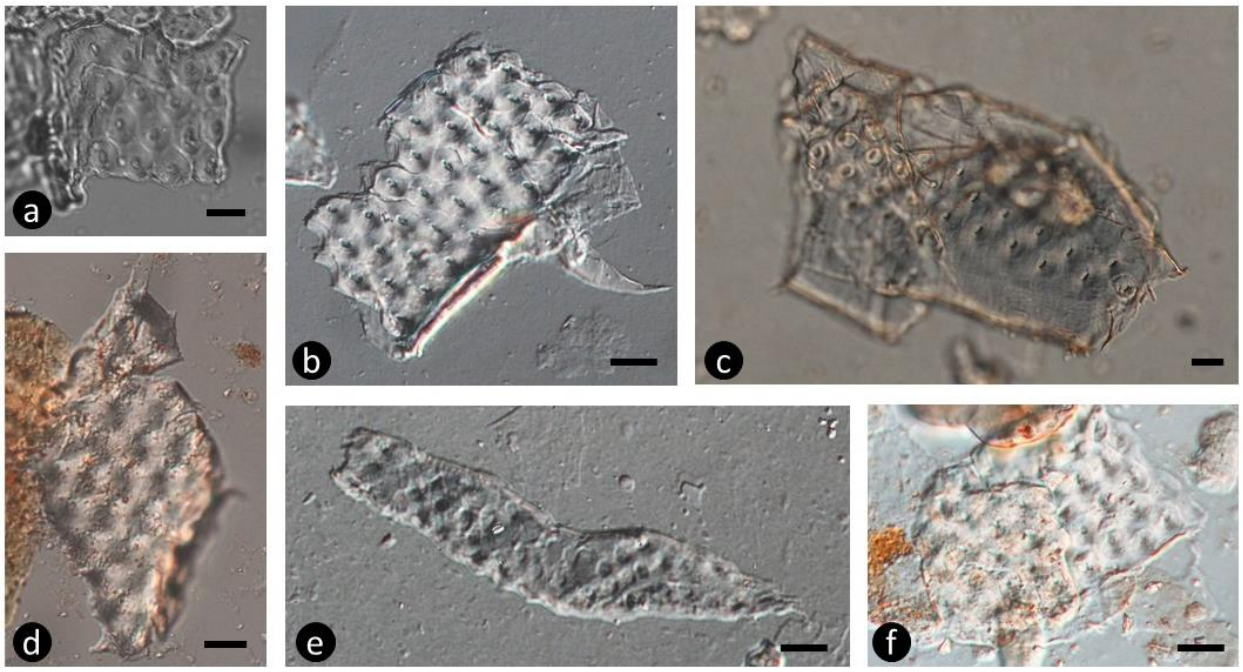

Plate 2. *Phytoliths extracted from rock. Sample ID in brackets.* ***a - f:*** *araucariod pitting (a: 60.4 SPQM; b: 22.1 NPQM; c: 53.3 SPQM; d: 60.4 SPQM; e: 70.4 SPQM; f: CC80AWhB). Scale bar 10μm.*

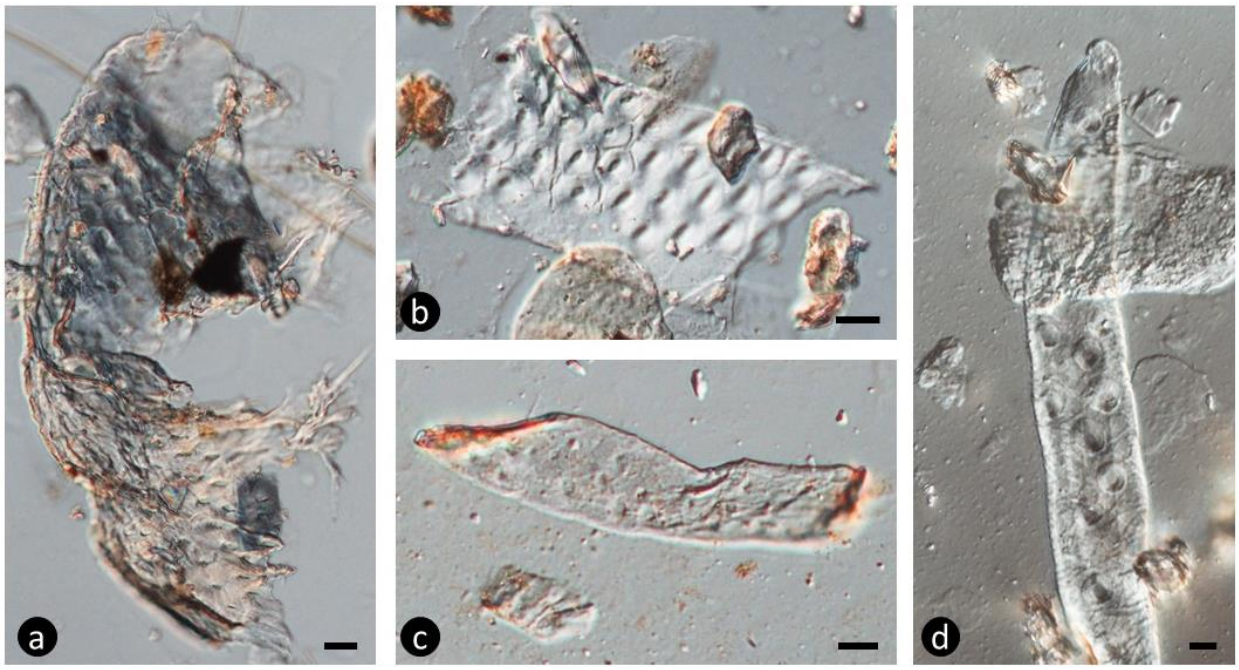

Plate 3. *Phytoliths extracted from rock. Sample ID in brackets.* ***a - d:*** *araucariod pitting (a: NPQM 15.8-C; b: PD915A; c: D 25.4 0.6 BU; d: NPQM 22.1-D). Scale bar 10μm.*

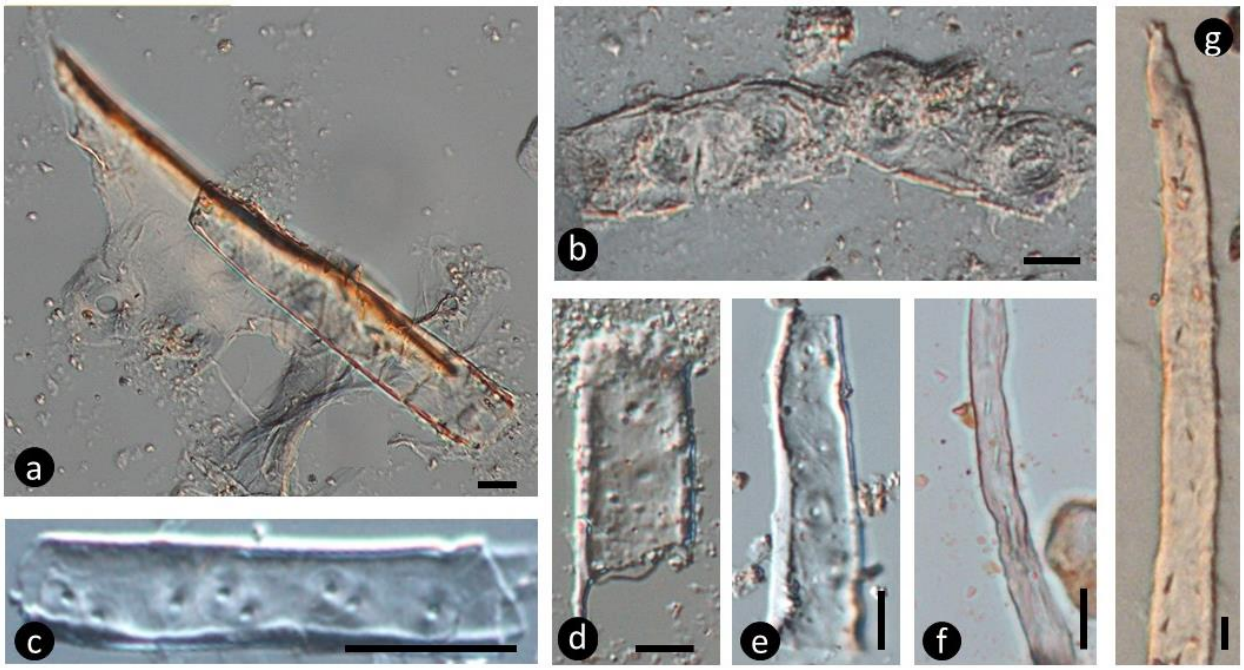

Plate 4. *Phytoliths extracted from rock. Sample ID in brackets.* ***a - e:*** *uniseriate circular bordered pitting (a: NPQM 32.9; b: CCC70CM; c: 45.9m NPQM; d: 36.2 NPQM; e: 6.0 NPQM);* ***f – g****: Perforated strands (f: CC980AWh; g: SPQM 69.7). Scale bar 10μm.*

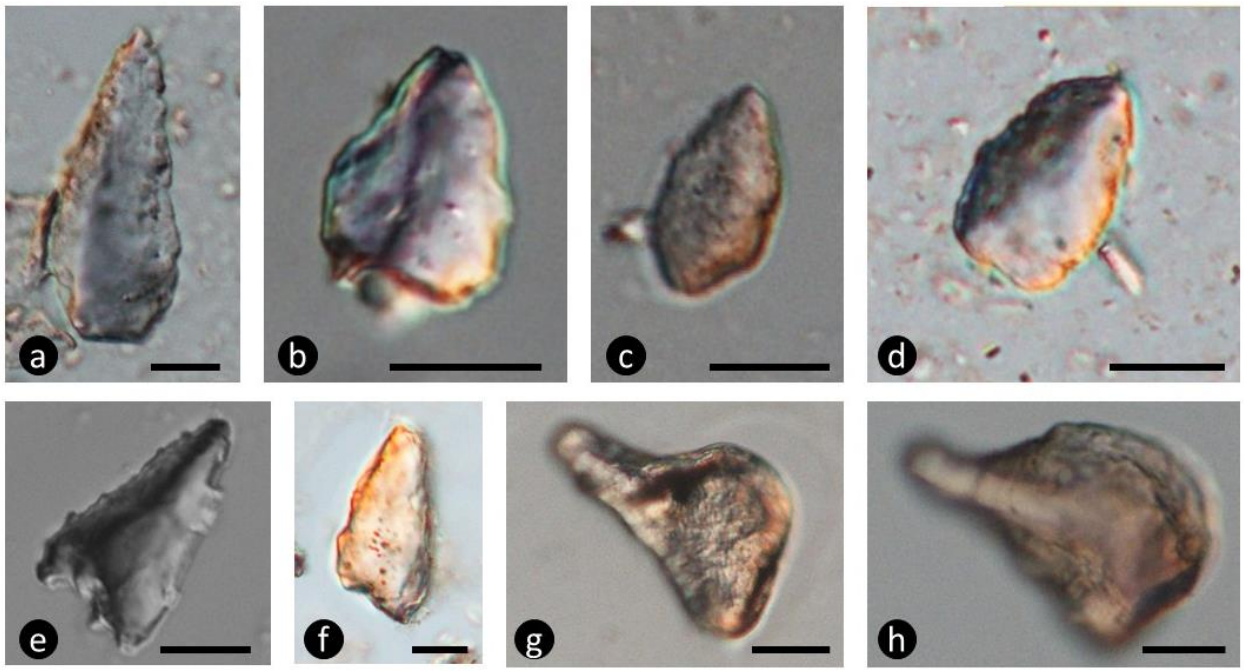

Plate 5. *Phytoliths extracted from rock. Sample ID in brackets.* ***a - f:*** *Clavate. a, b and d show a crest along the long axis (a: 1.1 NPQM; b: NPQM 15.3-B; c: NPQM 50.4m B; d: TX-CC-29-100BLQMA; e: 47.7 NPQM; f: PD65AWHB);* ***g – h****: cuneiform (g: NPQM 39.7-B; h: ash). Scale bar 10μm.*

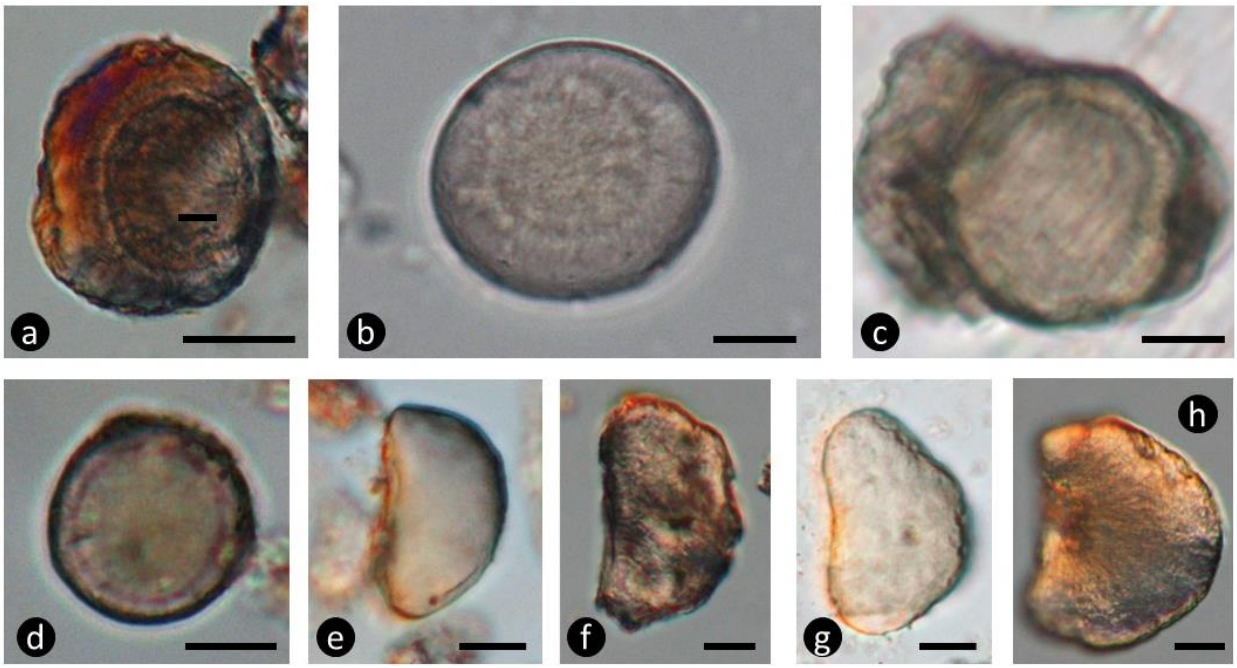

Plate 6. *Phytoliths extracted from rock. Sample ID in brackets.* ***a – d:*** *hair base (a: 22.1 NPQM; b: TX - D – 25.1 – 0.90 BUA; c: 15.8 NPQM; d: 6.0m NPQM);* ***e – h:*** *reniform (e: NPQM 26.0m-A; f: 14.9 NPQM; g: TX-CC-29-100BLQM; h: 15.8 NPQM). Scale bar 10μm.*

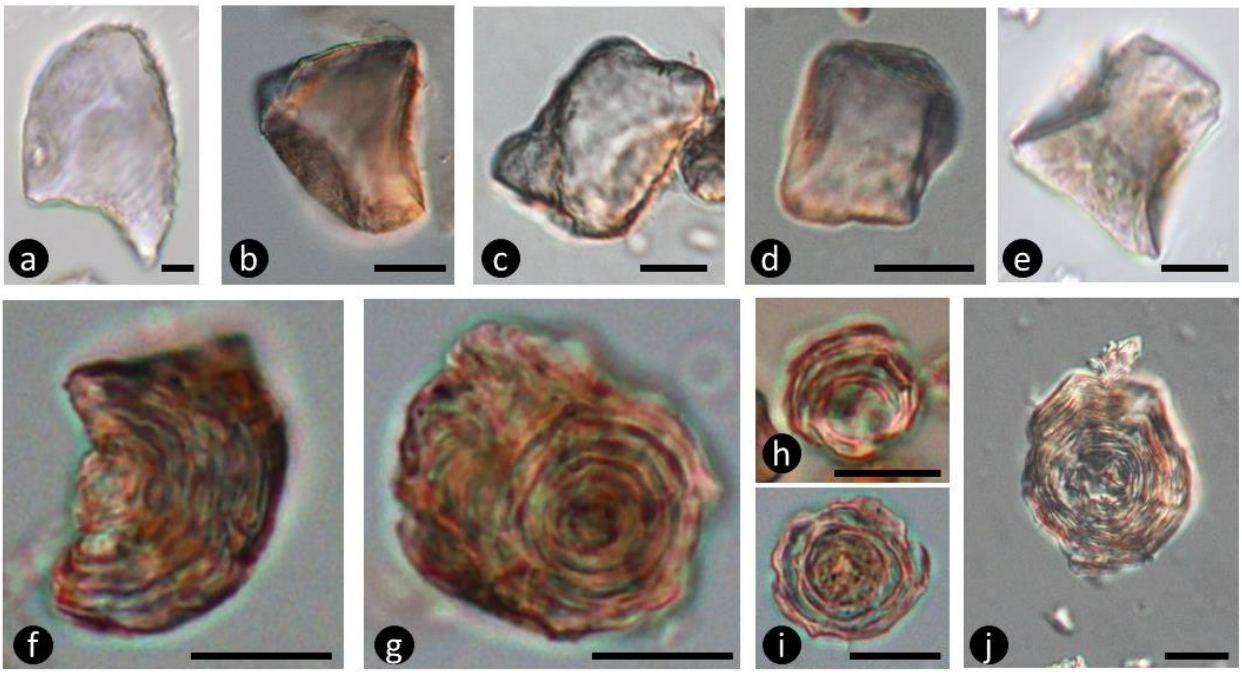

Plate 7. *Phytoliths extracted from rock. Sample ID in brackets.* ***a:*** *scutiform (TX-CCH-70cm-BLQMA_D);* ***b – e****: parallelepipedal bulliform (b: PD70AWHB; c: CCH15ALQ; d: NPQM 15.3-D; e: TX-CCH-70cm-BLQMA_D);* ***f – j****: Vesticular infilling (f – i: 6.0 NPQM; j: 14.9 NPQM) . Scale bar 10μm.*

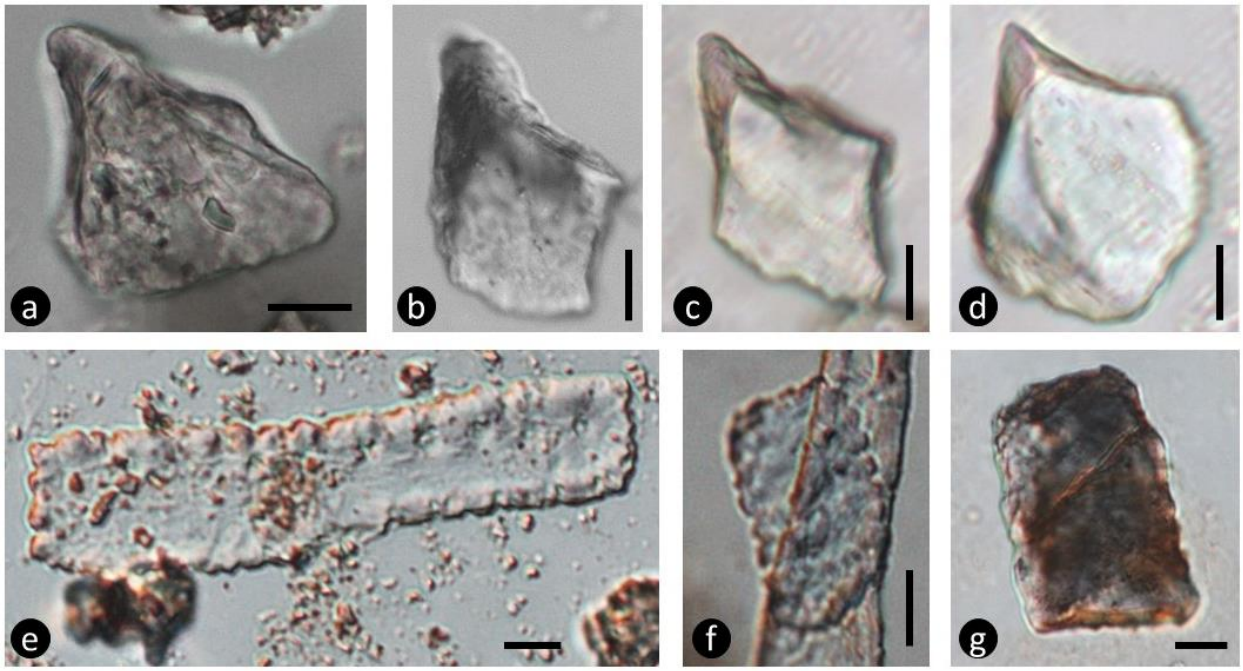

Plate 8. *Phytoliths extracted from rock. Sample ID in brackets.* ***a - d:*** *Cuneiform (2D) with nib (a: 7.4 NPQM; b: 47.7 NPQM; c – d: TX-CCH-70cm-BLQMA_D);* ***e – g****: Rectangular (2D) with undulated margin (e: D2555045; f: D266060A; g: CCH70CMB). Scale bar 10μm.*

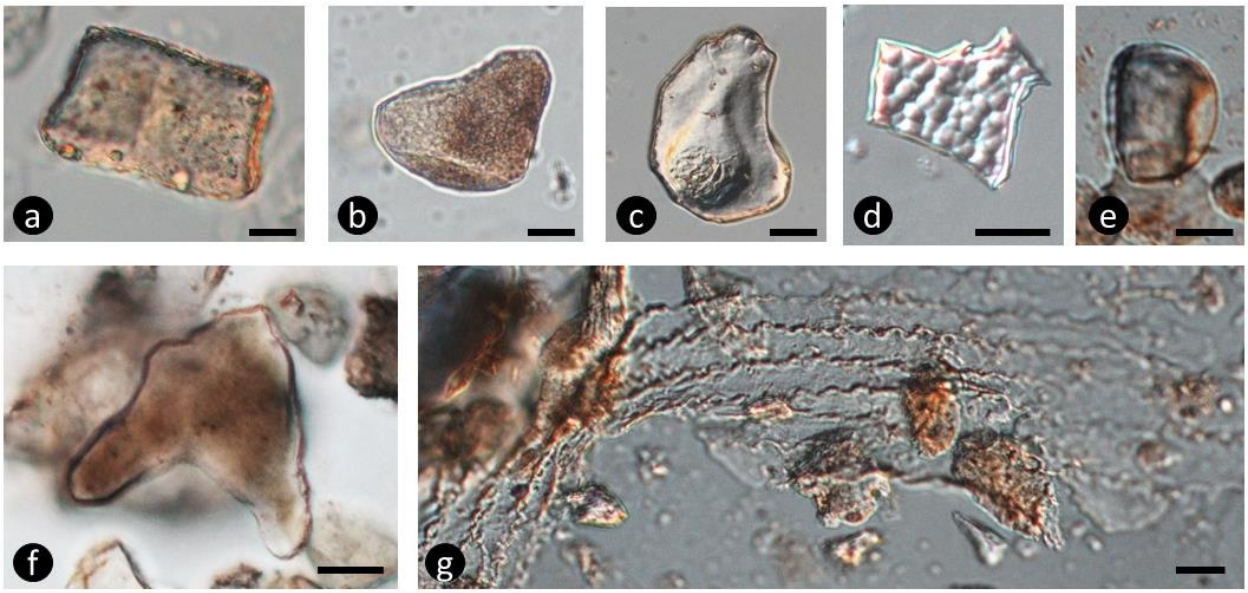

Plate 9. *Phytoliths extracted from rock. Sample ID in brackets.* ***a - g:*** *Indeterminate (a: 15CMAQMA; b: 33.5 NPQM; c: 39.7 NPQM-B; d: 25.0 NPQM-C, e: 135AWHA; f: 26.0 NPQM-A; g: CC-11-Awh). Scale bar 10μm.*

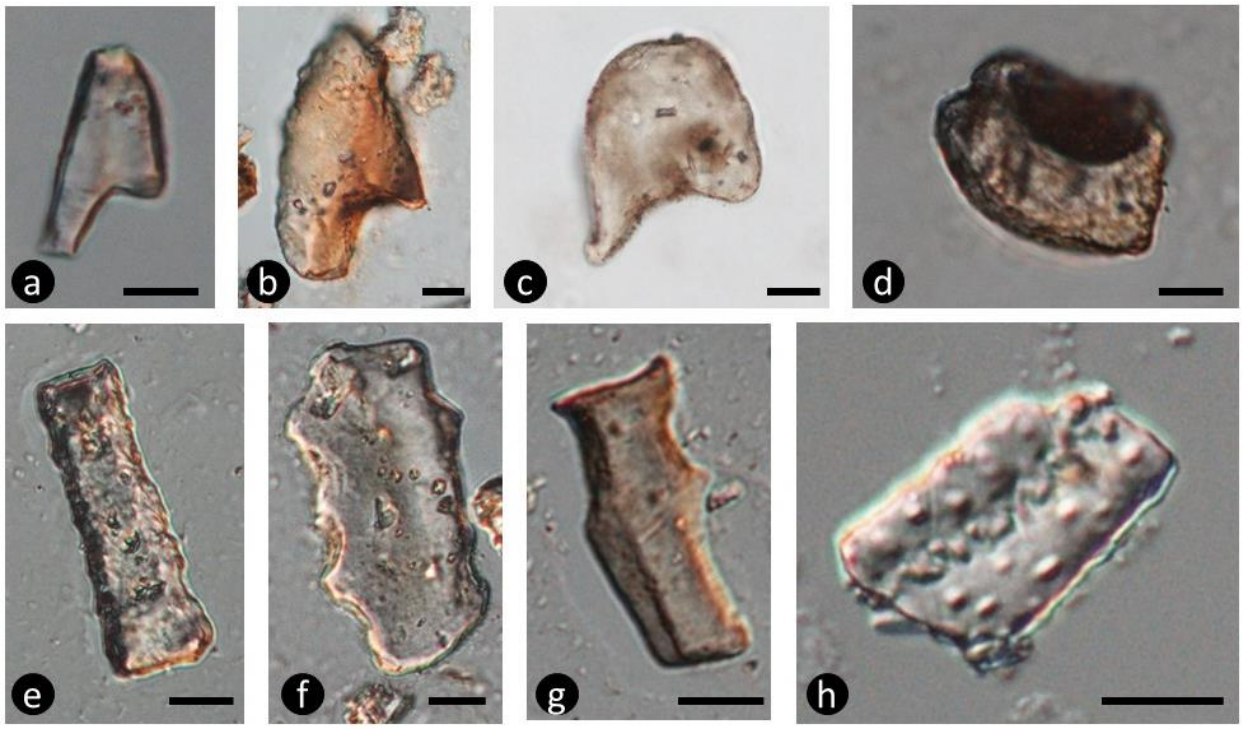

Plate 10. *Phytoliths extracted from rock. Sample ID in brackets.* ***a - g:*** *Indeterminate (a: 25.0 NPQM; b: TX-CCH-70cm-BLQMA; c: TX-D25_4-060BUA; d: CCH70CMB, e: 52.2 SPQM; f: CCC110BQ; g: CCC15CM; h: 19.6 NPQM). Scale bar 10µm.*

3.2 Phytolith reference collection

Photo plates 11 through 38 show phytoliths representatives of clades that evolved in the Paleozoic (see Appendix 1). For collection and processing details, refer to section *2.3 Building a phytolith reference collection* of this chapter.

3.3 Numerical analysis of phytolith assemblages

In this section we explore the similarity or dissimilarity between different sample profiles taken at different locations, to test whether sections of a similar age (based on the ages of the various dated ash layers) show any similar patterns. 3.3.1 Location of sample A in section B

The assemblage composition for the eight aggregate samples from section B with the aggregate sample from section A are graphically presented (Fig. 7). Dickens' aggregate sample A, from 26 meter above the Whitehorse-Quartermaster contact, contained 27 phytoliths. The aggregate samples from Caprock Canyon's section B, with average heights ranging from 5-67 meters above the Whitehorse-Quartermaster contact, contained between 45 and 59 phytoliths. If the vegetation, taphonomic regimes and depositional environment was similar in the same sample, one would expect similar assemblages in aggregated sample A and sample B which originates from around 23 meters above the Whitehorse-Quartermaster contact. The sediments from both locations are sampled close to the second Quartermaster ash, which are thought to

represent the same event. Dickens' sample A most common phytolith morphotypes are Perforated Strands (group 7, 30%), Orbicular Carbon Cores (groups 2, 26%) and Circular bordered pits (group 4, 18%). The only sample from the Caprock Canyon section B with the same three phytolith morphotype groups as most common contributors, is the sample from ~23m above the Whitehorse-Quartermaster contact. In section B the samples from 11m, 53m and 67m are dominated by the Perforated Strands morphotype (group 7, >2/3 of the assemblages). Unlike any of the other samples, sample from 15m in section B lacks Perforated Strands phytoliths, the sample from 67m in section has a large proportion of Orbicular carbon core phytoliths (group 2, 18%), and the samples from 15m and 43 m in section B have large proportions of Cuneiform phytoliths (> 25%).

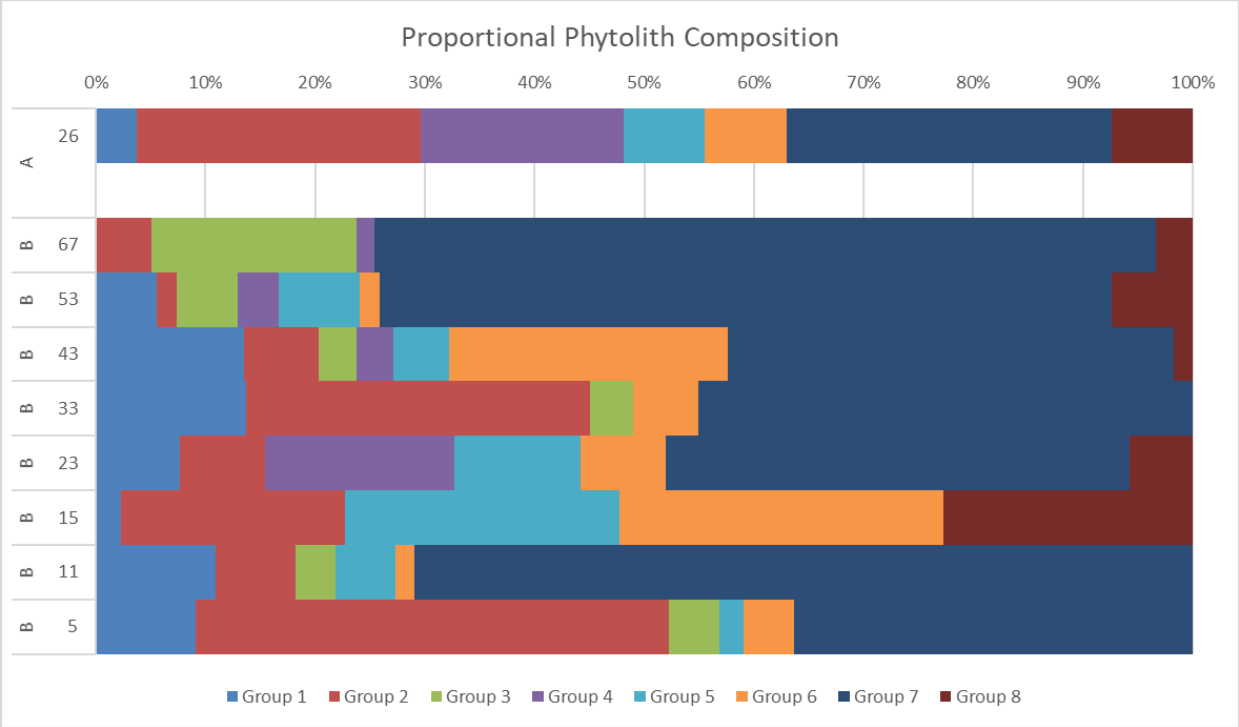

Fig 7. *Proportional occurrence of eight phytolith morphotype groups in Dickens' aggregate sample A and eight aggregated samples from Caprock Canyon's section B, Palo Duro Basin, Texas. The phytolith morphotype groups comprise: 1) Orbicular ornamented, 2) Carbon core orbicular, 3) Carbon core square, 4) Circular bordered pits (uniseriate), 5) Clavate, 6) Cuneiform, 7) Perforated strands and 8) Reniform. Indicated in the left margin are the average sample heights (m) above the Whitehorse-Quartermaster contact.*

Table 4. *Squared differences between in the proportional occurrences of each of the eight morphotype groups between Dickens' aggregate sample A from the Dickens' section, and aggregated samples from Caprock Canyon's section B, Palo Duro Basin, Texas. The phytolith morphotype groups comprise: 1) Orbicular ornamented, 2) Carbon core orbicular, 3) Carbon core square, 4) Circular bordered pits (uniseriate), 5) Clavate, 6) Cuneiform, 7) Perforated strands and 8) Reniform. Indicated in the left margin are the average sample heights (m) above the Whitehorse-Quartermaster contact. Lower numbers represent better similarity.*

Profile B	**Morphotype**								**Dissimilarity Metric**
Aggregated Location	Group 1	Group 2	Group 3	Group 4	Group 5	Group 6	Group 7	Group 8	
67	0.00	0.04	0.03	0.03	0.01	0.01	0.17	0.00	**19%**
53	0.00	0.06	0.00	0.02	0.00	0.00	0.14	0.00	**17%**
43	0.01	0.04	0.00	0.02	0.00	0.03	0.01	0.00	**12%**
33	0.01	0.00	0.00	0.03	0.01	0.00	0.02	0.01	**10%**
23	**0.00**	**0.03**	**0.00**	**0.00**	**0.00**	**0.00**	**0.02**	**0.00**	**8%**
15	0.00	0.00	0.00	0.03	0.03	0.05	0.09	0.02	**17%**
11	0.01	0.03	0.00	0.03	0.00	0.00	0.17	0.01	**18%**
5	0.00	0.03	0.00	0.03	0.00	0.00	0.00	0.01	**10%**

In order to compare Dickens Sample A and the aggregated Caprock Canyon samples from section B a dissimilarity test (see Equation 2) was carried out (Table 4). This dissimilarity metric combines the dissimilarities of each of the eight phytolith assemblages into a single number, with lower values indicating higher similarity. When compared to Dickens' sample A, the section B samples from 11m, 53m and 67m height have a large squared difference (0.14-0.17) in the proportional occurrence of Perforated strands (group 7 phytoliths). The absence of this morphotype in the sample from 15m results in a squared difference of 0.09, when compared to sample A. The dissimilarity metric of 8% confirms that the assemblages sampled close to the highest ash in the Dickens (sample A) and Caprock Canyon (sample 23m section B) are indeed the most similar. When compared to sample A, section B samples from 5, 33, and 43 meters show a slightly higher dissimilarity metric (10-12%). Sample A was retrieved 25 to 27 meters above the Whitehorse-Quartermaster contact. Based on the distance between this contact and the highest ash layer is the Dickens' and Caprock Canyon section sample A partially overlaps the depth range of the aggregate sample from profile B (19.6 – 25.6 m above the contact). The dissimilarity evaluation thus correctly identified the appropriate location of the aggregated sample within these two sections.

3.3.2 Location of samples C, D and E in B

Non-aggregated samples from Caprock Canyon sections C, D and E were collected below (BLQMA) and above (ALQMA) the Lower Quartermaster Ash layer, which outcrops 6 meters above the Whitehorse-Quartermaster contact (Fig. 8). Just like Dickens' sample A, the phytolith assemblages from these samples were compared to the aggregate samples of section B. The samples from sections C, D and E contained

between 17 and 37 identifiable phytoliths each. The most dominant phytolith morphotype in all but one samples is Carbon core square morphotype (group 3, 39-89%), in the other sample (section C 5.3 m) it is co-dominant with the Clavate morphotype (group 5, 28%).

The overwhelming abundance of the Carbon core square morphotype in the C, D and E samples, which is present only in very small proportions in section, are a cause for high dissimilarity metric scores between the two cores (Table 5). Overall, the average dissimilarity metrics are much higher (18-35%) than those found in the comparison between samples from sections A and B (8-19%). The lowest metrics correspond to the aggregated sample from 5m in profile B for two of the nine samples in C, D or E, correctly identifying the location. The seven other samples are more similar to other samples in section B. In this case, the similarity evaluation did not correctly identify the corresponding level of the samples within the section.

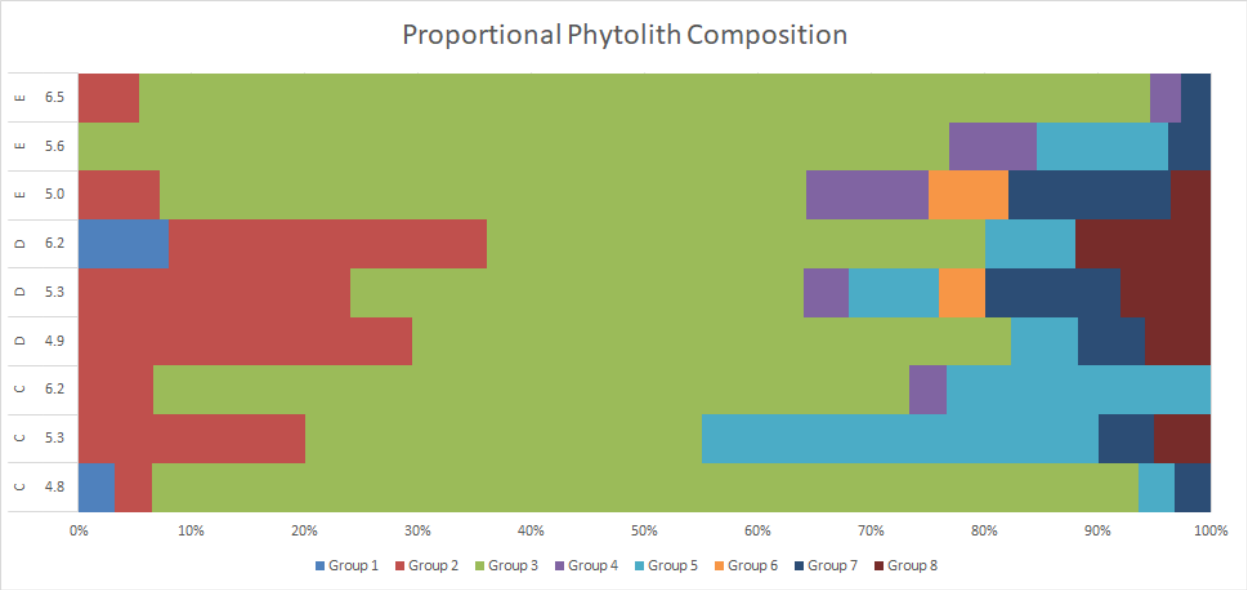

Fig 8. *Proportional occurrence of eight phytolith morphotype groups in a total of nine samples from sections C, D and E, Caprock Canyon, Palo Duro Basin, Texas. The phytolith morphotype groups comprise: 1) Orbicular ornamented, 2) Carbon core orbicular, 3) Carbon core square, 4) Circular bordered pits (uniseriate), 5) Clavate, 6) Cuneiform, 7) Perforated strands and 8) Reniform. Indicated in the left margin are the average sample heights (m) above the Whitehorse-Quartermaster contact.*

Table 5: *Dissimilarity Metric for non-aggregated phytolith samples from sections C, D and E, compared to aggregated samples from section B, Caprock Canyon, Palo Duro Basin, Texas. The lowest dissimilarity values are in bold. Shading of column headings indicate relative position below (darker) or above (lighter) Lower Quartermaster Ash layer. Location is in meters above the Whitehorse-Quartermaster contact.*

	Profile	C	C	C	D	D	D	E	E	E
Profile	Location above WHF (m)	4.8	5.3	6.15	4.9	5.3	6.15	5	5.6	6.5
B	67	34%	28%	31%	28%	24%	28%	25%	32%	35%
B	53	37%	27%	33%	29%	24%	29%	26%	34%	37%
B	43	**34%**	23%	29%	25%	20%	24%	**23%**	31%	**35%**
B	33	35%	23%	30%	23%	19%	22%	24%	32%	35%
B	23	35%	22%	29%	25%	20%	24%	23%	**31%**	35%
B	15	35%	**18%**	**27%**	24%	19%	**20%**	26%	32%	36%
B	11	38%	29%	34%	30%	26%	30%	28%	36%	39%
B	5	35%	21%	30%	**21%**	**17%**	20%	24%	32%	35%
Lowest dissimilarity metric		**34%**	**18%**	**27%**	**21%**	**17%**	**20%**	**23%**	**31%**	**35%**
Location of lowest dissimilarity in profile B (m)		**43**	**15**	**15**	**5**	**5**	**15**	**43**	**23**	**43**

3.3.3 The position of the Lower Quartermaster Ash layer in profiles C, D and E

Sections C, D and E all straddle the Lower Quartermaster Ash (LQMA) layer, with two samples collected below and one sample above the ash layer at very similar distances in all three profiles. The average similarity of the samples collected below the LQMA was calculated and compared to the similarity across the LQMA, both within the same profile, across profiles, and overall (Table 6). The two samples collected below the LQMA are on average less similar (17%, within the same section) than the samples across the LQMA within the same section (8%). Comparing across profiles, below the LQMA samples appear more similar (15%) than across the LQMA (22%). Overall, the similarity of the samples collected below the LQMA (16%) is very close to the similarity of samples collected across the LQMA (15%). The similarity evaluation thus did not reveal a coherent change in phytolith composition across the LQMA.

Table 6. *Dissimilarity Metric for aggregated phytolith samples from sections C, D and E, Caprock Canyon, Palo Duro Basin, Texas. Compared are samples below and across the Lower Quartermaster Ash within the same section, across sections and all sections.*

Dissimilarity Metric		profile within	profile across	profile all
LQMA position	below	17%	15%	16%
	across	8%	22%	15%

3.3.4 Phytolith compositions across the Permian-Triassic transition

Based on the ash dates, profiles F and G both straddle the Permian-Triassic Boundary at approximately 9 meters above the Whitehorse-Quartermaster contact at Caprock Canyon and Palo Duro. Because of the limited number of identified phytoliths, all samples from each of these sections were combined (Figure 9; Table 7). The samples collected at 9m were excluded from this analysis because this test focuses on distinguishing only two categories, Permian and Triassic. The assemblages of the four aggregated samples contained between 21 and 64 identified phytoliths. These aggregate samples represent a vertical distance varying from 0.5 m to 3.5 meters. The presumed Permian aggregate samples overlap the same location range, while the presumed Triassic samples of profile F were collected entirely from above the Triassic samples in profile G.

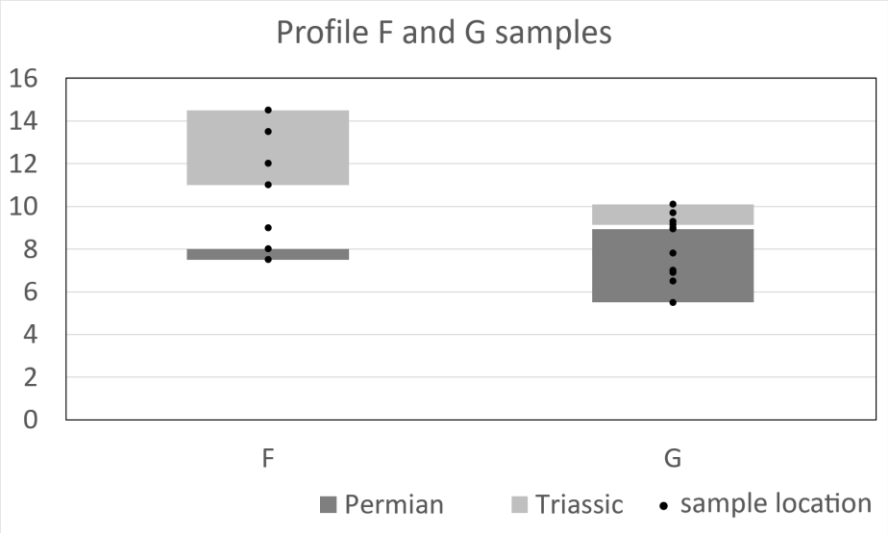

Fig 9. *Caprock Canyon section F, and Palo Duru section G, Palo Duro Basin, Texas, with all the sample locations indicated, combined in two aggregated samples each which exclusively contain samples from above or below the presumed boundary.*

Tabel 7. *Caprock Canyon section F, and Palo Duru section G, Palo Duro Basin, Texas, with their respective number of samples included, their physical position in the field in meters from above or below the presumed boundary, and the total number of phytoliths in each aggregate sample.*

Profile	Period	Samples	Location (m)			Phytoliths
			bottom	top	range	Total
F	Triassic	4	11	14.5	3.5	64
F	Permian	2	7.5	8.0	0.5	41
G	Triassic	4	9.15	10.1	0.95	21
G	Permian	6	5.5	8.95	3.45	49

The composition of the phytolith assemblage of the presumed Triassic aggregate sample of section F is distinctly different from the other three samples in sections F and G (Fig. 10). It contains a larger proportion of the "carbon core square" morphotype (group 3, 42%) and a small proportion of "reniform" phytoliths (group 8, 9%), but "perforated strands" phytoliths are almost absent. The other three samples contain on average 31 (±13) % to 44 (±15) % of "perforated strands" phytoliths and varying proportions of the other morphotypes, but the reniform

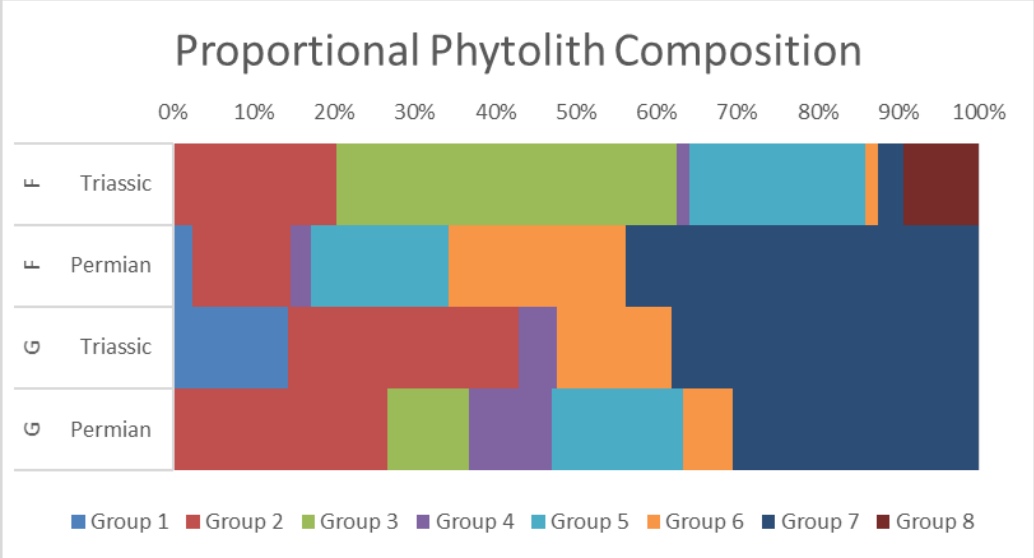

Fig 10. *Proportional occurrence of eight phytolith morphotype groups in four aggregated samples Caprock Canyon section F, and Palo Duro section G, Palo Duro Basin, Texas. The phytolith morphotype groups comprise: 1) Orbicular ornamented, 2) Carbon core orbicular, 3) Carbon core square, 4) Circular*

bordered pits (uniseriate), 5) Clavate, 6) Cuneiform, 7) Perforated strands and 8) Reniform. Indicated in the left margin are the presumed period ages these samples represent.

The dissimilarity metric comparing Triassic and Permian samples from sections F and G confirms the differences that were noted visually from the proportional phytolith composition (Fig. 10). Table 8 shows that the Permian sample from Caprock Canyon section F is quite similar to the Permian and Triassic samples from Palo Duro section G (with a dissimilarity metric of 10% for both). The Triassic sample from section F is less similar to the Permian sample from G (16%). As visually noted, the dissimilarity between the Triassic sample in F and the Triassic sample in G is the largest (22%) of all comparisons.

Tabel 8. *Dissimilarity Metric for two aggregated samples of Caprock Canyon section F, and two aggregated samples from Palo Duro section G, Palo Duro Basin, Texas. Indicated in the left margin are the presumed period ages these samples represent.*

Profile	Period	F Triassic	F Permian
G	Triassic	22%	10%
G	Permian	16%	10%

The similarity evaluation did show a coherent change in phytolith composition across the Permian-Triassic transition.

4 Discussion

The end-Permian biotic crisis caused floral turnovers and the gradual extinction of several dominant arborescent plant groups from the tropics to the polar regions. In the more temperate northern and southern floral realms, Angara and Gondwana, the plant groups that become dominant in the subsequent survival and recovery intervals include plant lineages that originated in equatorial Euramerica. One of the plant groups that migrates into Gondwana is the seed fern *Dicroidium*, which was during Permian times only known from deposits in Jordan (Kerp et al. 2006). Another plant group that becomes more widespread are the Voltzian conifers (voltzian Voltziales, sensu Escapa et al. 2010), the only conifer lineage that survived the crisis, and becomes a major component of both the Angaran and Gondwanan floras.

After a gap in their micro- and macrofossil record of 4-5 million years the Voltzian conifers are also return to the equatoral Euramercian realm. They are considered to be immigrants that survived in refugia outside the eastern part of Euramerica (Looy et al., 1999). These areas could have been located in northern Africa and Arabia, where during the Late Permian floras with both Euramerican and Gondwanan elements existed

(e.g., El-Khayal and Wagner 1985). Western Euramerica has also been mentioned as a region for potential refugia, but unfortunately conditions for preservation in this area were very low from the mid-Guadalupian to mid-Triassic on, and there are no pollen or macrofossils known from this interval (DiMichele et al. 2008). The aim of this study was 1) to extract and describe phytoliths and their distribution patterns from latest Permian and early-middle Triassic sediments from the Palo Duro Basin north-central Texas, 2) discuss the potential botanical affinities of the fossil morphotypes, and the evidence for conifer refugia, and (3) test the potential of phytolith assemblages to support biostratigraphy of Permian and Triassic strata.

71 of the 74 samples processed latest Permian to Triassic age samples from the Dickens, Caprock Canyon and Palo Duro sites proved to be productive. A total of thirty-three morphotypes were identified (Plates 1-10) and the samples were quantitatively analyzed. Because the phytolith yield per sample was relatively low, the phytolith morphotypes were combined into 8 morphotype groups (Table 4), and the less productive samples were combined into aggregated samples.

The most notable phytoliths have imprints of circular boarded pits which are characteristic features of the coniferous wood macrofossil petrifactions found in the same section (compare Plate 2C-D and appendix 2).

Botanical affinities. It has proven to be most challenging to associate the botanical affinities with the fossil morphotypes. The preservation of the material and potentially the extraction procedures do not lend themselves to an optimal phytolith recovery and identification. The most intriguing morphotype encountered are phytoliths that were deposited in coniferophyte tracheids: 1) Araucarioid pitting, 2) Uniseriate circular bordered pitting, and 3) Vesticular infillings. The Araucarioid pitting types are heptaseriate, alternate bordered pits (Plate 3a-d) are similar to those found in conifers with araucarioid wood. While they have superficially similar pitting patterns as those seen in e.g., *Betula* and *Cedar*, both of which are commonly used in the paper industry, but the apertures in Betula are slitted and those in Cedar show an opposite pattern. This morphotype was exceedingly rare and was observed only 8 times in total, twice in what is assumed to be Permian strata and 6 times in sediments of Triassic age. Narrowing down its botanical affinity would be very informative with regard to its geographical spread and its response to the end Permian biotic crisis. A wood fragment found in the Early Triassic sediments in Caprock Canyon State Park (GPS coordinates known by the author) was studied by Marion Bamford and is potentially related to Agathis and Araucaria, both of which have uniseriate vascular rays (Marion Bamford, pers. comm.) These uniseriate circular bordered pits are relatively common phytolith morphotype in the Permian and Triassic samples. For a comparison between the fossil wood and the fossil phytolith see Appendix 2.

The vesticular infillings morphotype is one of the few morphotypes that are comparable to "siliceous spherules" described from tracheid of silicified Cordaitalean wood from the Pennsylvanian, Oklahoma (Wilson and Clark 1960). The authors believed that the 10-70 micron concentrically layered spherules formed around organic nuclei during the petrification process. The specimens observed in the Texan samples have concentric layers as well, but do not show evidence of nuclei. They are similar to morphotypes observed by Strömberg (pers. comm.). Another less taxon-specific morphotype are the infillings of cells that form the base of epidermal hairs. These circular to oval cells are common in Paleozoic conifers and seed ferns (e.g., Clement-Westerhof 1984; Kerp 1990).

Biostratigraphy. We also tested the potential of phytolith assemblages to support biostratigraphy of Permian and Triassic strata. The phytolith composition in a sample from a distant profile (A, C, D, or E) was most similar to the phytolith composition at the correct depth range within a longer profile (B) in only one (A) of the four examples. We did not demonstrate that phytolith composition can consistently identify the correct depth range.

None of the samples collected above and below a geological feature (i.e. the Lower Quartermaster Ash layer show the greatest similarity with samples collected from the same position with respect to the geological strata in a distant profile. We did not demonstrate that phytolith composition can identify the correct position (above or below) a geological boundary.

The phytolith yield of the rock samples may be correlated with the types of sediment that make up the various strata as well as with the various depositional environments with which these strata are associated. The Whitehorse Group goes from perimarine gypsiferous sandstones, mudstones, gypsum and dolomites to the intertidal and supratidal calcareous mudstones and sandstones which are interpreted to be fluvial channel deposits of the Quartermaster Formation. Besides different taphonomical regimes for the range of environments the Whitehorse to Quartermaster represent, it is also likely the near shore plant communities and those fringing the river channels are different in composition.

Data aggregation. Our current approach aggregates samples to a total of approximately 50 identified phytoliths. As a result, the depth representation varies from a single point sample to a range of 16 meters. Alternatively, a fixed depth range can be aggregated and a weighted average could be applied to achieve consistency. Total phytolith abundance is discarded in our approach. Abundance could be incorporated as an additional metric to quantify similarity. Phytolith yield may be the product of production rate and volume by the vegetation, sedimentation and preservation or—more likely—a combination of both (e.g. Mulholland and Rapp 1992). Increasing the yield of certain samples would require processing a greater volume of rock sample. For some of the more sparse samples, it would mean having to process 50 times as much material.

The uncertainty around the proportion of each morphotype could be incorporated into the dissimilarity metric. Smaller proportions have a smaller confidence interval (e.g. 8% for a proportion of 10% with n=50) than larger proportions (e.g. 14% for a proportion of 50% with n=50). Because the aggregated samples had similar sizes (approximately 50 identified phytoliths), the uncertainty around each calculated proportion is in the same order of magnitude.

While phytolith-based biostratigraphy has been unsuccessful in this study, we demonstrated that phytoliths of Permian and Triassic age can serve as evidence of plant life at the western portion of the supercontinent Pangea, a region previously believed to be barren.

Conclusion. This study showed that diverse phytolith assemblages can be isolated from sediments of late Permian and Triassic age, that more research needs to be done to establish the botanical affinity of the recovered phytoliths, and shows that phytolith assemblages have some potential use for biostratigraphy of regional Permian and Triassic strata. The presence of phytoliths with circular bordered pits throughout the sections suggests that woody vegetation was present along the coastal margin of Panthalassa on western Pangea before, during, and after the Permian mass extinction. A layer with petrified wood fragments with a similar pitting higher up in the Caprock Canyon section, known to represent conifers (Marion Bamford, pers. comm.), is additional proof that these plants were present in the region (see Appendix 2). These finds, both phytoliths and wood, are the first evidence for late Permian - Early Triassic plant life in the continental US. Assuming that the probable PTB transition in the Quartermaster fm proves to be stratigraphically conformable, then these results imply that—contrary to what has been generally suggested—the tropical Panthalassa margin of Pangea was not barren, but preserved woodland ecological elements throughout the troublesome time period crossing the Permian-Triassic transition.

Work cited

Benton, M.J., and Andrew J. Newell. 2014. “Impacts of Global Warming on Permo-Triassic Terrestrial Ecosystems.” *Gondwana Research* 25 (4): 1308–37. https://doi.org/10.1016/j.gr.2012.12.010.

Black, Benjamin A, Jean-François Lamarque, Christine A Shields, Linda T Elkins-Tanton, and Jeffrey T Kiehl. 2014. “Acid Rain and Ozone Depletion from Pulsed Siberian Traps Magmatism.” *Geology* 42 (1): 67–70.

Blinnikov, M. 1999. “Late-Pleistocene History of the Columbia Basin Grassland Based on Phytolith Records in Loess.” PhD dissertation, University of Oregon, Eugene, OR.

Brodribb, Tim, and Robert S Hill. 2004. “The Rise and Fall of the Podocarpaceae in Australia—A Physiological Explanation.” In *The Evolution of Plant Physiology*, 381–99. Elsevier. https://doi.org/10.1016/B978-012339552-8/50020-2.

Burgess, Seth D., and Samuel A. Bowring. 2015. “High-Precision Geochronology Confirms Voluminous Magmatism before, during, and after Earth’s Most Severe Extinction.” *Science Advances* 1 (7): e1500470. https://doi.org/10.1126/sciadv.1500470.

Burgess, Seth D., Samuel Bowring, and Shu-zhong Shen. 2014. “High-Precision Timeline for Earth’s Most Severe Extinction.” *Proceedings of the National Academy of Sciences* 111 (9): 3316–21. https://doi.org/10.1073/pnas.1317692111.

Campbell, Malcolm M., and Ronald R. Sederoff. 1996. “Variation in Lignin Content and Composition (Mechanisms of Control and Implications for the Genetic Improvement of Plants).” *Plant Physiology* 110 (1): 3.

Chang, S. 2008. “Applications of High-Precision Geochronology in Evolution and Mass Extinctions.” PhD dissertation, University of California Berkeley.

Chave, Keith E. 1984. “Physics and Chemistry of Biomineralization.” *Annual Review of Earth and Planetary Sciences* 12 (1): 293–305.

Clement-Westerhof, Johanna A. 1984. “Aspects of Permian Palaeobotany and Palynology. IV. The Conifer Ortiseia Florin from the Val Gardena Formation of the Dolomites and the Vicentinian Alps (Italy) with Special Reference to a Revised Concept of the Walchiaceae (Göppert) Schimper.” *Review of Palaeobotany and Palynology* 41 (1–2): 51–166.

Crisp, Michael D., and Lyn G. Cook. 2011. “Cenozoic Extinctions Account for the Low Diversity of Extant Gymnosperms Compared with Angiosperms.” *New Phytologist* 192 (4): 997–1009. https://doi.org/10.1111/j.1469-8137.2011.03862.x.

Cui, Ying, Antoine Bercovici, Jianxin Yu, Lee R. Kump, Katherine H. Freeman, Shangguo Su, and Vivi Vajda. 2017. “Carbon Cycle Perturbation Expressed in Terrestrial Permian–Triassic Boundary Sections in South China.” *Global and Planetary Change* 148 (January): 272–85. https://doi.org/10.1016/j.gloplacha.2015.10.018.

DiMichele, W, H Kerp, N Tabor, and C Looy. 2008. “The So-Called ‘Paleophytic–Mesophytic’ Transition in Equatorial Pangea — Multiple Biomes and Vegetational Tracking of Climate Change through Geological Time.” *Palaeogeography, Palaeoclimatology, Palaeoecology* 268 (3–4): 152–63. https://doi.org/10.1016/j.palaeo.2008.06.006.

El-Khayal, AA, and RH Wagner. 1985. “Upper Permian Stratigraphy and Megafloras of Saudi Arabia: Palaeogeographic and Climatic Implications.” In *Compte Rendu*, 10:17–26.

Erwin, D. H. 2006. *Extinction : How Life on Earth Nearly Ended 250 Million Years Ago*. Princeton, N.J.: Princeton University Press.

Escapa, Ignacio H., Anne-Laure Decombeix, Edith L. Taylor, and Thomas N. Taylor. 2010. “Evolution and Relationships of the Conifer Seed Cone *Telemachus* : Evidence from the Triassic of Antarctica.” *International Journal of Plant Sciences* 171 (5): 560–73. https://doi.org/10.1086/651948.

Fang, Jiang-yu, and Xue-long Ma. 2006. “In Vitro Simulation Studies of Silica Deposition Induced by Lignin from Rice.” *Journal of Zhejiang University SCIENCE B* 7 (4): 267–71. https://doi.org/10.1631/jzus.2006.B0267.

Gradstein, Felix M., James G. Ogg, and Alan G. Smith, eds. 2005. *A Geologic Time Scale 2004*. Cambridge: Cambridge University Press. https://doi.org/10.1017/CBO9780511536045.

Grauvogel-Stamm, L., and S. Ash. 2005. "Recovery of the Triassic Land Flora from the End-Permian Life Crisis." *Comptes Rendus Palevol* 4 (6–7): 593–608. https://doi.org/10.1016/j.crpv.2005.07.002.

Gustavson, Thomas C., William W. Smpkins, Alan Alhades, and Ann Hoadley. 1982. "Evaporite Dissolution and Development of Karst Features on the Rolling Plains of the Texas Panhandle." *Earth Surface Processes and Landforms* 7 (6): 545–63. https://doi.org/10.1002/esp.3290070604.

Kerp, Hans. 1990. "The Study of Fossil Gymnosperms by Means of Cuticular Analysis." *Palaios*, 548–569.

Kerp, Hans, Abdalla Abu Hamad, Birgit Vörding, and Klaus Bandel. 2006. "Typical Triassic Gondwanan Floral Elements in the Upper Permian of the Paleotropics." *Geology* 34 (4): 265. https://doi.org/10.1130/G22187.1.

Klavins, Sharon D., Derek W. Kellogg, Michael Krings, Edith L. Taylor, and Thomas N. Taylor. 2005. "Coprolites in a Middle Triassic Cycad Pollen Cone: Evidence for Insect Pollination in Early Cycads?"

Knoll, A.H. 1984. "Patterns of Extinction in the Fossil Record of Vascular Plants." In *Extinctions*, edited by M.H. Nitecki, 21–68. Chicago: The University of Chicago.

Kunzmann, Lutz. 2007. "Araucariaceae (Pinopsida): Aspects in Palaeobiogeography and Palaeobiodiversity in the Mesozoic." *Zoologischer Anzeiger - A Journal of Comparative Zoology* 246 (4): 257–77. https://doi.org/10.1016/j.jcz.2007.08.001.

Labandeira, Conrad C., and J. John Sepkoski. 1993. "Insect Diversity in the Fossil Record." *Science* 261 (5119): 310–15.

Lehman, Tom., John. Schnable, Craig. Bunting, Geological Society of America., South-Central Section., and Meeting. 1999. *Guidebook for the Stratigraphy of the Caprock Escarpment as Exposed at Caprock Canyons State Park, Briscoe County, Texas : Prepared for Spring 1999 Fieldtrip for the South-Central Section Meeting of the Geological Society of America, March 14, 1999*. Lubbock, TX: The Dept.

LePage, B.A. 2003. "THE EVOLUTION, BIOGEOGRAPHY AND PALAEOECOLOGY OF THE PINACEAE BASED ON FOSSIL AND EXTANT REPRESENTATIVES." *Acta Horticulturae*, no. 615 (September): 29–52. https://doi.org/10.17660/ActaHortic.2003.615.1.

Looy, Brugman, Dilcher, and Visscher. 1999. "The Delayed Resurgence of Equatorial Forests After the Permian–Triassic Ecologic Crisis." *Proceedings of the National Academy of Sciences* 96 (24): 13857–62. https://doi.org/10.1073/pnas.96.24.13857.

Looy, C., H. Kerp, I. Duijnstee, and B. DiMichele. 2014. "The Late Paleozoic Ecological-Evolutionary Laboratory, a Land-Plant Fossil Record Perspective." *The Sedimentary Record* 12 (4): 4–18.

Looy, C., R. Twitchett, D. Dilcher, J. Van Konijnenburg-Van Cittert, and H. Visscher. 2001. "Life in the End-Permian Dead Zone." *Proceedings of the National Academy of Sciences of the United States of America* 98 (14): 7879–83. https://doi.org/10.1073/pnas.131218098.

Lucas, S.G., and O.J. Anderson. 1993. "Stratigraphy of the Permian-Triassic Boundary in Southeastern New Mexico and West Texas." *New Mexico Geological Society 44th Annual Fall Field Conference Guidebook*, Carlsbad Region (New Mexico and West Texas), , 219–30.

McElwain, Jennifer C., and Surangi W. Punyasena. 2007. "Mass Extinction Events and the Plant Fossil Record." *Trends in Ecology & Evolution* 22 (10): 548–57. https://doi.org/10.1016/j.tree.2007.09.003.

Metzgar, Jordan S., Judith E. Skog, Elizabeth A. Zimmer, and Kathleen M. Pryer. 2008. "The Paraphyly of *Osmunda* Is Confirmed by Phylogenetic Analyses of Seven Plastid Loci." *Systematic Botany* 33 (1): 31–36. https://doi.org/10.1600/036364408783887528.

Mitchell, W.S. 2014. "High-Resolution U-Pb Geochronology of Terrestrial Cretaceous-Paleogene and Permo-Triassic Boundary Sequences in North America." PhD dissertation, Berkeley CA USA: University of California Berkeley.

Mulholland, Susan C, and George Rapp. 1992. “Phytolith Systematics: An Introduction.” In *Phytolith Systematics*, 1–13. Springer.
Nance, H.S. 1988. “Interfingering of Evaporites and Red Beds: An Example from the Queen/Grayburg Formation, Texas.” *Sedimentary Geology* 56 (1–4): 357–81. https://doi.org/10.1016/0037-0738(88)90061-9.
Padian, Kevin. 2018. “Measuring and Comparing Extinction Events: Reconsidering Diversity Crises and Concepts.” *Integrative and Comparative Biology*, July. https://doi.org/10.1093/icb/icy084.
Payne, and Clapham. 2012. “End-Permian Mass Extinction in the Oceans: An Ancient Analog for the Twenty-First Century?” *Annual Review of Earth and Planetary Sciences* 40.
Payne, J. L. 2004. “Large Perturbations of the Carbon Cycle During Recovery from the End-Permian Extinction.” *Science* 305 (5683): 506–9. https://doi.org/10.1126/science.1097023.
Pearsall, DM. 2000. “Paleoethnobotany: A Handbook of Procedures Academic Press.” *San Diego, Calif.*
Piperno, D. R., and Sues. 2005. “PALEONTOLOGY: Dinosaurs Dined on Grass.” *Science* 310 (5751): 1126–28. https://doi.org/10.1126/science.1121020.
Piperno, Dolores R. 2006. *Phytoliths : A Comprehensive Guide for Archaeologists and Paleoecologists*. Lanham, Md.: AltaMira.
Poort, Ruud J., Johanna A. Clement-Westerhof, Cindy V. Looy, and Henk Visscher. 1997. “Aspects of Permian Palaeobotany and Palynology. XVII. Conifer Extinction in Europe at the Permian-Triassic Junction: Morphology, Ultrastructure and Geographic/Stratigraphic Distribution of Nuskoisporites Dulhuntyi (Prepollen of Ortiseia, Walchiaceae).” *Review of Palaeobotany and Palynology* 97 (1–2): 9–39. https://doi.org/10.1016/S0034-6667(96)00072-3.
Prasad, V., C. A. E. Strömberg, H. Alimohammadian, and A. Sahni. 2005. “Dinosaur Coprolites and the Early Evolution of Grasses and Grazers.” *Science* 310 (5751): 1177–80. https://doi.org/10.1126/science.1118806.
Ran, Jin-Hua, Hui Gao, and Xiao-Quan Wang. 2010. “Fast Evolution of the Retroprocessed Mitochondrial Rps3 Gene in Conifer II and Further Evidence for the Phylogeny of Gymnosperms.” *Molecular Phylogenetics and Evolution* 54 (1): 136–49. https://doi.org/10.1016/j.ympev.2009.09.011.
Rees, P. McAllister. 2002. “Land-Plant Diversity and the End-Permian Mass Extinction.” *Geology* 30 (9): 827–30. https://doi.org/10.1130/0091-7613(2002)030<0827:LPDATE>2.0.CO;2.
Retallack, G. J. 1995. “Permian-Triassic Life Crisis on Land.” *Science* 267 (5194): 77–80. https://doi.org/10.1126/science.267.5194.77.
Rydin, Catarina, Kaj Raunsgaard Pedersen, Peter R. Crane, and Else Marie Friis. 2006. “Former Diversity of Ephedra (Gnetales): Evidence from Early Cretaceous Seeds from Portugal and North America.” *Annals of Botany* 98 (1): 123–40. https://doi.org/10.1093/aob/mcl078.
Schneebeli-Hermann, Elke, Peter A. Hochuli, and Hugo Bucher. 2017. “Palynofloral Associations before and after the Permian–Triassic Mass Extinction, Kap Stosch, East Greenland.” *Global and Planetary Change*, July. https://doi.org/10.1016/j.gloplacha.2017.06.009.
Stanley, Steven M. 2016. “Estimates of the Magnitudes of Major Marine Mass Extinctions in Earth History.” *Proceedings of the National Academy of Sciences* 113 (42): E6325–34. https://doi.org/10.1073/pnas.1613094113.
Strömberg, C. 2004. “Using Phytolith Assemblages to Reconstruct the Origin and Spread of Grass-Dominated Habitats in the Great Plains of North America during the Late Eocene to Early Miocene.” *Palaeogeography, Palaeoclimatology, Palaeoecology* 207 (3–4): 239–75. https://doi.org/10.1016/j.palaeo.2003.09.028.
———. 2009. “Methodological Concerns for Analysis of Phytolith Assemblages: Does Count Size Matter?” *Quaternary International* 193 (1–2): 124–40. https://doi.org/10.1016/j.quaint.2007.11.008.
Struve, G.A. 1835. “Silica in plantis nonnullis.” Thesis, Universitate Litteraria Friderica Guilelma.
Tabor, Neil J., and Christopher J. Poulsen. 2008. “Palaeoclimate across the Late Pennsylvanian–Early Permian Tropical Palaeolatitudes: A Review of Climate Indicators, Their Distribution, and

Relation to Palaeophysiographic Climate Factors." *Palaeogeography, Palaeoclimatology, Palaeoecology* 268 (3–4): 293–310. https://doi.org/10.1016/j.palaeo.2008.03.052.
Tabor, N.J., T.S. Myers, G.H. Mack, J.W. Geissman, D. Collins, P.R. Renne, R. Mundil, W.S. Mitchell, C V Looy, and R. Kirchholtes. in prep. "A Revised Age for the Quartermaster Formation (Lower Triassic): Evidence of a Continuous Permian-Triassic Boundary Section in the Palo Duro Basin, North-Central Texas, U.S.A."
Tabor, N.J., T.S. Myers, G.H. Mack, C.V. Looy, P.R. Renne, R. Bateman, and J.W. Geissman. 2011. ""Ochoan" Quatermaster Formation of North Texas, USA, Part I: Litho- and Chemostratigraphy." presented at the GSA Annual Meeting, Minneapolis, October. https://gsa.confex.com/gsa/2011AM/finalprogram/abstract_195308.htm.
Trembath-Reichert, Elizabeth, Jonathan Paul Wilson, Shawn E. McGlynn, and Woodward W. Fischer. 2015. "Four Hundred Million Years of Silica Biomineralization in Land Plants." *Proceedings of the National Academy of Sciences*, March, 201500289. https://doi.org/10.1073/pnas.1500289112.
Veevers, J. J. 1994. *Permian-Triassic Pangean Basins and Foldbelts Along the Panthalassan Margin of Gondwanaland*. Geological Society of America.
Visscher, H., H. Brinkhuis, D L Dilcher, W C Elsik, Y. Eshet, C V Looy, M R Rampino, and A. Traverse. 1996. "The Terminal Paleozoic Fungal Event: Evidence of Terrestrial Ecosystem Destabilization and Collapse." *Proceedings of the National Academy of Sciences* 93 (5): 2155–58.
Wang, Shi-Jun, Xiao-Yuan He, and Long-Yi Shao. 2011. "Cycad Wood from the Lopingian (Late Permian) of Southern China: Shuichengoxylon Tianii Gen. et Sp. Nov." *International Journal of Plant Sciences* 172 (5): 725–34. https://doi.org/10.1086/659454.
Wellman, Charles H., Peter L. Osterloff, and Uzma Mohiuddin. 2003. "Fragments of the Earliest Land Plants." *Nature* 425 (6955): 282–85. https://doi.org/10.1038/nature01884.
Wilson, L.R., and R.T. Clark. 1960. "Siliceous Spherules in Tracheids of Codaitean Wood." *Oklahoma Geology Notes* 20 (5): 106–10.
Wit, Maarten J. de, Joy G. Ghosh, Stephanie de Villiers, Nicolas Rakotosolofo, James Alexander, Archana Tripathi, and Cindy Looy. 2002. "Multiple Organic Carbon Isotope Reversals across the Permo-Triassic Boundary of Terrestrial Gondwana Sequences: Clues to Extinction Patterns and Delayed Ecosystem Recovery." *The Journal of Geology* 110 (2): 227–40. https://doi.org/10.1086/338411.
Xiong, Conghui, and Qi Wang. 2011. "Permian–Triassic Land-Plant Diversity in South China: Was There a Mass Extinction at the Permian/Triassic Boundary?" *Paleobiology* 37 (1): 157–67. https://doi.org/10.1666/09029.1.
Yang, Zu-Yu, Jin-Hua Ran, and Xiao-Quan Wang. 2012. "Three Genome-Based Phylogeny of Cupressaceae s.l.: Further Evidence for the Evolution of Gymnosperms and Southern Hemisphere Biogeography." *Molecular Phylogenetics and Evolution* 64 (3): 452–70. https://doi.org/10.1016/j.ympev.2012.05.004.
Zhou, Zhi-Yan. 2009. "An Overview of Fossil Ginkgoales." *Palaeoworld* 18 (1): 1–22. https://doi.org/10.1016/j.palwor.2009.01.001.

APPENDIX 1

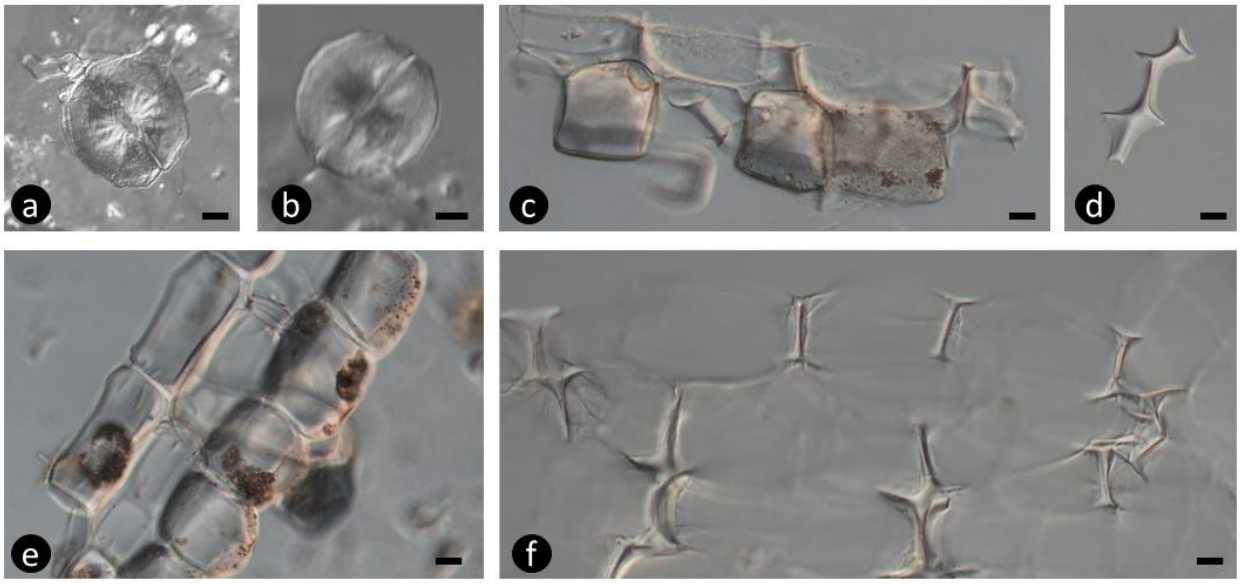

Plate 11. Phytoliths extracted from extant plants. Morphological description in brackets. **a - b**: *Huperzia phlegmari* (a and b: silicified stomata; **c - f**: *Isoetes* sp. (c and e: polyhedral bulliform; d and f: polyhedral epidermal). Scale bar is 10µm.

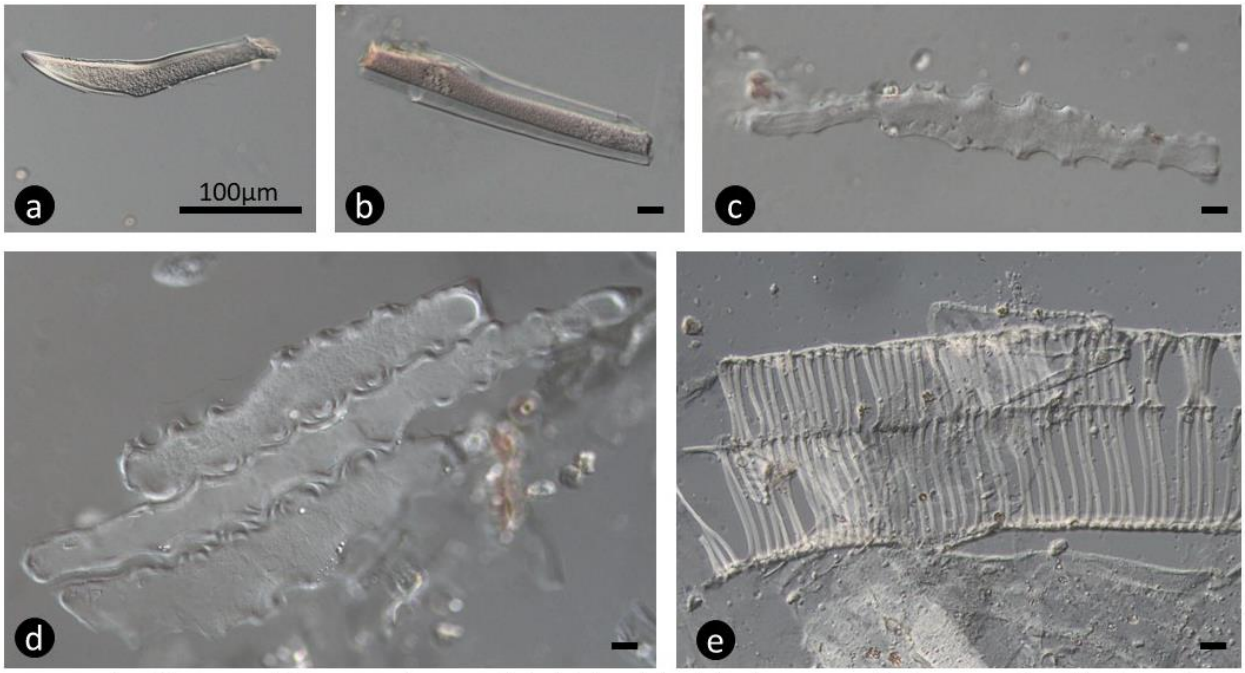

Plate 12. Phytoliths extracted from extant plants. Morphological description in brackets. **a - e**: *Palhinhaea cernua* (a and b: Elongated with centrally raised parallelepipedal feature; c and d: elongate crenate on both sides, e: vascular tissue) Scale bar is 10µm unless noted otherwise.

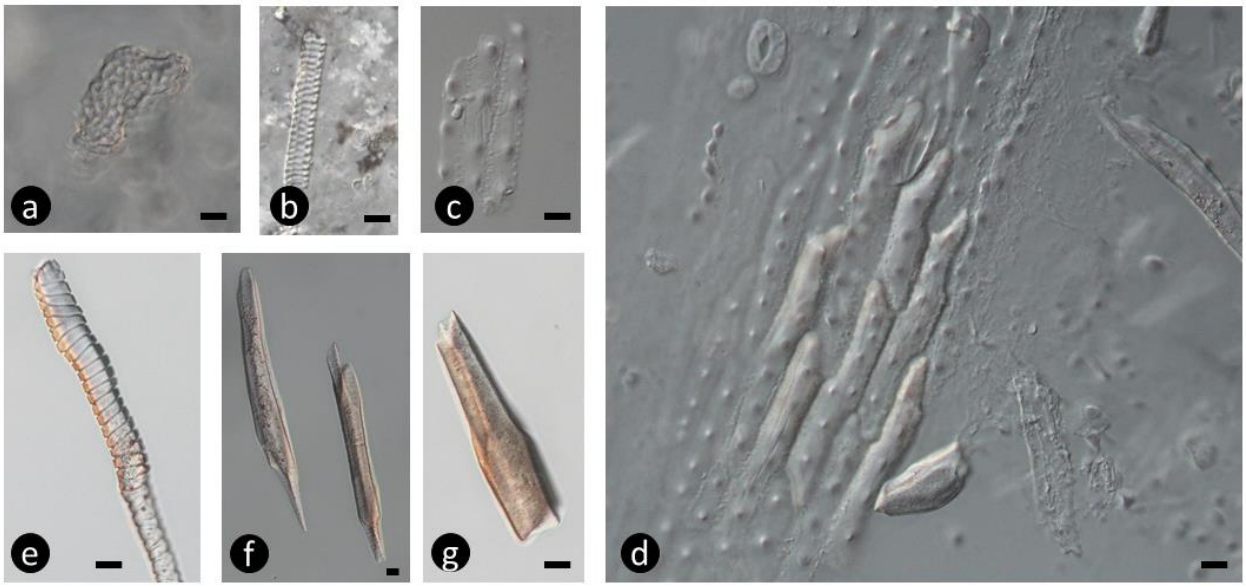

Plate 13. Phytoliths extracted from extant plants. Morphological description in brackets. **a**: *Lycopodium venustulum* (a: Irregular body with lacunose depressions); **b - d**: *Selaginella pallescens* (b: vascular tissue; c and d: irregular body with verrucate nodes) **e - g**: *Selaginella plana* (e: tracheid; f and g: elongate smooth rod with edges along the body). Scale bar is 10µm.

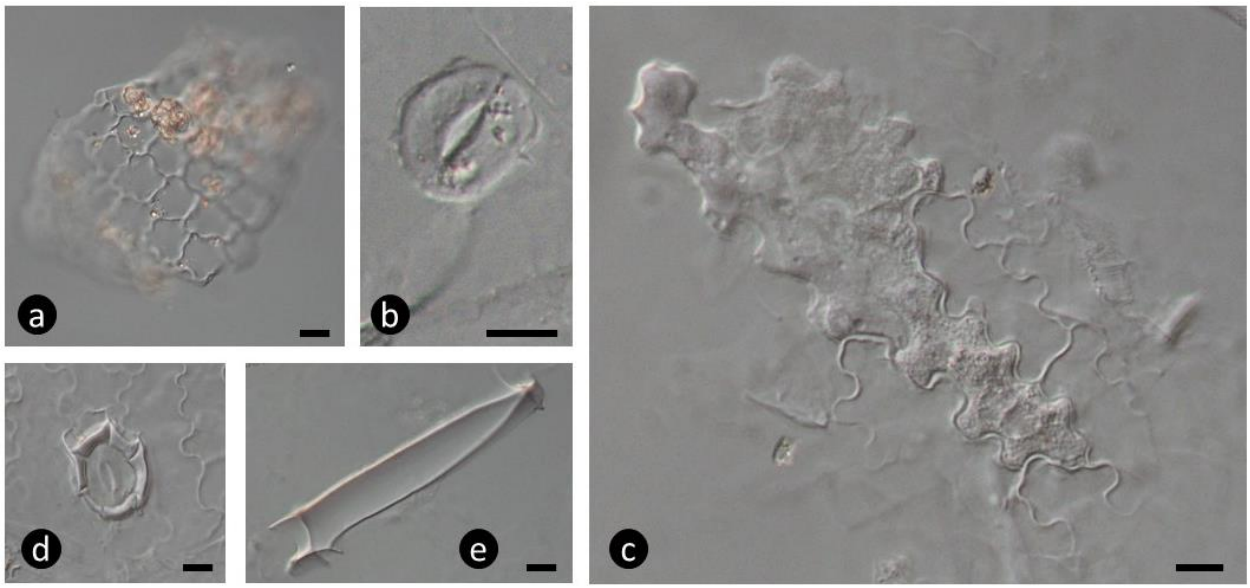

Plate 14. Phytoliths extracted from extant plants. Morphological description in brackets. **a**: *Selaginella plana* (a: lobular epidermal cell); **b - e**: *Selaginella willdenowii* (b: silicified stomata; c: lobular epidermal cell; d: silicified subsidiary cells; e: polyhedral elongate). Scale bar is 10µm.

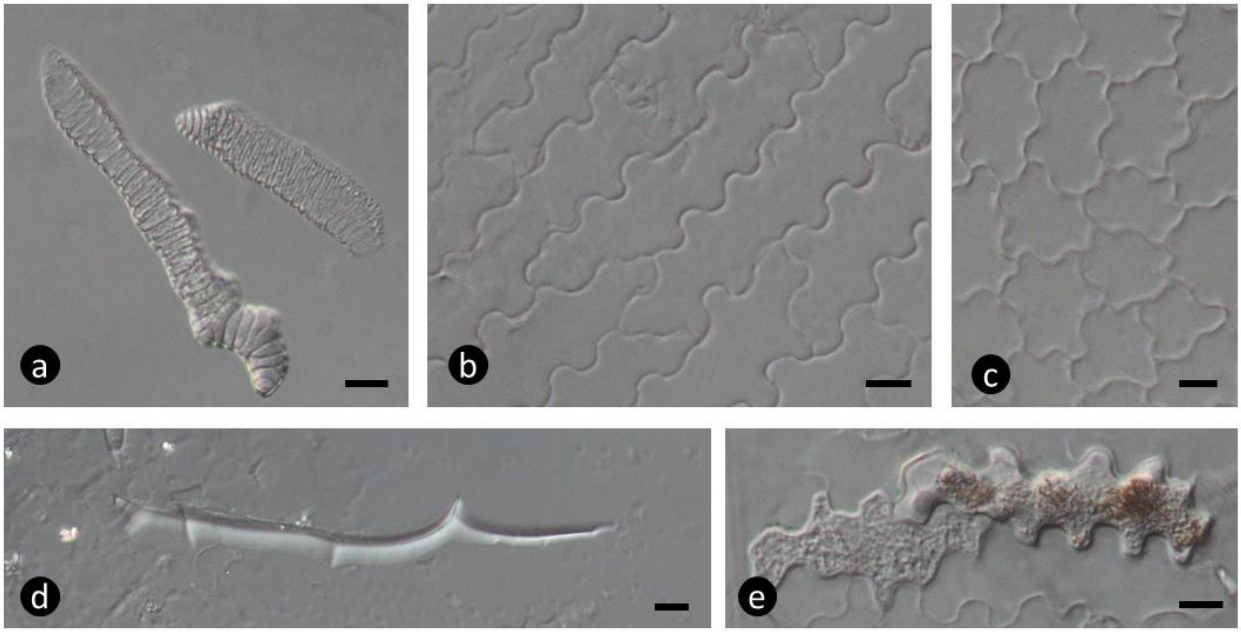

Plate 15. Phytoliths extracted from extant plants. Morphological description in brackets. **a**: *Selaginella plana*; **b, c, d** and **e**: *Selaginella willdenowii* (a: tracheid; b and c: lobular epidermal cells; d: polyhedral epidermal; e: lobular epidermal cells). Scale bar is 10μm.

Plate 16. Phytoliths extracted from extant plants. Morphological description in brackets. **a - c**: *Psilotum nudum* (a – c: cubical to elongate bulliform); **d - f**: *Psilotum X intermedium* (a: elongate echinate single side; e and f: tracheid). Scale bar is 10μm.

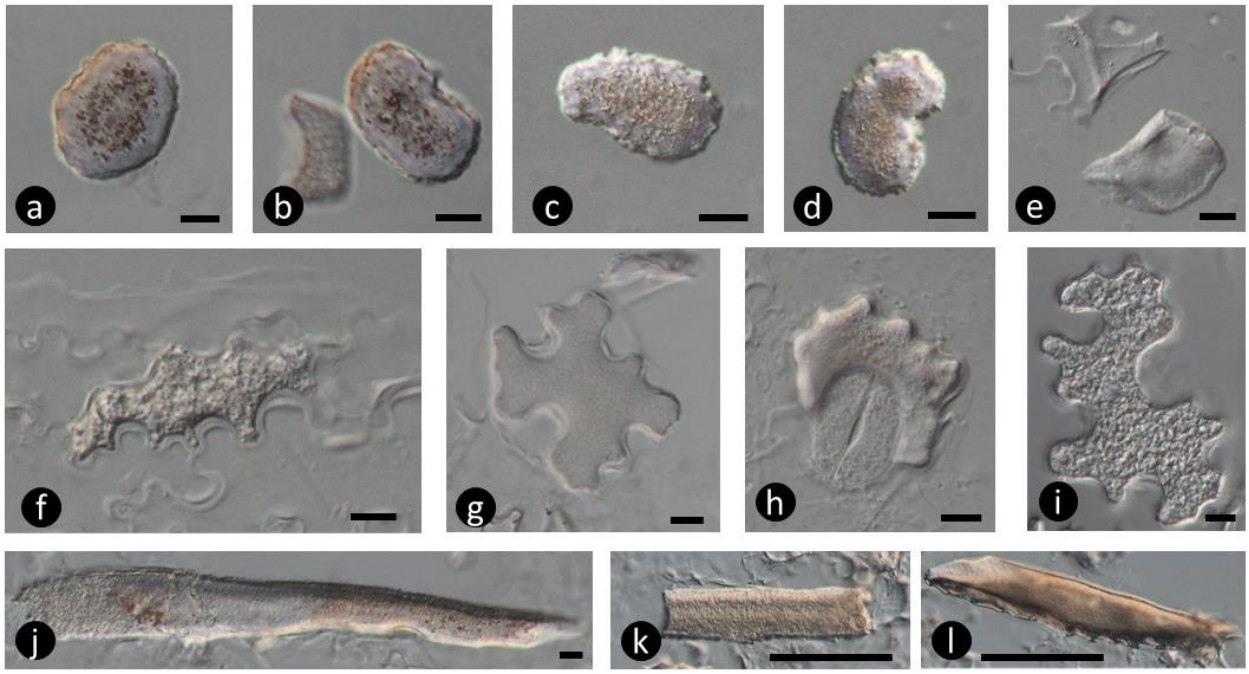

Plate 17. Phytoliths extracted from extant plants. Morphological description in brackets. **a - d**: *Angiopteris evecta* (a – d: globular irregular with granulate surface)*; **e - l:** Blechnum gibbum* (e: cuneiform bulliform cell; f – i: lobular epidermal cell, with h showing silicified stomata; j – l: elongated trapeziform). Scale bar a – j: 10µm, k and l: 100µm.

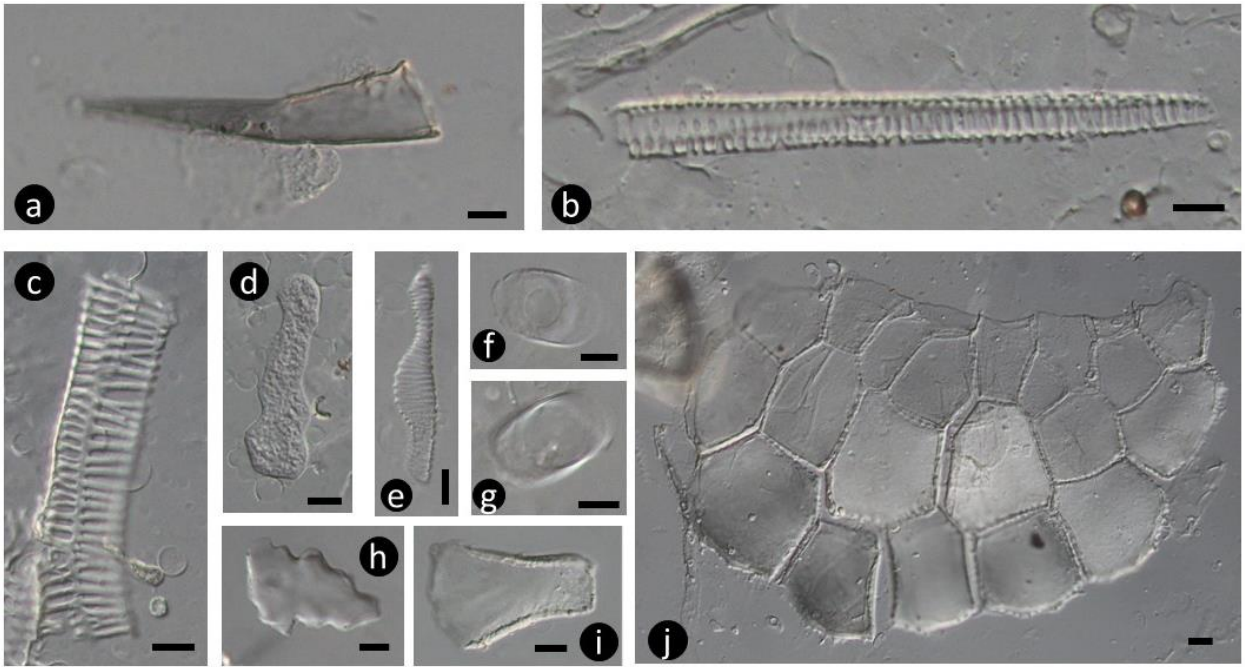

Plate 18. Phytoliths extracted from extant plants. Morphological description in brackets. **a – g**: *Cyathea cooperi* (a: hair segmented; b: vascular tissue; d: polylobate irregular with lacunose surface; e: tracheid; f and g: oblong with circular depression, depression has smooth raised edge); **h – j**: *Cyathea poeppigii (*h: irregular polylobate with psilate surface; i – j: flat, irregular with complete or incomplete castelate ornamentation along the raised edge). Scale bar 10µm.

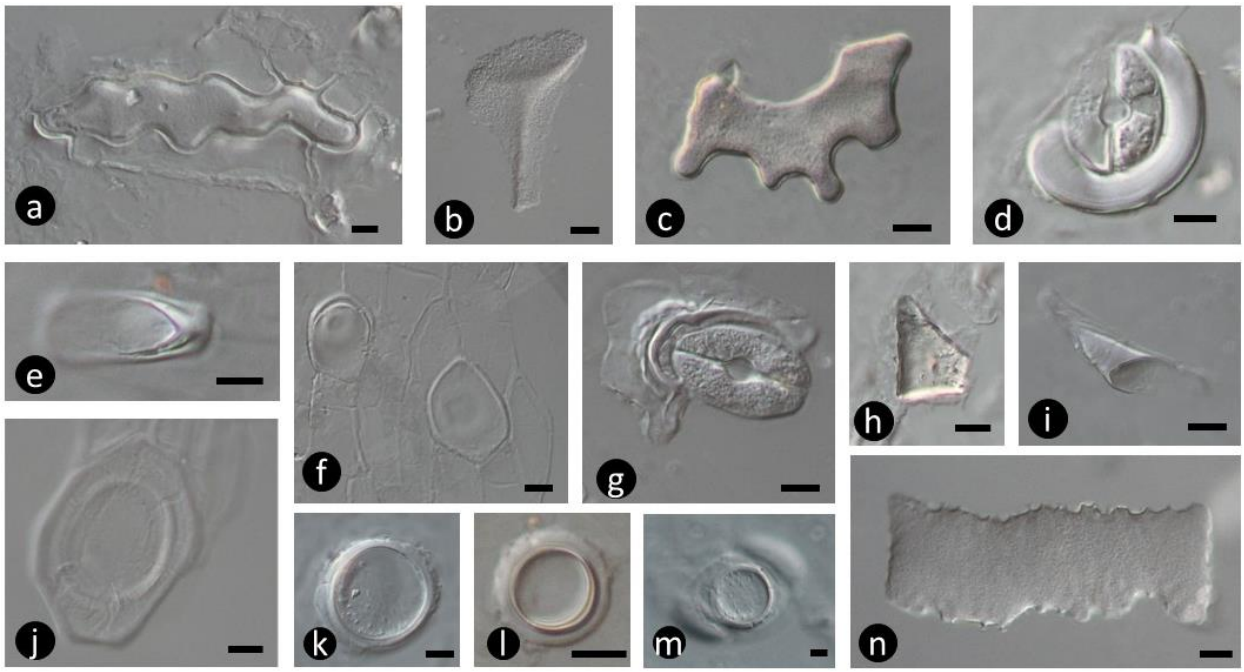

Plate 19. Phytoliths extracted from extant plants. Morphological description in brackets. **a – n**: *Dicksonia Antarctica* (a: Elongated lobular epidermal cell; b: triangular keeled; c: lobular epidermal cell, potentially a silicified subsidiary cell; d, g: silicified stomata and subsidiary cells; e: oval with one short side folded; f and j: oblong with circular depression, depression has smooth raised edge; h: cuneiform; i: hair segmented; k - m: concave circular disc with raised psilate edges; n: elongate with small granulate surface and irregular edges). Scale bar is 10µm.

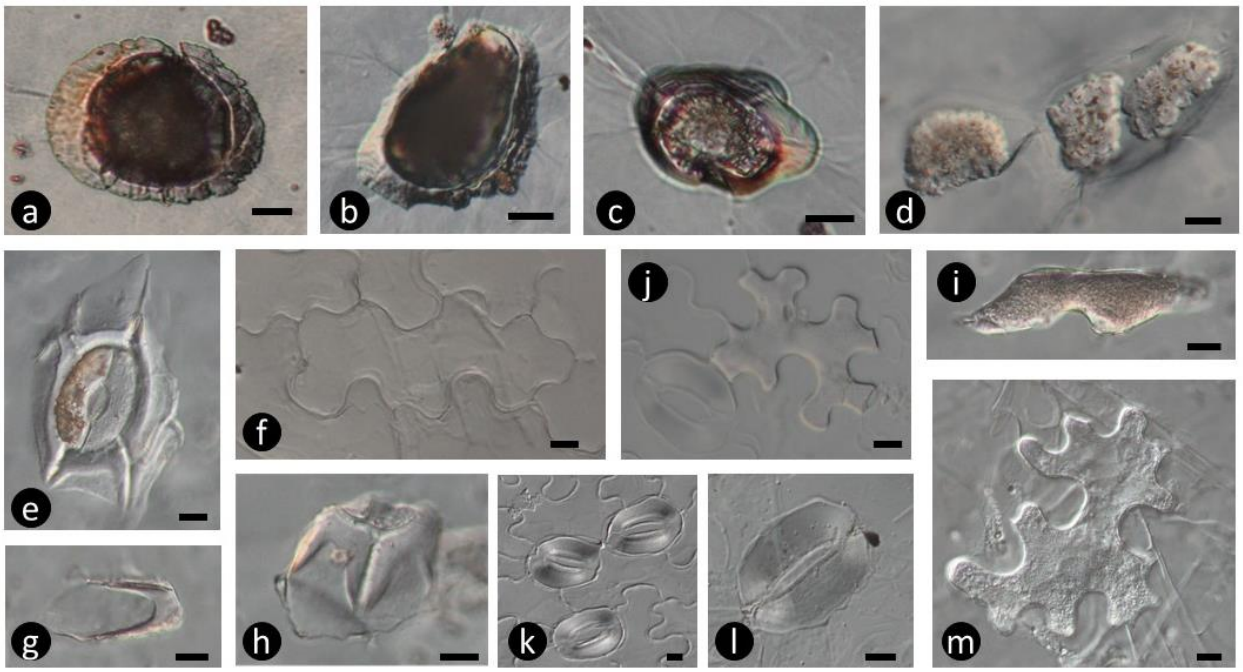

Plate 20. Phytoliths extracted from extant plants. Morphological description in brackets. **a - d**: *Marattia sp.* (a - c: circular to oval with often dark, central depression); ***e – i****: Microlepia platyphylla* (e: silicified stomata; f: lobular epidermal cell; g and h: subsidiary cells; i: elongate irregular with small granular surface texture)*;* **j** and **k:** *Osmunda regalis* (j: lobular epidermal cell ; k: silicified stomata and lobular epidermal cell)*;* **l and m**: *Osmunda japonica* (l: silicified stomata; m: lobular epidermal cell). Scale bar 10µm.

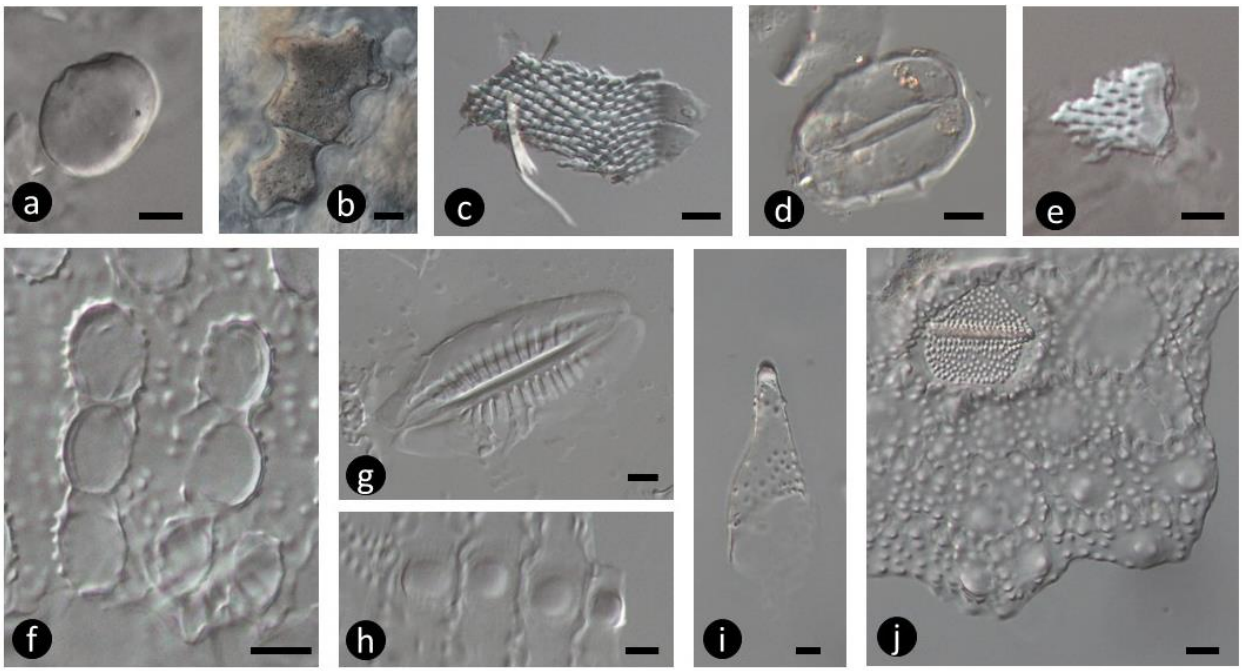

Plate 21. Phytoliths extracted from extant plants. Morphological description in brackets. **a – e**: *Pellaea rotundifolia* (a: flat smooth orbicular; b: lobular epidermal cell; c and e: perforated platelet; d: silicified stomata); **f – h**: *Equisetum myriochaetum* (f and h: tuberculate node on epidermal cells; g: silicified stomata)*;* **i and j**: *Equisetum telmateia* (i and j: tuberculate node on epidermal cells, j includes stomata). Scale bar 10μm.

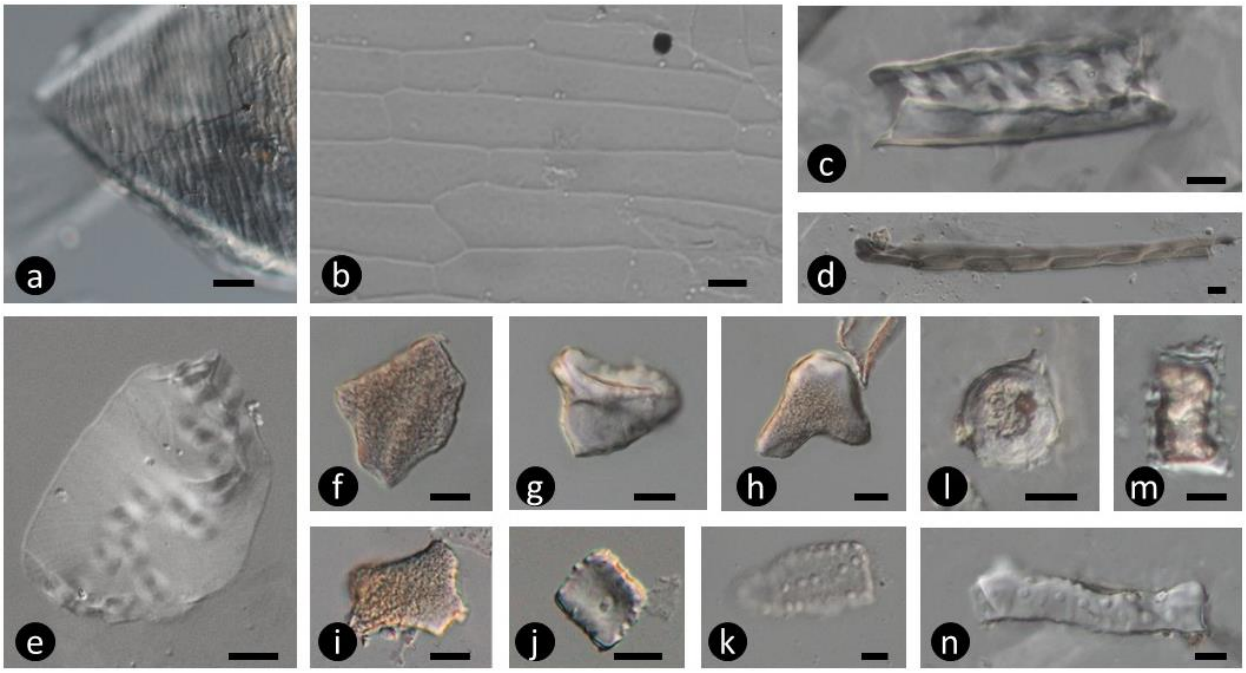

Plate 22. Phytoliths extracted from extant plants. Morphological description in brackets. **a**: *Austrocedrus chilensis* (a: plate with even striations)*;* **b**: *Calocedrus decurrens* (b: elongated irregular epidermal cells)*;* **c - e**: *Calocedrus formosana* (vascular tissue); **f – k**: *Cryptomeria japonica* (f and i: irregular flat with small granular surface texture; g: unclear; h: scutiform with blunt point; j and k: irregular flat with small irregular tuberculate protrusions); **l – n**: *Cunninghamia konishii* (l: demi globular with central circular depression; m; long cell, elongated with echinate ornamentation along edge; n: irregular elongate with small irregular tuberculate protrusions). Scale bar 10μm.

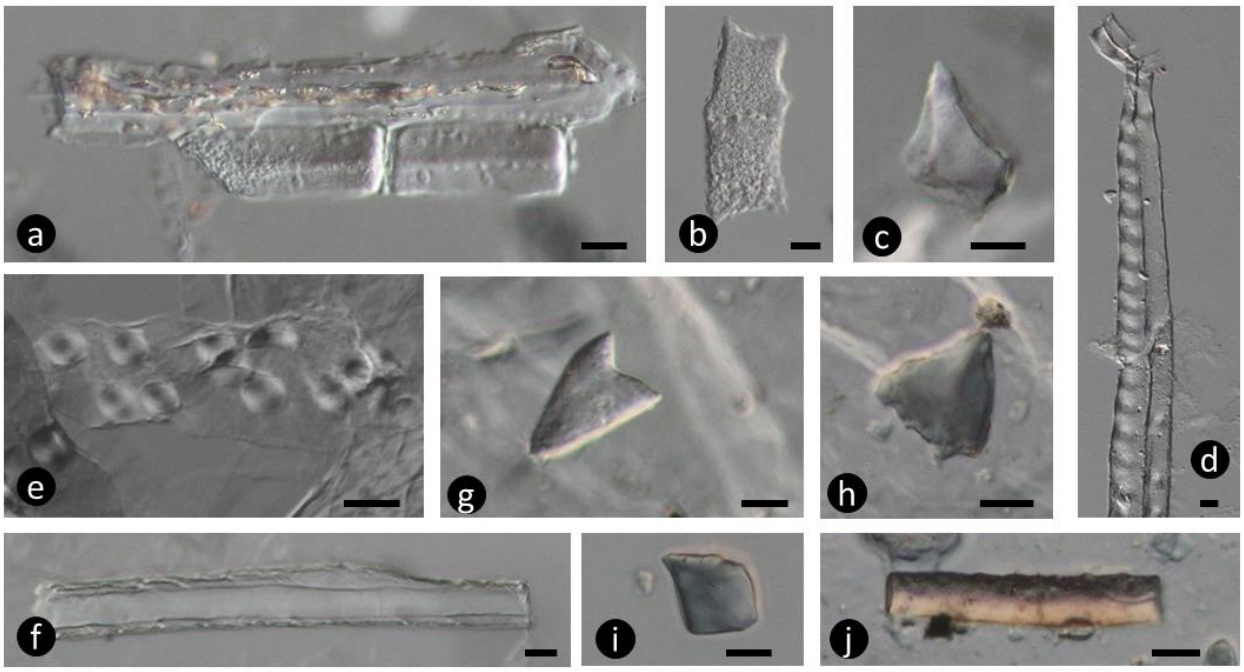

Plate 23. Phytoliths extracted from extant plants. Morphological description in brackets. **a – d**: *Cunninghamia konishii* (a: longate with keel down the long axis and small irregular tuberculate protrusions; b: irregular flat with small granular surface texture; c: cuneiform; d: vascular tissue)*;* **e**: *Cupressus abramsiana* (e: vascular tissue); **f**: *Cupressus lusitanica* (f: vascular tissue); **g – j**: *Juniper virginiana* (g: scutiform; h and i: cuneiform; j: smooth cylindrical cell). Scale is 10µm.

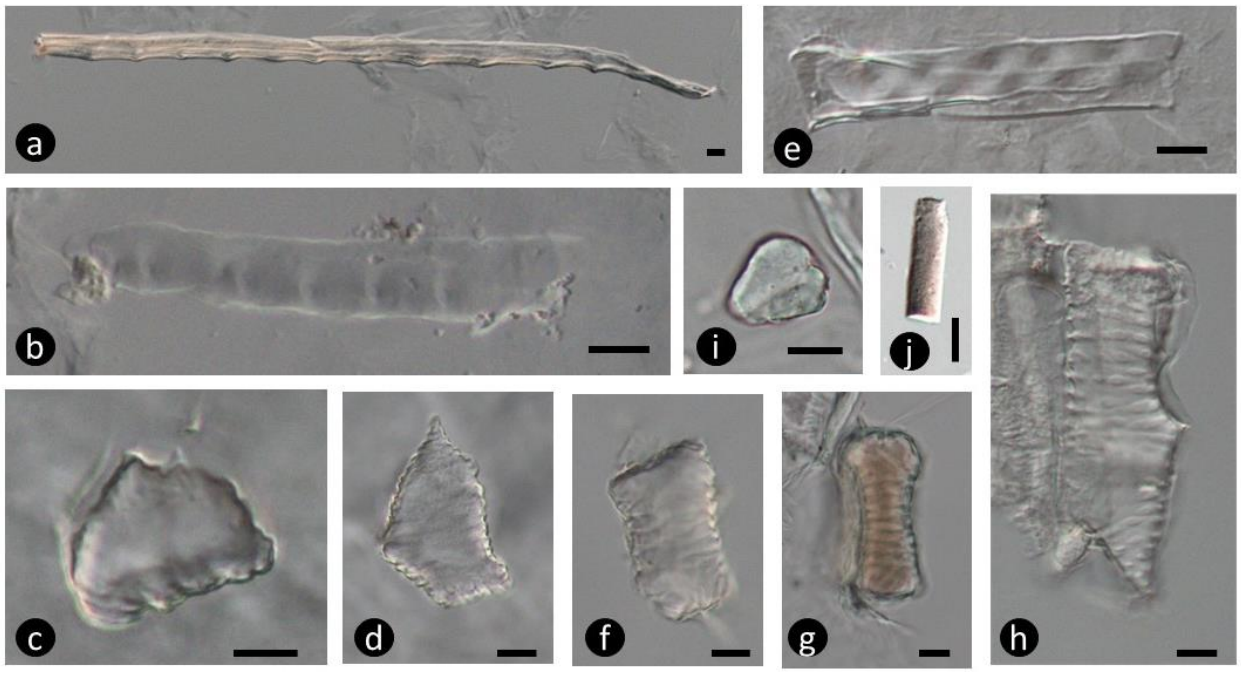

Plate 24. Phytoliths extracted from extant plants. Morphological description in brackets. **a** and **b**: *Sciadopitys verticillate* (a and b: vascular tissue); **c – e**: *Sequoia sempervirens* (c: bulliform ; d: tracheid; e: vascular tissue); **f - h***: Taxus brevifolia* (f – h: tracheid)*;* **i – j**: *Tetraclinis articulate* (i: keeled cuneiform; j: smooth cylindrical cell). Scale is 10µm.

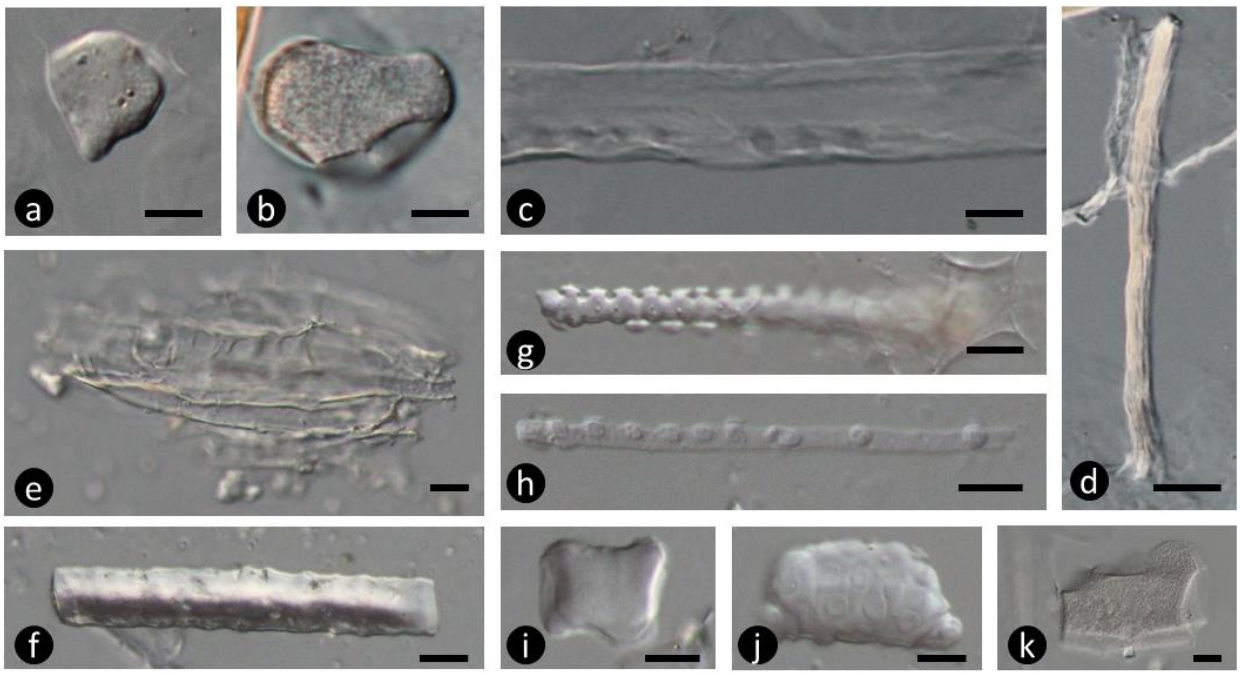

Plate 25. Phytoliths extracted from extant plants. Morphological description in brackets. **a – c**: *Thuja plicata* (a: cuneiform; irregular flat with small granular surface texture; c: vascular tissue); **d**: *Widdringtonia schwarzii (cellulose);* **e**: *Dacrycarpus dacrydioides* (vascular tissue)*;* **f**: *Dacrydium cupressinum* (smooth cylindrical cell)*;* **g - k**: *Phyllocladus trichomanoides* (g and h: elongate with evenly distributed pilate processes; i: bulliform; j: tracheid; k: facetate tabular with irregular flat with small granular surface texture). Scale bar 10µm.

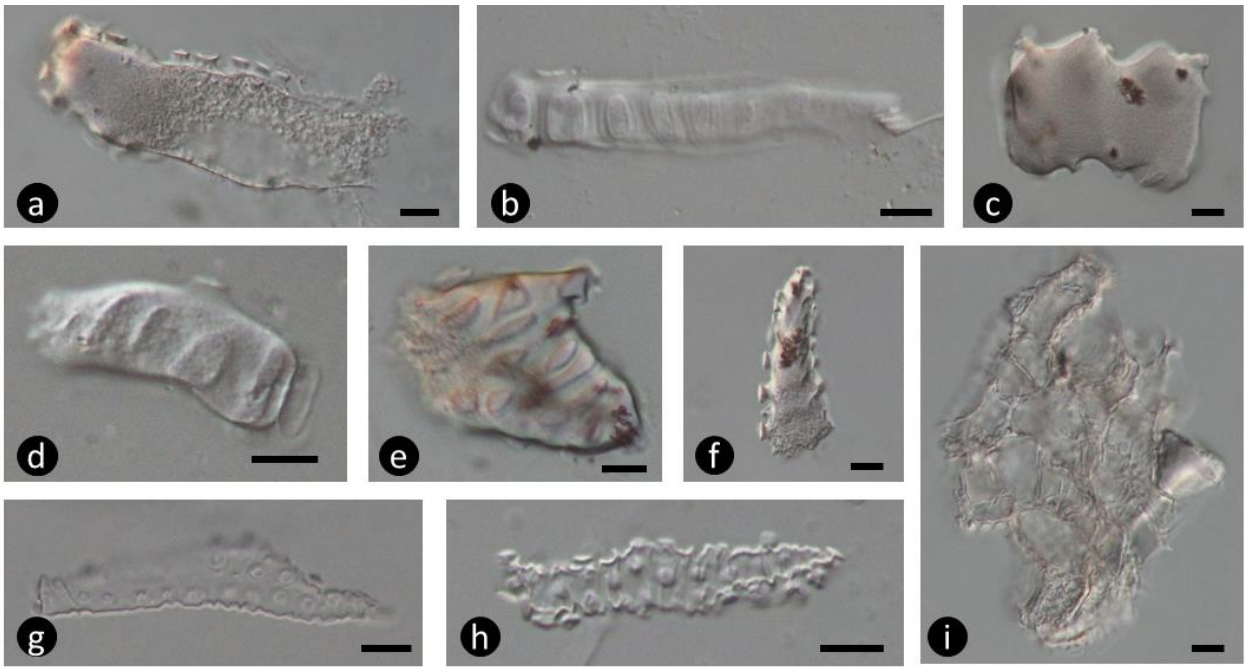

Plate 26. Phytoliths extracted from extant plants. Morphological description in brackets. **a - f**: *Podocarpus latifolius* (a and f: elongate with evenly distributed pilate processes; b, d and e: tracheid; c: elongate with small granulate surface and irregular edges)*;* **g - i**: *Podocarpus nivalis* (g and h: irregular elongate with irregularly distributed pilate processes; i: flat, irregular with complete or incomplete crenate ornamentation along the raised edge. Scale bar 10µm.

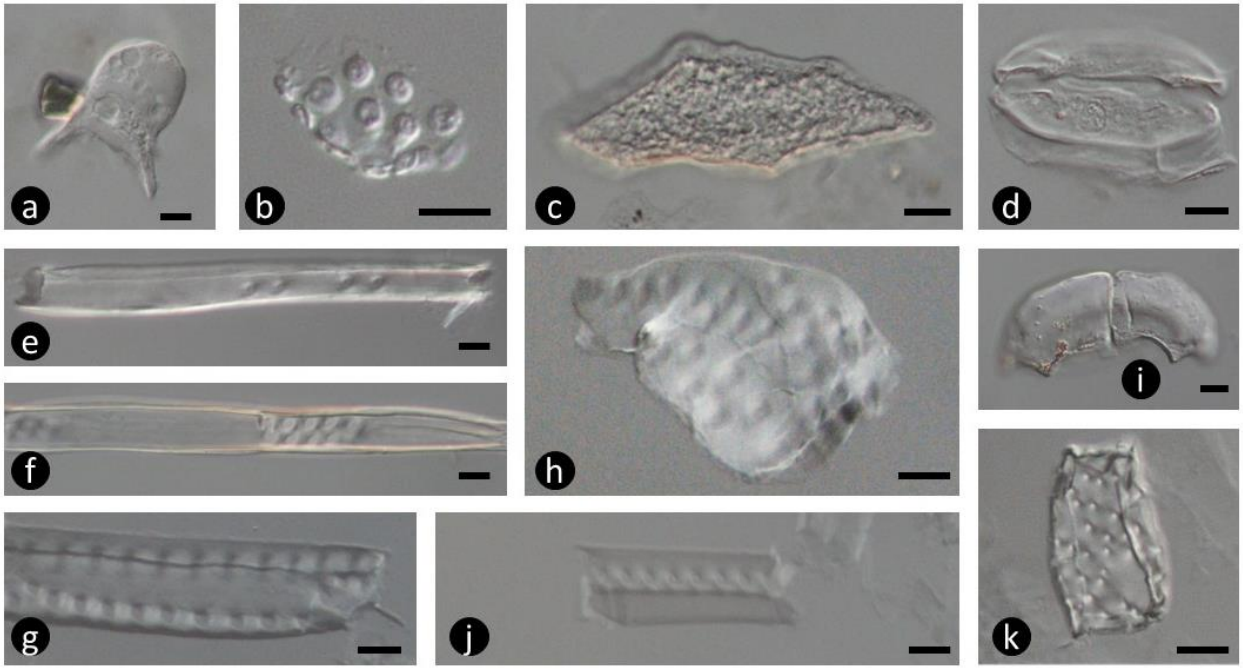

Plate 27. Phytoliths extracted from extant plants. Morphological description in brackets. **a - i**: *Agathis australis* (a: scutiform; b: irregular flat body with pilate processes; c: irregular trapeziform with regular scrobiculate surface; d: silicified stomata e – h: vascular) **j - k**: *Agathis robusta* (i: subsidiary cell; j –k: vascular). Scale bar 10µm.

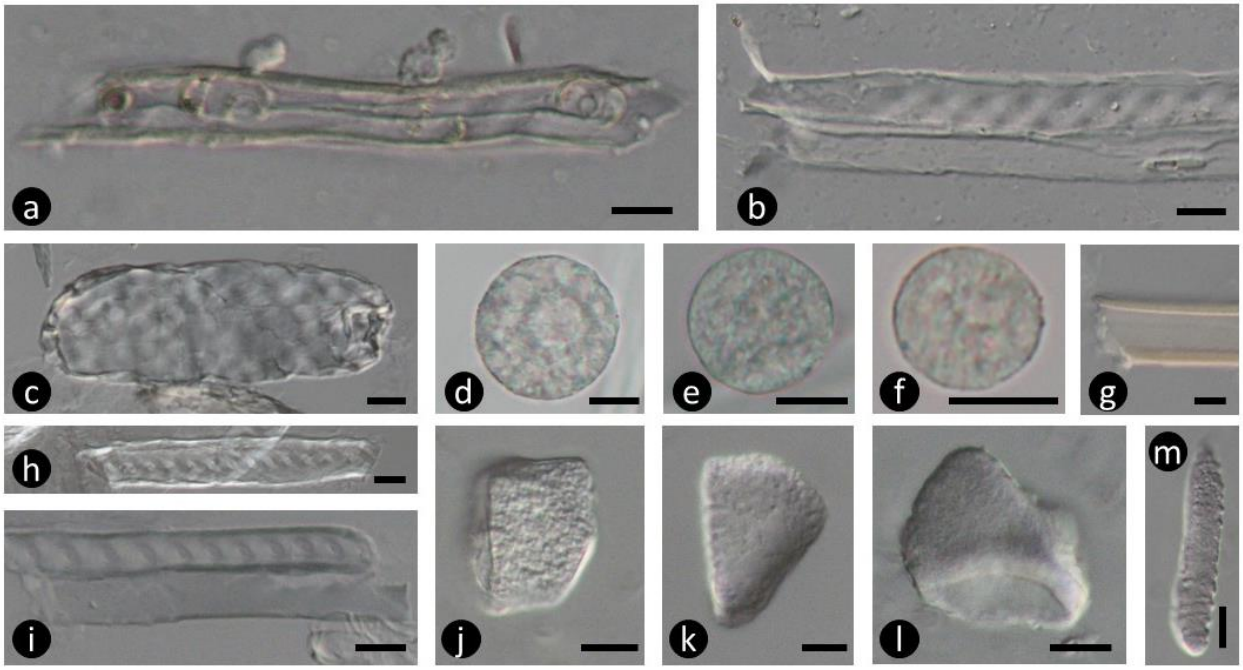

Plate 28. Phytoliths extracted from extant plants. Morphological description in brackets. **a – b:** *Araucaria Araucana* (vascular tissue); **c – i:** *Araucaria cunninghamii* (c, g – i: vascular tissue; d – f: flat orbicular with lacunose surface); **j – m:** *Wollemia nobilis* (j: tabular with small granular surface texture; k: cuneiform; l: saddle shape; m: tracheid). Scale bar 10µm.

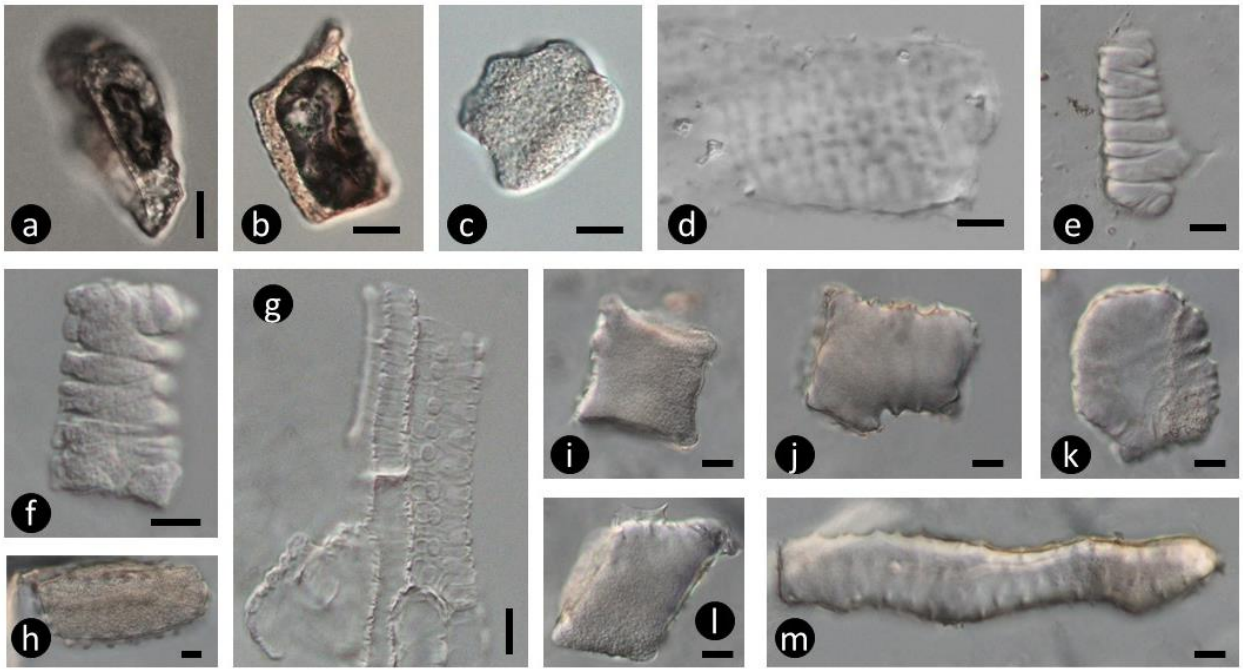

Plate 29. Phytoliths extracted from extant plants. Morphological description in brackets. **a – d:** *Abies forrestii* (a and b: irregular elongate to oval with central irregular depression; c: tabular with small granular surface texture; d:perforated platelet); **e – g:** *Cephalotaxus harringtonii* (e – g: tracheid, with g showing tuberculate nodes); **h – m:** *Keteleeria evelyniana* (h: irregular flat to oblong with small irregular tuberculate protrusions; i, j – k: psilate tabular to psilate ovate with j showing echinate ornamentation and k showing discontinuous striations; m: tracheid). Scale bar 10µm.

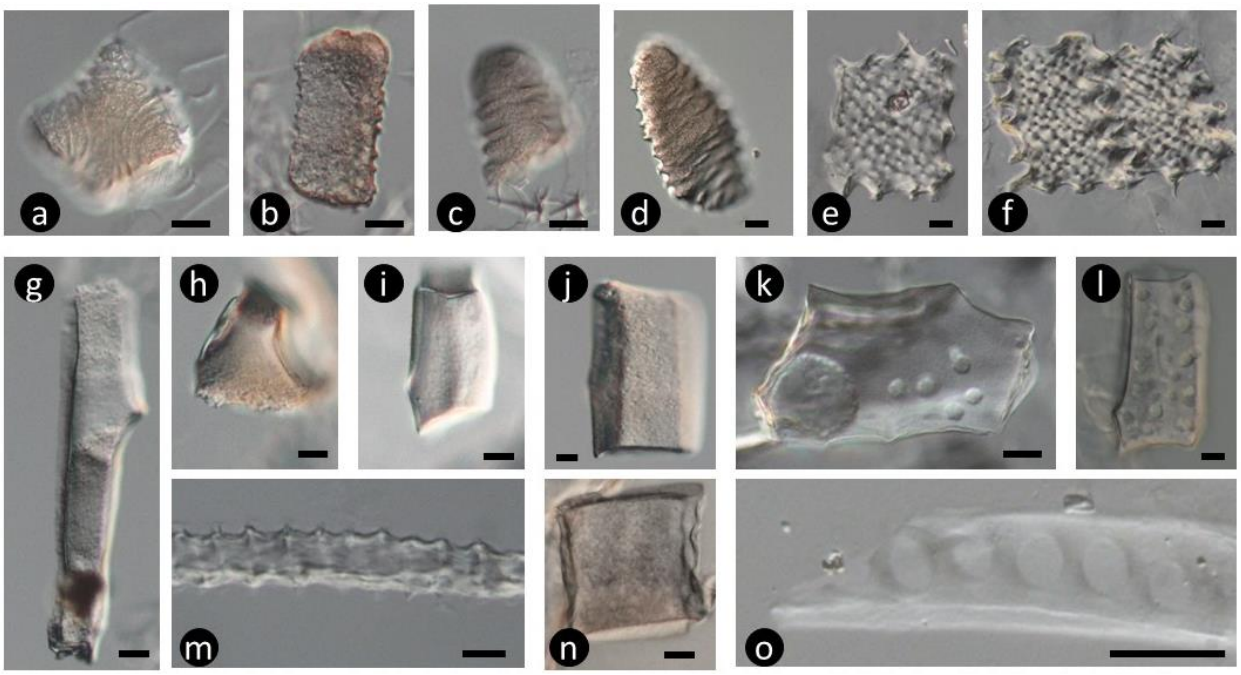

Plate 30. Phytoliths extracted from extant plants. Morphological description in brackets. **a – d:** *Abies forrestii* (a: Irregular body with discontinuous striate ornamentation; b – d: tracheid); **e – o:** *Pinus morrisonicola* (e and f: perforated platelets with echinate interlocking ornamentation; g: elongate facetate; h – l and n: Parallepipedal bulliform with k and l showing irregular pitting; m: elongate echinate; o: vascular tissue). Scale bar 10µm.

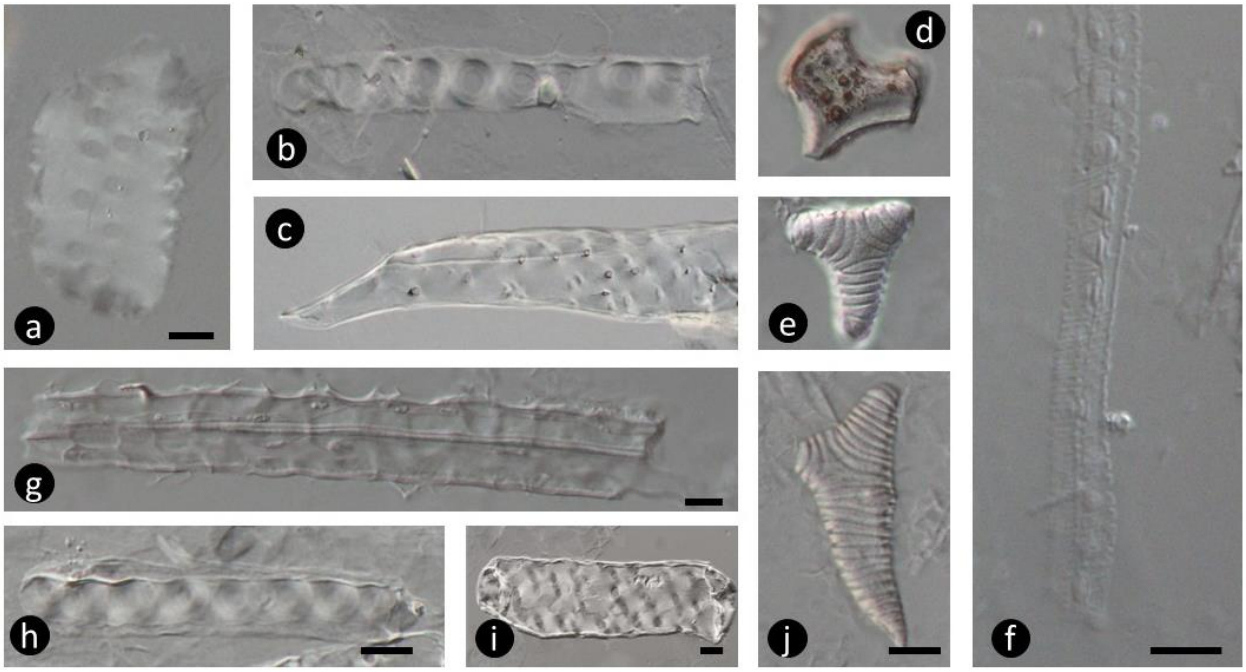

Plate 31. Phytoliths extracted from extant plants. Morphological description in brackets. **a – b:** *Pseudolarix amabilis* (vascular tissue); **c:** *Ephedra californica* (vascular tissue); **d:** *Ephedra chilensis* (cuneiform?); **e - j:** *Gnetum ula* (e and j: Irregular body with continuous striate ornamentation; f – i: vascular tissue). Scale bar 10µm.

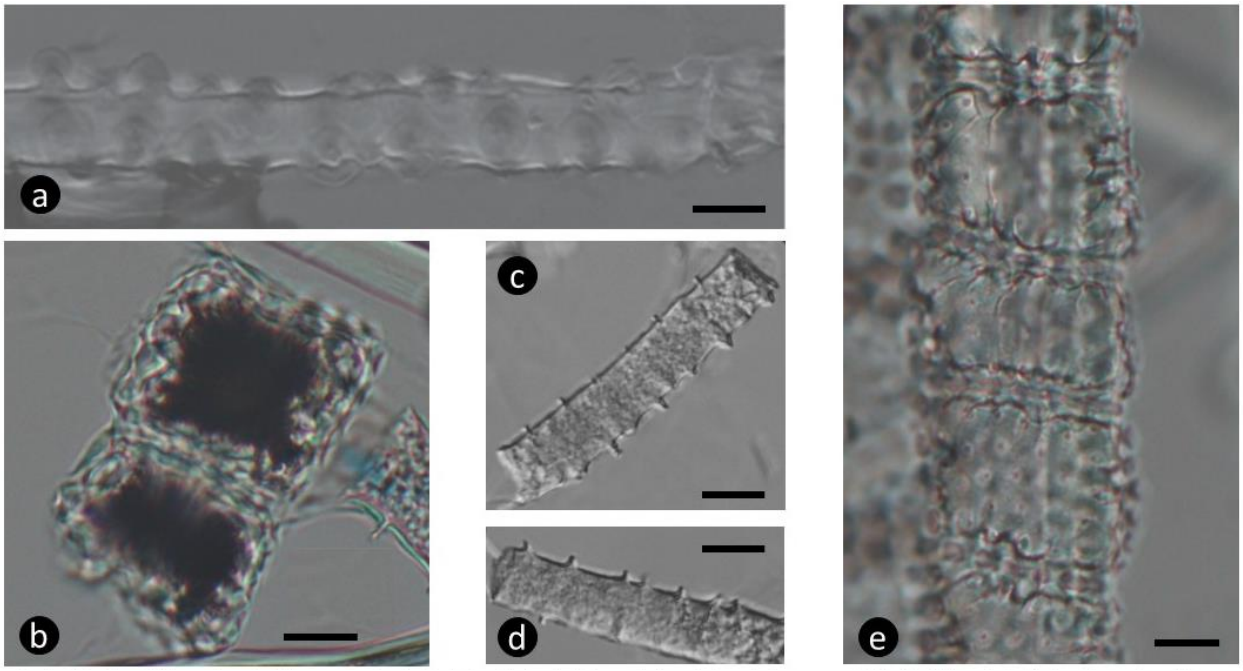

Plate 32. Phytoliths extracted from extant plants. Morphological description in brackets. **a – e:** *Welwitschia mirabilis* (a: Elongate with pilate processes; b and e: perforated platelets with interlocking crenate ornamentation; c and d: elongate with single echinate margin). Scale bar 10µm.

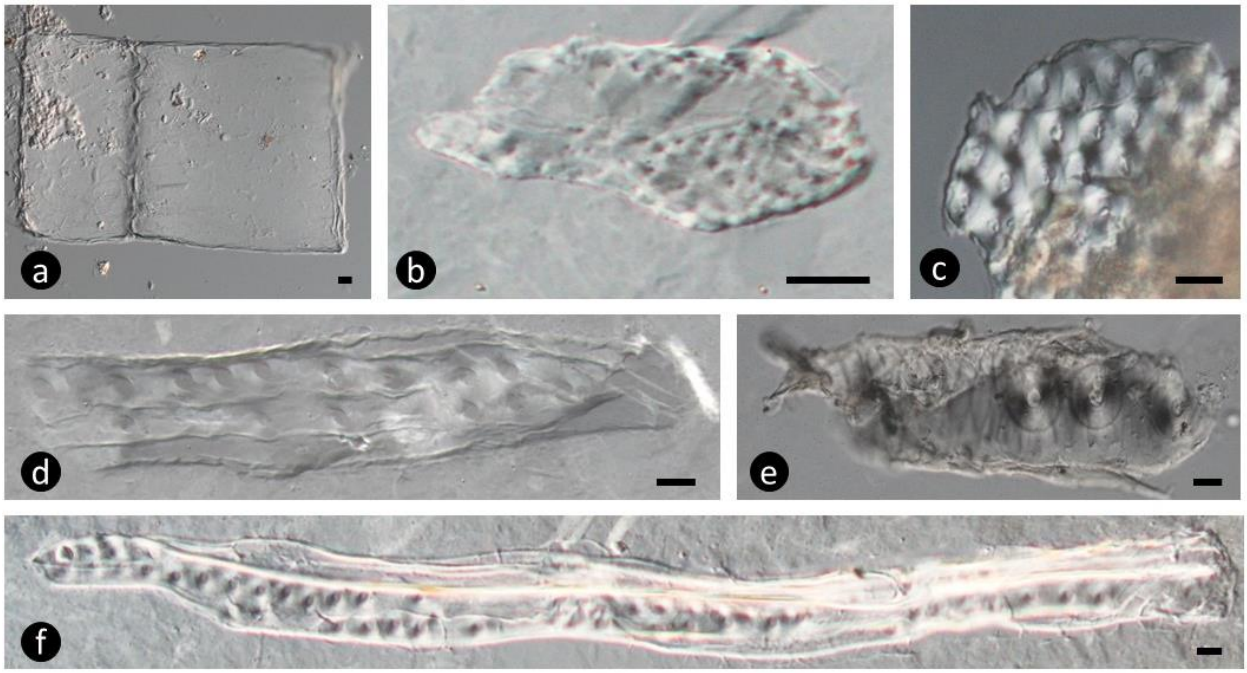

Plate 33. Phytoliths extracted from extant plants. Morphological description in brackets. **a – f:** *Ginkgo biloba* (a: flat rectangular to square with sinuate interlocking margin; b: perforated platelet; c – f: vascular tissue with c showing araucariod pitting). Scale bar 10µm.

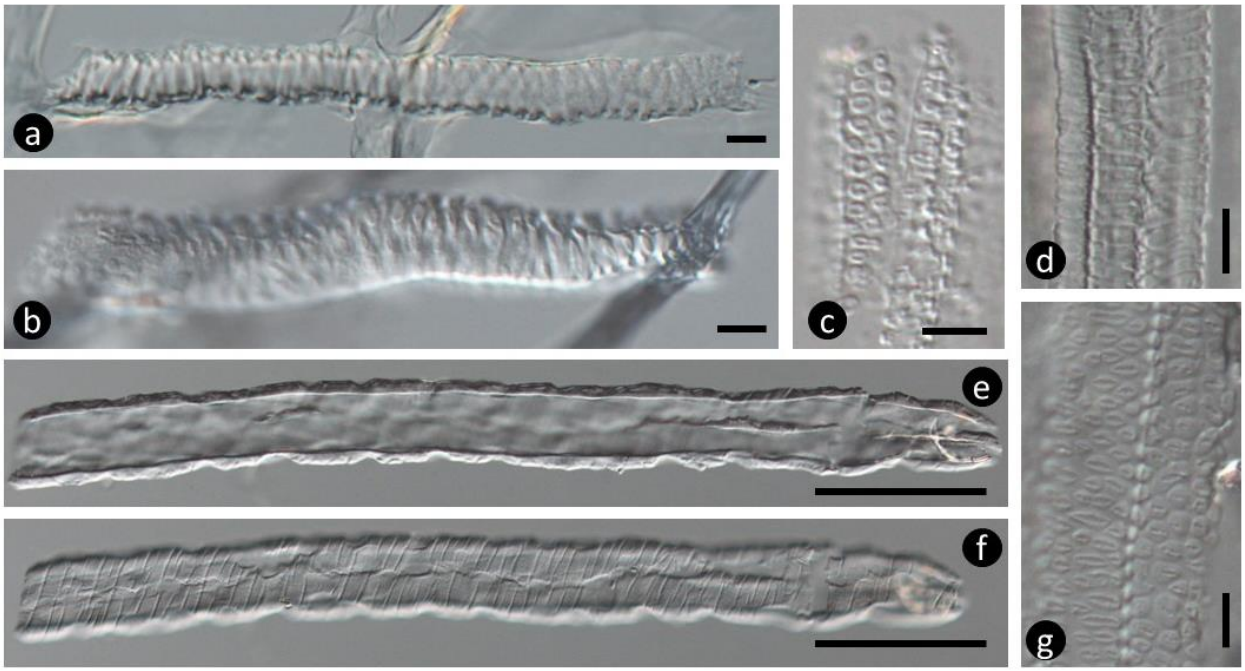

Plate 34. Phytoliths extracted from extant plants. Morphological description in brackets. **a – c:** *Ceratozamia zaragozae* (a – c: elongated tracheid, with c showing evenly spaced circular processes); **d – g:** *Dioon tomasellii* (d and g: tracheid with g showing evenly spaced circular processes; e and f: same phytolith focused in a different plane. Elongate with irregular raised border along the long axis, with striation along the short axis of the element). Scale bar 10µm.

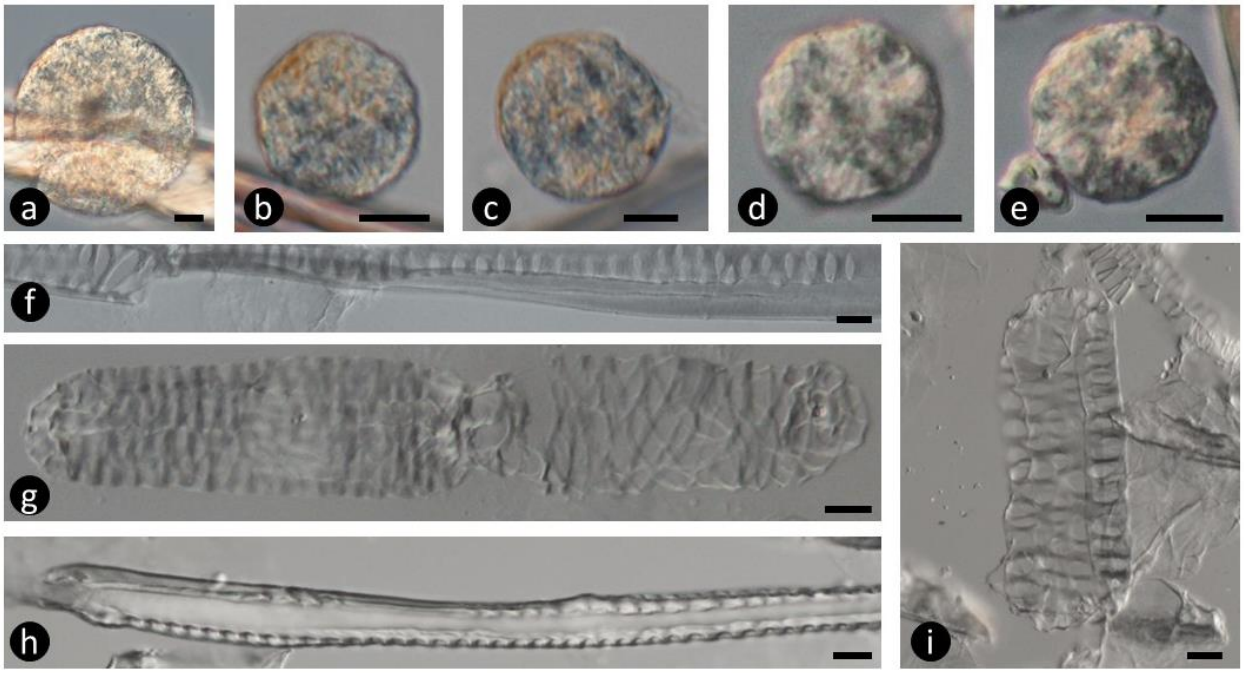

Plate 35. Phytoliths extracted from extant plants. Morphological description in brackets. **a – g:** *Encephalartos trispinosus* (a – e: flat orbicular with lacunose surface; f and g: vascular tissue); **h – i:** *Lepidozamia peroffskyana* (h and i: vascular tissue). Scale bar 10µm.

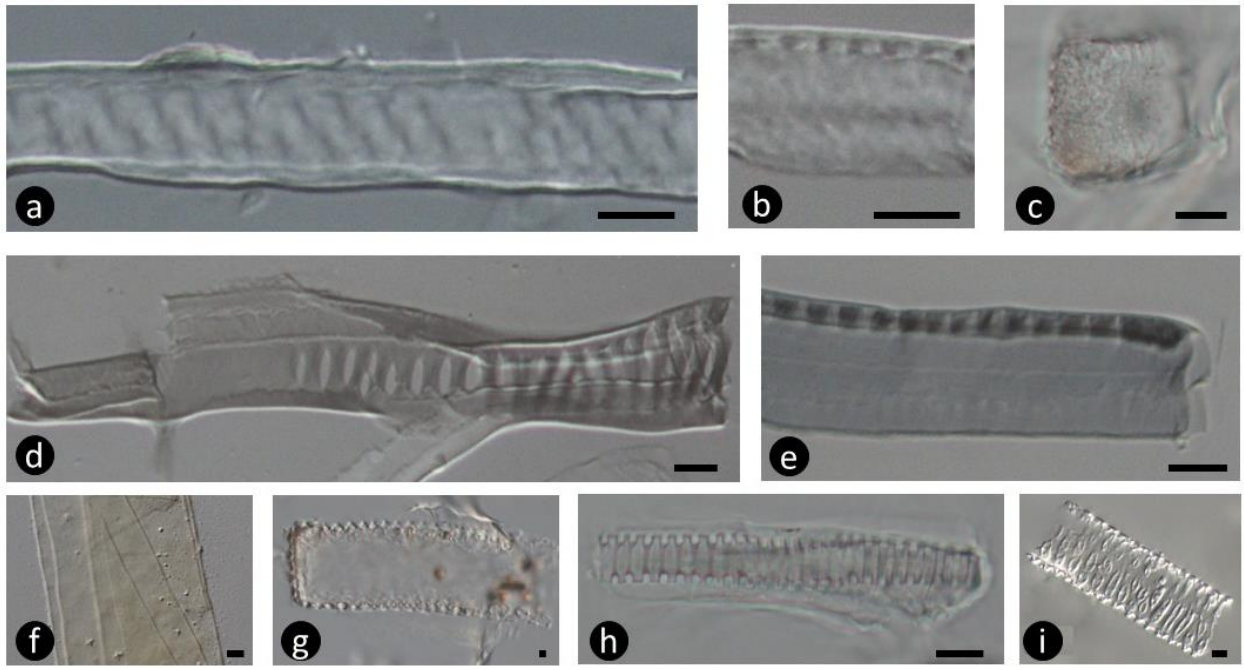

Plate 36. Phytoliths extracted from extant plants. Morphological description in brackets. **a – c:** *Macrozamia secunda* (a and b: vascular tissue; c: psilate tabular with echinate ornamentation and discontinuous striations; **d – e:** *Zamia integrifolia* (d and e: vascular tissue); **f:** *Cycas pectinata* (elongate flat psilate); **g – i:** *Microcycas calocoma* (g: elongate with regular echinate ornamentation; h and i: tracheid with i showing evenly spaced circular processes). Scale bar 10µm.

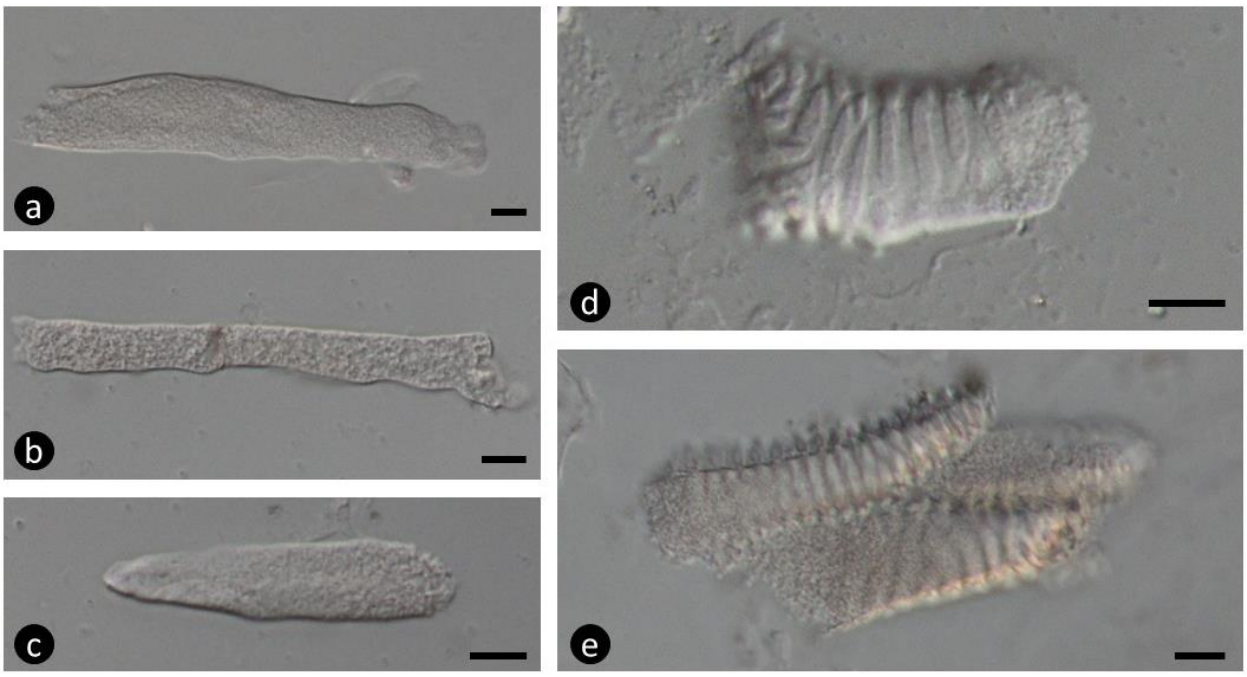

Plate 37. Phytoliths extracted from extant plants. Morphological description in brackets. **a – e:** *Stangeria eriopus* (a – c: Elongate with small granular surface texture; d and e: tracheid). Scale bar 10µm.

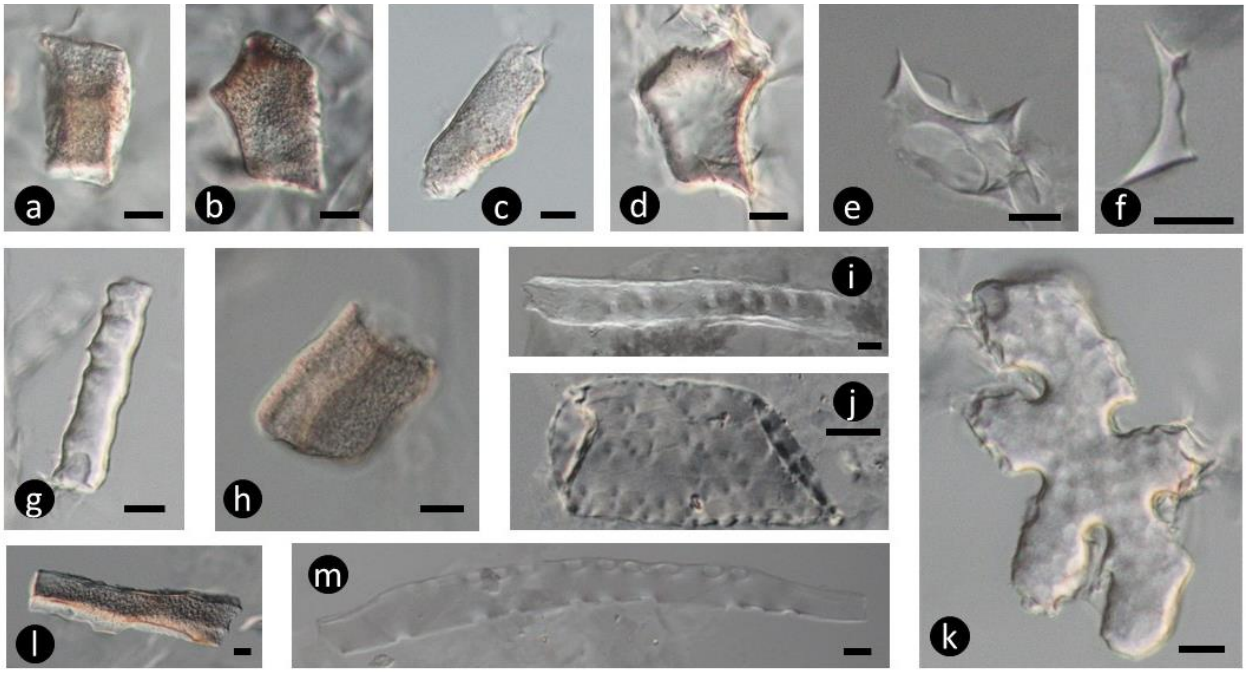

Plate 38. Phytoliths extracted from extant plants. Morphological description in brackets. **a - k**: *Cathaya argyrophyll* (a – d, h and l: tabular to parallelepipedal body with a faceted surface; e and f: polyhedral epidermal; g: cylindrical with slight sinuations; i and m: vascular tissue; j: perforated platelet; k: lobular epidermal cell with lacunose surface); Scale bar is 10µm.

APPENDIX 2

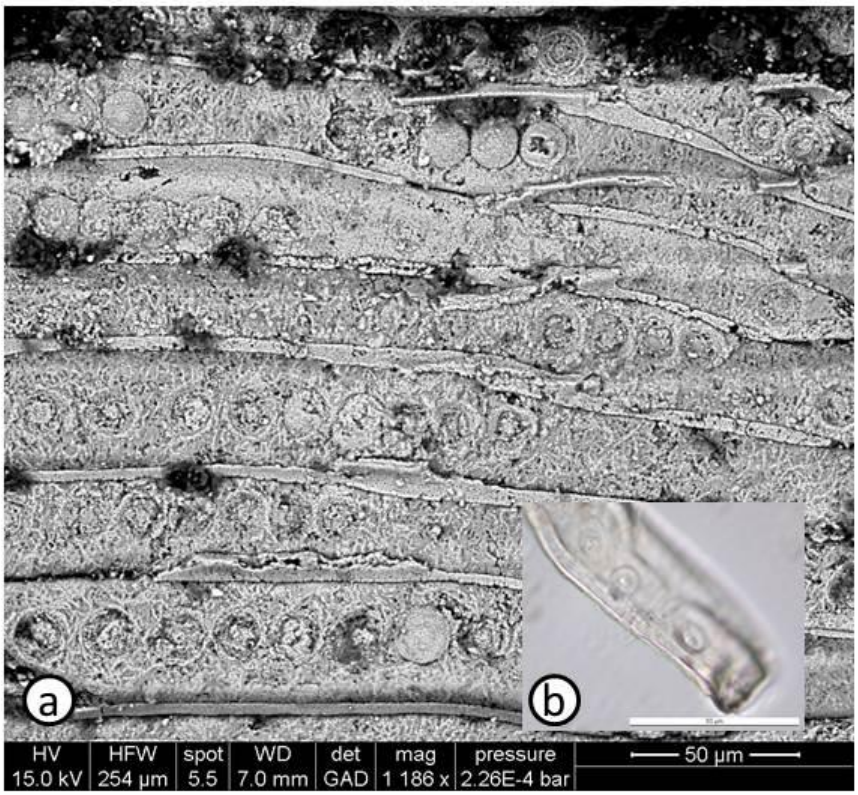

Appendix 2. **a**: SEM of petrified wood fragments known to represent conifers, found in Early Triassic sediments in Caprock Canyon State Park (Marion Bamford, pers. comm.); **b** (insert): uniseriate circular bordered pit phytolith extracted from rock sample of Early Triassic age from Caprock Canyon State Park. Scale bars: 50µm